

**FLUORESCENCE RELAXATION SPECTROSCOPY:
light on dynamical structures of flavoproteins**

Philippe Burten-Bastiaens

Cover illustration: Willem Burten



CENTRALE LANDBOUWCATALOGUS

0000 0429 2716

Promotor : Dr. C. Veeger
hoogleraar in de Biochemie

Co-promotor : Dr. A.J.W.G. Visser
universitair hoofddocent

Philippe I.H. Burten-Bastiaens

**FLUORESCENCE RELAXATION SPECTROSCOPY:
light on dynamical structures of flavoproteins**

Proefschrift
ter verkrijging van de graad van
doctor in de landbouw- en milieuwetenschappen,
op gezag van de rector magnificus,
Dr. H.C. van der Plas,
in het openbaar te verdedigen
op maandag 27 april 1992
des namiddags te vier uur in de aula
van de Landbouwuniversiteit te Wageningen

BIBLIOTHEEK
LANDBOUWUNIVERSITEIT
WAGENINGEN

aan mijn
ouders

STELLINGEN

- 1 De korte correlatietijd die is waargenomen bij het fluorescentieanisotropie-verval van lipoamide dehydrogenase, al dan niet gebonden aan een multienzym complex, is in het verleden verkeerd geïnterpreteerd als flexibiliteit binnen het eiwit.

Fluorescence Polarization Study of the α -Ketoglutarate Dehydrogenase Complex from *Escherichia coli*.
Waskiewicz, D.E. and Hammes, G.G. (1982) *Biochemistry* 21, 6489-6496.

Pyruvate Dehydrogenase Complex from *Azotobacter vinelandii*: Structure Function, and Inter-Enzyme Catalysis.
Bosma, H.J., de Graaf-Hess, A.C., de Kok, A., Veeger, C., Visser, A.J.W.G. and Voordouw, G. (1982) *Ann. N.Y. Acad. Sci.* 378, 265-286.

Dit proefschrift

- 2 De door Weber en Shinitzky gegeven verklaring voor het verdwijnen van energieoverdracht tussen identieke moleculen bij excitatie aan de rode kant van het absorptiespectrum, kan op grond van de in hoofdstuk 4 van dit proefschrift beschreven experimenten worden verworpen.

Failure of Energy Transfer between Identical Aromatic Molecules on Excitation at the Long Wave Edge of the Absorption Spectrum.
Weber, G. and Shinitzky, M. (1970) *Proc. Natl. Acad. Sci.* 65, 823-830

- 3 Dynamische eigenschappen van eiwitten verkregen met NMR zijn niet vergelijkbaar met de "in vivo" situatie vanwege de hoge viscositeit van een eiwitoplossing in een NMR buis.

- 4 Het valt te betreuren dat de discipelen van "Our Father, Who art in Urbana" niet het licht der impulsen hebben gezien, maar star vasthouden aan het geloof der ongevoelige modulatie.

Uit "The Biochemical Fluorometrist's Prayer" Anonieme dichter

- 5 Het model dat superactiviteit van eiwitten in omgekeerde micellen door demping van fluctuaties verklaart, is in tegenspraak met de rol van fluctuaties in de katalyse zoals beschreven in hoofdstuk 2 van dit proefschrift.

Micellar Enzymology: Its Relation to Membranology.
Martinek, K., Klyachko, N.L., Kabanov, A.V., Khmel'nitsky, Yu.L. and Levashov, A.V. (1989) *Biochim. Biophys. Acta* 981, 161-172

- 6 Energieoverdracht volgens Förster reikt voorbij de magische grens van 20 Ångström.

Dit proefschrift.

- 7 Gemengde micellen vormen geen goed systeem om proteïne kinase C activering te bestuderen daar Triton-X100 de membraan-geïnserteerde vorm destabiliseert.

Activation of Protein Kinase C by Triton X-100 Mixed Micelles Containing Diacylglycerol and Phosphatidylserine.
Hannun, Y.A., Loomis, C.R. and Bell, R.M. (1985) J. Biol. Chem., 260, 10039-10043

- 8 Aangezien de thermodynamica van levende systemen als ver-uit-evenwicht beschouwd mag worden, is het niet verwonderlijk dat celbiologen de maanstand en het weer de schuld geven voor het mislukken van een weefselkweek.

Orde uit Chaos.
Prigogine, I. en Stengers, I. (1988) Uitgeverij Bert Bakker, Amsterdam

- 9 Het feit dat bureaucratie geestdodend werkt geeft aan dat hiervoor een Turing-machine bestaat.

The Emperor's New Mind.
Penrose, R. (1989) Oxford University Press, New York.

- 10 Het binnenhalen van een universitaire onderzoeksschool heeft veel weg van een Pyrrus-overwinning.

- 11 Het verheffen van monogaam gedrag tot norm heeft tot gevolg dat Amerikanen blijven zitten met de verkeerde president.

- 12 Het Nederlandse bedrijfsleven zou er wel bij varen indien de RDM zich helemaal toelegt op het vervaardigen van papieren duikboten.

Philippe Burten-Bastiaens

Fluorescence relaxation spectroscopy: light on dynamical structures of flavoproteins.

Wageningen, 27 april 1992

Voorwoord

Hoe vaak heb ik niet gezegd dat het proefschrift over 2 weken af zou zijn (waarschijnlijk ongeveer 20 keer). Mijn begeleider Ton Visser keek me dan glimlachend aan en wist de juiste tijdsfactor in te schatten (1:10). Maar het zit er op, mede dankzij de hulp van een aantal mensen die ik hierbij zou willen bedanken. Ton, zonder je enthousiasme, opbouwende kritiek en vertrouwen had ik het niet gered. Ik hoop dat we in de toekomst nog vele wetenschappelijke en niet-wetenschappelijke avonturen zullen beleven. Veel van de experimenten die in dit boekje staan beschreven waren niet mogelijk geweest zonder het vakmanschap en de kennis van Arie van Hoek, "the laser wizard for whom the impossible is possible". Arie, ik heb veel van je geleerd en de samenwerking als bijzonder plezierig ervaren. De dag dat we kreupel van de blaren het hotel in Los Angeles binnenkwamen zal ik niet gauw vergeten. Cees Veeger wil ik bedanken voor het nauwgezet doorlezen en becomingentariëren van dit proefschrift waardoor de resultaten in een bredere context geplaatst konden worden. Mijn collega en vriend Eward Pap heeft door zijn relativerend vermogen er een aantal keer voor gezorgd dat ik de grens der waanzin niet heb overschreden. De vele discussies die we hebben gehad, hebben tot ideeën geleid die in dit proefschrift verwerkt zijn. Buiten dat stond hij altijd klaar om me op "de wereld daarbuiten" te wijzen. Door Rik Leenders (voor ingewijden "de chef"), met wie ik drie jaar een kamer heb gedeeld, heb ik geleerd dat samenwerken met mensen die het anders doen dan ik bijzonder goed kan zijn. We hebben veel gelachen in die kamer. Jacques Benen heeft er voor gezorgd dat ik een overmaat lipoamide dehydrogenase ter beschikking had en stond altijd klaar om me ergens mee te helpen. Ik hoop dat we de tijdopgeloste fluorescentie-quenching experimenten nog zullen publiceren. Willem van Berkel ben ik erkentelijk voor zijn bijdrage aan hoofdstuk drie. Jillert Santema heeft flavine-dimeren gesynthetiseerd die prachtige resultaten hebben opgeleverd, welke ik helaas niet heb kunnen verwerken in dit proefschrift. Jillert, maak je geen zorgen, de nieuwe post-doc heeft een vruchtbare start. De bloederige avonturen met Wim Wolkers hebben tot zuiver glutathione reductase geleid dat gebruikt is in de experimenten beschreven in hoofdstuk twee. Raymond Verhaert, bedankt voor het kritisch doorlezen van hoofdstuk twee en vier en in het algemeen voor je interesse. De morele steun van de "Loburg clan" (Antonio, Axel, Marc en Wicher) en van Jacques en Ivonne heeft me menig keer uit de put getrokken. Arjan Kindermans, ziehier een boekje over "klepperende klepjes en klapperende

deurtjes" in eiwitten. Ik heb onze gesprekken over ver uiteenlopende vakgebieden altijd buitengewoon stimulerend gevonden. Dirk, bedankt voor het in vorm houden van mijn lachspieren. Lenie, je steun en menselijk inzicht was voor mij van onschatbare waarde. Je remercie Jean-Claude Brochon d'avoir bien voulu participer à ce projet. Vous m'avez beaucoup aidé à minimaliser l'entropie des informations sur la méthode de l'entropie maximale. Als laatste wil ik "La Famiglia" bedanken. Willem (pa), Sonia (ma), Raymond (broer) en Pawla (zus), jullie hebben me altijd gestimuleerd en onvoorwaardelijk gesteund.

Abbreviations

ADC	analog to digital converter
CFD	constant fraction discriminator
CS	conformational substate
CW	continuous wavelength
DCPIP	dichlorophenol-indophenol
EB	erythrosine B
EDTA	ethylenediamine tetraacetic acid
eq.	equation
ETF	electron transferring flavoprotein
Fig.	figure
FWHM	full width half maximum
GR	glutathione reductase
GSSG	oxidized glutathione
GSH	reduced glutathione
Lip	lipoamide
LipDH	lipoamide dehydrogenase
LipDH-AV	lipoamide dehydrogenase from <i>Azotobacter vinelandii</i>
LipDH- Δ 14	deletion mutant of lipoamide dehydrogenase from <i>Azotobacter vinelandii</i>
MCA	multichannel analyzer
MCP	microchannel plate
MCS	multichannel scaling
MEM	maximum entropy method
SDS-PAGE	sodium dodecylsulfate-polyacryl gelelectrophoresis
SV	Stern-Volmer
TCSPC	time-correlated single photon counting
Tyr	tyrosine

CONTENTS

1. General Introduction	1
1.1 Flavin as a natural fluorescent reporter group	1
1.2 Lipoamide dehydrogenase and glutathione reductase as biophysical systems	3
1.3 Fluorescence methodology	5
1.3.1 Molecular relaxation spectroscopy	5
1.3.2 Fluorescence lifetime distributions	8
1.3.3 Fluorescence anisotropy	10
1.3.3.1 General description	10
1.3.3.2 Rotation of the protein	10
1.3.3.3 Restricted reorientational motion	11
1.3.3.4 Homo-energy transfer	11
1.4 Aim of this thesis	14
1.5 References	15
2. Comparison of the Dynamical Structures of Lipoamide Dehydrogenase and Glutathione Reductase by Time-Resolved Polarized Flavin Fluorescence	19
2.1 Introduction	19
2.2 Materials	22
2.3 Methods	22
2.3.1 Time-resolved fluorescence	22
2.3.2 Data analysis	23
2.4 Results	26
2.4.1 Total fluorescence decay analysis	26
2.4.2 Fluorescence anisotropy analysis	32
2.5 Discussion	42
2.6 Appendix	46
2.7 References	48
3. Molecular Relaxation Spectroscopy of Flavin Adenine Dinucleotide in Wild Type and Mutant Lipoamide Dehydrogenase from <i>Azotobacter vinelandii</i>	51
3.1 Introduction	51
3.2 Theory	53
3.3 Materials	54
3.4 Instrumentation	55
3.5 Computational methods	56
3.6 Results	57
3.6.1 Fluorescence quenching by iodide	57
3.6.2 Spectral Shifts	58

3.6.3	Interpretation of the data according to continuous relaxation models	62
3.7	Discussion	68
3.8	References	71
4.	Conformational Dynamics and Intersubunit Energy Transfer in Wild Type and Mutant Lipoamide Dehydrogenase from <i>Azotobacter vinelandii</i> . A multidimensional time-resolved polarized fluorescence study.	73
4.1	Introduction	74
4.2	Materials and Methods	76
4.2.1	Biochemical preparations	76
4.2.2	Instrumental	77
4.2.3	Generation of fluorescence data surface	80
4.2.4	Data analysis	80
4.3	Results	82
4.3.1	Total fluorescence decay	82
4.3.2	Fluorescence anisotropy decay	90
4.4	Discussion	103
4.5	References	107
5.	Energy Transfer between the Two Flavin Chromophores of Electron-Transferring Flavoprotein from <i>Megasphaera elsdenii</i> as Inferred from Time-Resolved Red-Edge and Blue-Edge Fluorescence Spectroscopy	111
5.1	Introduction	111
5.2	Materials and methods	114
5.2.1	Biochemical manipulation	114
5.2.2	Steady-state spectra	114
5.2.3	Time-resolved fluorometry	114
5.2.4	Data analysis	115
5.3	Results	116
5.3.1	Fluorescence decay	116
5.3.2	Fluorescence anisotropy decay	117
5.4	Discussion	124
5.5	References	125
6.	Summarizing Discussion	127
	Samenvatting	131
	Curriculum vitae	138

Chapter 1

General Introduction

1.1 Flavin as a natural fluorescent reporter group

The biologically widespread group of flavoproteins have in common that they contain the yellow flavin molecule as prosthetic group. The most common natural flavins are flavin adenine dinucleotide (FAD) and flavin mononucleotide (FMN) which have both riboflavin as their biological precursor. In the majority of flavoproteins the prosthetic group is noncovalently bound to the apo-flavoprotein where the tight binding is a result of combined effects of electrostatic and hydrophobic interactions. However, a number of flavoproteins is known where FAD is covalently attached by the 8 α -position to the amino acid residues histidine, tyrosine or cysteine. Furthermore, a number of chemically modified flavins are found in flavoproteins such as 8-hydroxy-FAD and 6-hydroxy-FAD with altered physical-chemical properties.

To the biological chemist the most interesting feature of this versatile molecule consists of its redox properties which can be modulated by the (protein) environment. The redox active part of the natural flavins is the isoalloxazinic ring which can exist in the oxidized, one-electron reduced and two-electron reduced state. The redox potentials of the two one-electron steps vary largely among different flavoproteins and depend on the chemical nature of the active site in which the isoalloxazine resides. This property makes flavin suitable as an electron shuttle in very different chemical (redox) reactions which explains its widespread occurrence in nature [1].

For the biophysicist one of the most interesting properties of flavin is that it is a fluorescent molecule which spectral parameters depend on the particular characteristics of the molecular environment. In this respect the molecule is a natural reporter group from which information on the dynamical structure of proteins in solution can be extracted. The large variety of flavoproteins with their different biological functions provides a pool of material to undertake comparative studies on protein dynamics and structure in relation to catalytic function. Most of the fluorescence data are usually obtained by monitoring the protein fluorescence of the intrinsic probe tryptophan [2]. Although this amino acid is present in a diversity of proteins, several distinct disadvantages adhere to the use of this molecule

as a natural reporter group. First, most proteins contain several tryptophan residues which makes the interpretation of the data ambiguous because of the different contributions to the fluorescence from differently emitting classes of tryptophan [3]. Second, the photophysics of tryptophan is complicated because of the existence of almost degenerate energy levels belonging to the first absorption band [4]. Due to this latter property the fundamental polarization of this molecule is considerably lowered by interconversion between the two perpendicular transition moments [5]. Also, the intramolecular excited-state process considerably complicates the interpretation of the data in the picosecond time domain where rapid fluctuations of protein residues can take place [6, 7].

In comparison, the photophysical properties of the isoalloxazinic residue of natural flavins are somewhat simpler. The first electronic transition of free flavin in neutral aqueous solution has an absorption maximum at 445 nm ($\epsilon = 12.4 \text{ mM}^{-1}\text{cm}^{-1}$) and the second electronic transition has an absorption maximum at 367 nm ($\epsilon = 10.0 \text{ mM}^{-1}\text{cm}^{-1}$) [8]. The geometry of the first electronic transition moment in the molecular frame is known (Fig.1) [9].

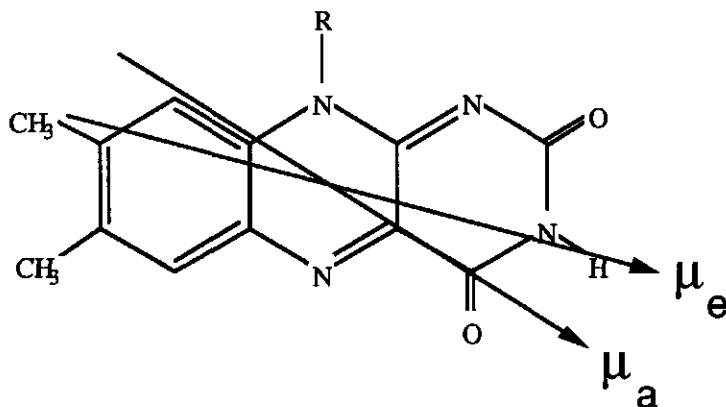


Fig.1: Molecular structure of flavin with directions of absorption (μ_a) and emission (μ_e) transition moments.

From the fundamental anisotropy it was deduced that the emission transition moment makes an angle of 16° relative to the first absorption transition moment. Two possibilities then remain for the orientation of the emission transition moment in the molecular frame, assuming that it lies in plane with the isoalloxazinic plane. By monitoring energy transfer between the flavins it is possible to resolve the abovementioned ambiguity in

the direction of the emission transition moment. We determined that it lies almost parallel to the pseudo-symmetry axis of the molecule (Chapter 4 of this thesis).

The flavins fluoresce in the green spectral region where the position of the emission maximum is dependent on the dielectric and refractive properties of the solvent. The fluorescence quantum yield of riboflavin or FMN ($Q = 0.26$) in aqueous solution is much higher than that of free FAD ($Q = 0.03$) [10]. The quenching of the isoalloxazine fluorescence in FAD originates from intramolecular complex formation with the adenine moiety where both static and dynamic mechanisms account for the decrease in the quantum yield relative to FMN. Detailed thermodynamic and kinetic information on this complex have been obtained from steady-state and time-resolved fluorescence studies [11]. The fluorescence of flavin bound to apo-flavoproteins is in most cases rather weak which in some instances can be ascribed to a transient charge transfer mechanism with electron-rich aromatic residues (tyrosine, tryptophan) [12]. Although exceptions such as lipoamide dehydrogenase and electron transferring flavoprotein with high quantum yield exist, the weak fluorescence of flavoproteins demands sensitive detection systems to obtain accurate information on dynamics and structure of flavoproteins [13]. The advantage of the green fluorescence of flavins is that the signal is much less contaminated by fluorescence of (protein) impurities. However, extreme care should be taken to ascertain that the sample does not contain free flavin which can arise from the dissociation of the prosthetic group from the apo-protein.

Modern fluorescence techniques provide a vast arsenal to obtain information on structure and dynamic aspects of proteins in solution. The information that the (biological) fluorescence spectroscopist can retrieve from experiments include: hydrodynamic properties of macromolecules (*e.g.* shape and size), thermodynamic parameters of protein-protein and ligand-protein equilibria, kinetics and thermodynamics of conformational substates, flexibility in proteins, dipolar relaxation and estimation of polarity inside proteins, distances between chromophoric groups (geometric information) and kinetic parameters of excited state reactions.

1.2 Lipoamide dehydrogenase and glutathione reductase as biophysical systems

The structurally similar dimeric flavoproteins glutathione reductase (GR) and lipoamide dehydrogenase (LipDH) contain one FAD per subunit of 50 kDa molecular mass. Both enzymes have been characterized in considerable detail [14-20]. The chemical

mechanism of the enzymatic catalysis has been elucidated to a large extent. The enzymes have a redox-active disulfide group in common. LipDH functions within a multienzyme complex (e.g. the pyruvate dehydrogenase complex) [21]. In solution the enzyme catalyses the reversible oxidation of dihydrolipoamide coupled to the reduction of NAD⁺:



GR operates as a dimer in erythrocytes where it maintains a high value for the ratio of reduced to oxidized glutathione concentrations which is, among others, essential for proper function of erythrocytes by stabilizing thiols in the cell membrane. The enzyme utilizes NADPH instead of NADH and, in contrast to LipDH, irreversibly oxidizes the cofactor [18]:



The crystal structures of GR from human erythrocytes and LipDH from *Azotobacter vinelandii* have been solved to 1.54 Å and 2.2 Å, respectively [22-24]. Notwithstanding the 28% homology the three-dimensional structures are very similar. The genes of lipoamide dehydrogenase from *Azotobacter vinelandii* (LipDH-AV) and of glutathione reductase from *E.coli* have been cloned and brought to expression [25, 26]. In this way the enzymes can be overproduced. More important, the active site can be modified by site-directed mutagenesis [27]. This provides not only a way to study the role of amino acid residues in catalysis, but also to modulate physical factors (electrostatics and statistical mechanics) which have an influence on conformational dynamics.

In studying the fluorescence properties of GR and LipDH two viewpoints can be distinguished. From a biological point of view it is striking that two proteins with very similar tertiary structure catalyze different reactions and operate in different supramolecular organizations. It is then of interest to use spectroscopic methods to investigate the role of structural dynamics in relation to catalysis. The population of conformational substates and their dynamic interplay could have an important role in binding of the substrate and kinetics of the reaction catalyzed by the enzymes (chapter 2 of this thesis).

From a physical viewpoint, however, the unique spatial arrangement of the flavins in conjunction with the specific local environment, permits the development and testing of (photo)physical models. With site-directed mutagenesis we are then able to alter the local chromophore environment and to trace

its effect on the developed model. Frauenfelder has considered a protein as a physics laboratory [28], which is very appropriate in this context. One of the physical phenomena that can be investigated in these oxidoreductases, is radiationless energy transfer between alike chromophores (flavins), in relation with excitation energy and dipolar relaxation [29-31].

LipDH is one of the most fluorescent flavoproteins known with a flavin fluorescence quantum yield of about 0.1. In contrast, GR has very weak fluorescence ($Q \approx 0.01$) [32]. A tyrosine (Tyr197) in close proximity of the isoalloxazine of FAD, is responsible for a charge transfer exciplex reducing the fluorescence lifetime to the picosecond regime [33]. This tyrosine is absent in LipDH explaining its relatively strong fluorescence. The average fluorescence lifetimes of the two proteins follow the same tendency as their quantum yields. The polarized fluorescence decays are also widely different in both proteins. The decays as analysed by a discrete set of exponentials exhibited a complex kinetic pattern [32]. With sophisticated apparatus and modern methods of data analysis we are now able to explain the experimental results in an unambiguous way.

In the following section we will focus attention on three methodologies in fluorescence spectroscopy. From each method specific information on the protein system can be obtained.

1.3 Fluorescence methodology

1.3.1 Molecular relaxation spectroscopy

The interaction of a chromophore with the (dipolar) environment is characterized by the action of two forces:

- i) the polarizing force leading to the generation of the reactive field (R)
- ii) the restoring force tending to restore the configuration of the environment without the fluorescent molecule.

The definition of the restoring force is hypothetical in proteins since the tertiary structure is maintained by the interaction of the prosthetic group with the apo-flavoprotein. Despite this fact, the restoring force is valid as a theoretical concept where it only acts on local amino acid residues surrounding the chromophore. The expression relating the free energy of the solvate (chromophore surrounded by solvent or protein dipoles) to the reactive field has a parabolic form for both ground- and excited states [34]. This is schematically depicted in Fig.2. Excitation in the main-band of the

absorption spectrum with photons of frequency ν_m results in the population of nonequilibrium excited states. Excitation at the red-edge of the absorption band (frequency ν_r) photoselects chromophores with the smallest electronic transition frequencies [30, 35]. Both excited-state solvates, either obtained after red-edge or main-band excitation, will have a tendency to relax to the minimal energy configuration with a characteristic dipolar relaxation time τ_r (Fig.2). When the relaxation towards equilibrium is much faster than the *average* fluorescence lifetime $\bar{\tau}_f$, emission will predominantly take place from the lowest equilibrium excited state. The steady-state fluorescence spectrum will then be independent of excitation frequency. This situation is typically encountered in rapidly fluctuating fluorophore environments such as exposed tryptophan residues in proteins. In the reverse situation, where the dipolar relaxation time is much longer than the excited state lifetime, emission takes place from the energy levels of the nonequilibrium solvate. In that case the red-edge excited emission spectrum will be shifted longwave relative to the main-band excited spectrum [36, 37]. In the intermediate situation ($\bar{\tau}_f \approx \tau_r$), the relation between the *mean* wavenumber of the steady-state emission spectrum ($\bar{\nu}$), dipolar relaxation time and average fluorescence lifetime is [38]:

$$\frac{\bar{\nu} - \bar{\nu}_\infty}{\bar{\nu}_0 - \bar{\nu}_\infty} = \frac{\Delta\nu}{\Delta\nu_0} = \frac{\tau_r}{\tau_r + \bar{\tau}_f} \quad (1)$$

where $\bar{\nu}_0$ and $\bar{\nu}_\infty$ are the mean frequencies of the unrelaxed ($\tau_r \gg \bar{\tau}_f$) and completely relaxed ($\tau_r \ll \bar{\tau}_f$) spectrum, respectively.

The relaxed spectrum, typically observed at elevated temperatures, is difficult to monitor in proteins due to temperature denaturation and loss of tertiary structure. A useful expression was obtained which does not contain $\bar{\nu}_\infty$ by assuming:

- i) that a unique equilibrium excited state exists independent of excitation wavelength
- ii) that the mean fluorescence lifetime and dipolar relaxation time are invariant to excitation energy [30, 35, 39, 40]:

$$\frac{\bar{\nu} - \bar{\nu}^{\text{edge}}}{\bar{\nu}_0 - \bar{\nu}_0^{\text{edge}}} = \frac{\Delta\nu^{\text{edge}}}{\Delta\nu_0^{\text{edge}}} = \frac{\tau_r}{\tau_r + \bar{\tau}_f} \quad (2)$$

where $\bar{\nu}^{\text{edge}}$ is the mean wavenumber of the spectrum obtained upon red-edge excitation. From this expression the dipolar relaxation time in biological molecules can be estimated when the difference in mean frequencies of the unrelaxed spectra ($\bar{\nu}_0 - \bar{\nu}_0^{\text{edge}}$) is known. Unrelaxed spectra of chromophores in proteins are obtained at low temperatures in cryogenic solvents. With this spectroscopic technique in combination with fluorescence lifetime measurements one can probe the dynamics of the fluorophore environment in a protein [41, 42].

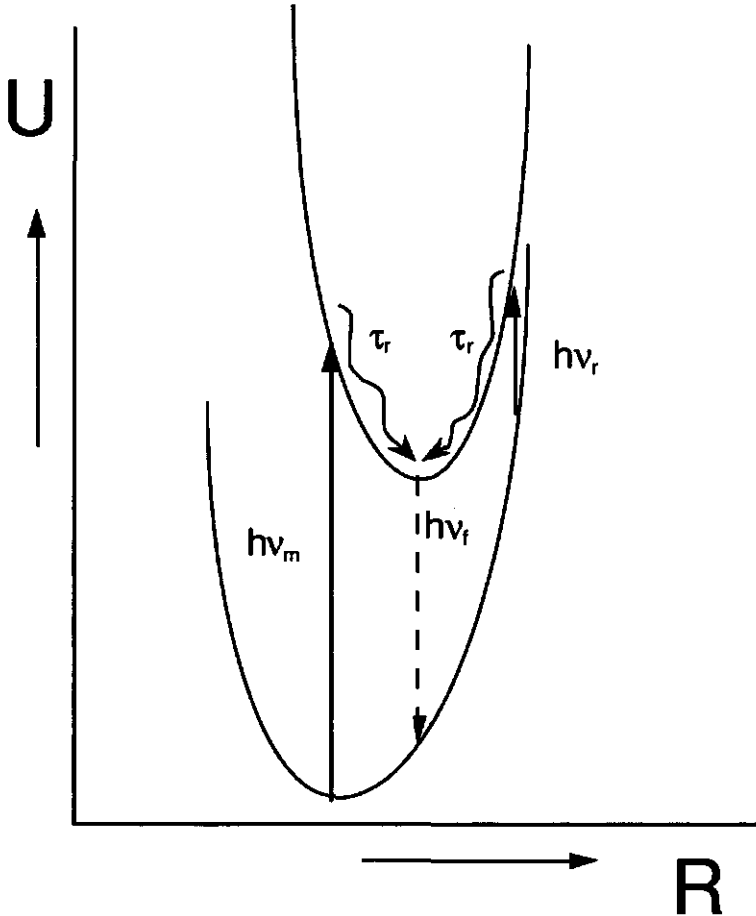


Fig.2: Field diagram describing free energy (U) of solvate in ground and excited state as function of reactive field (R). ν_m and ν_r are frequencies of photons corresponding to main-band and red-edge excitation, respectively. ν_f is the frequency of emitted photons and τ_r is the dipolar relaxation time. Solid arrows indicate absorption of photons, the broken arrow the emission of photons and the oscillating arrow dipolar relaxation towards the equilibrium excited state.

1.3.2 Fluorescence lifetime distributions

The excited-state lifetime of a fluorophore in a protein is extremely sensitive to the physical properties of its environment. A multitude of processes such as collisional quenching, thermal deactivation or energy transfer, causes radiationless decay resulting in a shortening of the lifetime. It has been proposed that proteins exist in multiple conformational substates (CS) [43, 44]. The population of the free energy levels of conformational substates obeys Boltzmann's distribution law. The rate of interconversion between the states is determined by the activation barrier between them. Each conformation has a different local fluorophore environment resulting in an altered fluorescence lifetime. When the rate of interconversion between conformational substates is much larger than the fluorescence rate of each state, an average fluorescence lifetime will be observed. In the slow exchange limit, each substate will give rise to its own characteristic fluorescence lifetime resulting in a spectrum of decay times. Frauenfelder and coworkers [43, 44] classified the conformational substates in a hierarchical system depending on the activation barrier between the states (abbreviated CS¹, CS² and CS³, see Fig.3). Exchange between CS¹ corresponds to conformational transitions involving the whole protein molecule and its hydration layer (activation energies in the order of 100 kJ/mol). CS² is a subgroup of CS¹, and exchange between them corresponds to protein domain movements (maximum barrier about 50 kJ/mol). CS³ transitions pertain to amino acid residue fluctuations (barrier less than 10 kJ/mol). In a protein at room temperature the exchange between states of CS³ is rapid on a fluorescence time scale. Heterogeneity in the fluorescence decay then originates from degeneracy of CS¹ or CS². In order to observe CS³, fluorescence must be studied in proteins dissolved in cryogenic solvents at low temperatures. In the light of this concept the fluorescence decay pattern of fluorophores in proteins has to be studied over a wide range of temperatures. Lifetime distributions instead of a limited set of discrete exponentials form now the preferential model to analyze the fluorescence decay. Two approaches can be followed. One can define *a priori* an analytical form of the distribution (*e.g.* uniform, Gaussian, Lorentzian, unimodal, bimodal). Rejection or acceptance of the model is then based on statistical fit criteria [45-47]. In the *non a priori* approach, the fluorescence decay is fitted to an exponential series (inverse Laplace transform) with evenly spaced lifetime components (τ) on a $\log(\tau)$ -axis. The optimal spectrum of decay times is recovered by maximizing the Shannon-Jaynes entropy and minimizing the χ^2 statistics. By using the Shannon-Jaynes

information entropy as a regularizing function in the maximum entropy method (MEM) a solution is chosen with no more correlation than inherent in the experimental data [48]. MEM is the preferable approach in analyzing time-resolved fluorescence in proteins considering the complexity of a multitude of conformational substates.

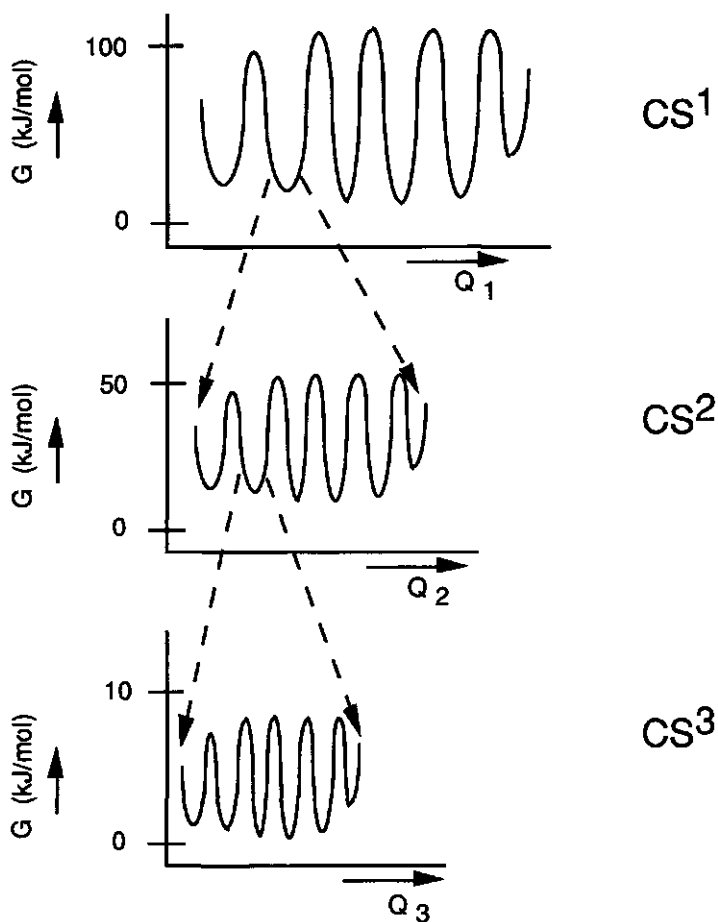


Fig.3: Hierarchy of conformational substates. G is the Gibbs free energy of a protein molecule in conformation Q . The broken arrows indicate the amplification of a substate in a certain tier.

1.3.3 Fluorescence anisotropy

1.3.3.1 General description

Time-resolved polarized fluorescence spectroscopy is a technique to monitor angular displacements of emission transition moments of fluorescent molecules. It has been applied to protein systems to investigate, among others, rapid angular fluctuations and protein hydrodynamics.

The experimental observable parameter is the fluorescence anisotropy defined as [49]:

$$r(t) = \frac{I_{\parallel}(t) - I_{\perp}(t)}{I_{\parallel}(t) + 2I_{\perp}(t)} \quad (3)$$

where $I_{\parallel}(t)$ and $I_{\perp}(t)$ are the observed time-dependent parallel and perpendicular polarized components relative to the polarization direction of the exciting beam. The vertically polarized excitation initially photoselects an anisotropic distribution of fluorophores from the macroscopic isotropic ensemble. This distribution has the form of a second order Legendre polynomial ($P_2(x)$). The information contained in the fundamental anisotropy is lost by several time-dependent mechanisms (*vide infra*). The general expression relating the time-dependent correlation function of the molecular transition moments with the experimental anisotropy is [50, 51]:

$$r(t) = \langle P_2 [\vec{\mu}_a(0) \cdot \vec{\mu}_e(t)] \rangle \quad (4)$$

$\vec{\mu}_a(0)$ and $\vec{\mu}_e(t)$ are unit vectors along the transition moment of absorption at time $t=0$ and emission at time t after excitation, respectively. In a dimeric flavoprotein there are three possible contributions to the depolarization of the fluorescence: rotational diffusion of the whole protein, restricted reorientational motion of flavin and interflavin energy transfer.

1.3.3.2 Rotation of the protein

When there is a rigid solution of the protein with non-interacting flavin moieties, the correlation function of the emission transition moments becomes time-independent. One then recovers the fundamental anisotropy containing information about the angle (δ) between absorption and emission transition moments:

$$r(t) = r(0) = \frac{2}{5}P_2(\cos\delta) \quad (5)$$

The correlation function is time-dependent for a protein rotating in solution. The anisotropy is given by a sum of five exponentials for a completely asymmetric body, which reduces to a triple exponential for a cylindrically symmetric protein [52]. In most experimental cases it is not possible to determine the three individual components by analysis of the fluorescence anisotropy. Instead, a single correlation time is often measured which is the harmonic mean of the three expected values [53].

1.3.3.3 Restricted reorientational motion

When the fluorescent molecule exhibits independent flexibility inside the protein, eq.4 can be factorized in three terms [51]:

$$r(t) = \frac{2}{5}P_2(\cos\delta).C_p(t).C_M(t) \quad (6)$$

where $C_p(t)$ and $C_M(t)$ are the correlation functions of protein tumbling and restricted motion, respectively. $C_M(t)$ is an infinite sum of exponentially decaying functions and cannot be described in close form [50]. Several approximations are described in the literature imposing exact solutions for the derivative at $t=0$ or the area under the decay [54-58]. All these expressions have the following functional form in common:

$$C_r(t) = \sum_{i=1}^N \beta_i \exp(-t/\phi_i) + r_{\infty} \quad (7)$$

where the ϕ_i 's are the correlation times associated with restricted reorientational dynamics. The value of N is determined by the selected model (typically, N is 1 or 3). It is reasonable to expect that the correlation times will be shorter at higher temperature as relaxation towards equilibrium (r_{∞}) is more rapidly attained.

1.3.3.4 Homo-energy transfer

The other time-dependent cause for fluorescence depolarization is intersubunit energy transfer between the flavins. This special case of energy transfer between identical chromophores, termed homo-transfer, cannot be observed in the total fluorescence decay. Instead, it is observable in the anisotropy decay when the direction of the transition moments

changes during energy transfer [31, 59]. We consider two chromophores with a defined fixed orientation, weakly interacting by dipole-dipole coupling through the Förster mechanism. This system is analogous to a two-state jump model for which the forward and reverse rates of interconversion are identical. It can be shown that the anisotropy decay has the following form [51, 60, 61]:

$$r(t) = \beta_1 \exp(-2k_T t) + \beta_2 \quad (8)$$

where the β_i 's are functions of the intra- and intermolecular angles between absorption and emission transition moments [61]. The rate of energy transfer k_T (in ns^{-1}) is related to geometrical and spectral parameters by the Förster equation [63]:

$$k_T = 8.71 \times 10^{17} R^{-6} \kappa^2 n^{-4} k_r J \quad (9)$$

where R is the intermolecular distance (in nm) between donor and acceptor, κ is the orientation factor [64] describing the relative orientation of donor and acceptor transition dipoles, n the refractive index of the intervening medium, k_r is the radiative rate of the donor (in ns^{-1}) and J is the overlap integral (in M^{-1}cm^3) given by:

$$J = \frac{\int_0^{\infty} \frac{F_d(\nu) \epsilon_a(\nu)}{\nu^4} d\nu}{\int_0^{\infty} F_d(\nu) d\nu} \quad (10)$$

$F_d(\nu)$ is the fluorescence intensity of the donor at frequency ν and ϵ_a is the extinction coefficient of the acceptor at ν .

The two-state model of energy transfer is valid for a system with uniform transition energies of donor and acceptor molecules. In an inhomogeneously broadened system the transition energies are distributed (Fig.2). This will have consequences for the temperature- and excitation wavelength dependence of the observed rate of transfer. In an inhomogeneously broadened system with $\tau_r \gg \tau_f$, the experimental overlap integral is a static average of the individual overlap integrals of the different dimers in a certain energy configuration. The rate of intersubunit energy transfer is then a distributed function. Upon main-band excitation dimers containing fluorophores with the most probable transition

energy, are preferentially photoselected. This is equivalent to dimers having the same transition energies for donor and acceptor molecules. The majority of excited molecules will then behave as a homogeneous system. Eq.8 is then a reasonable approximation for the time-dependent anisotropy.

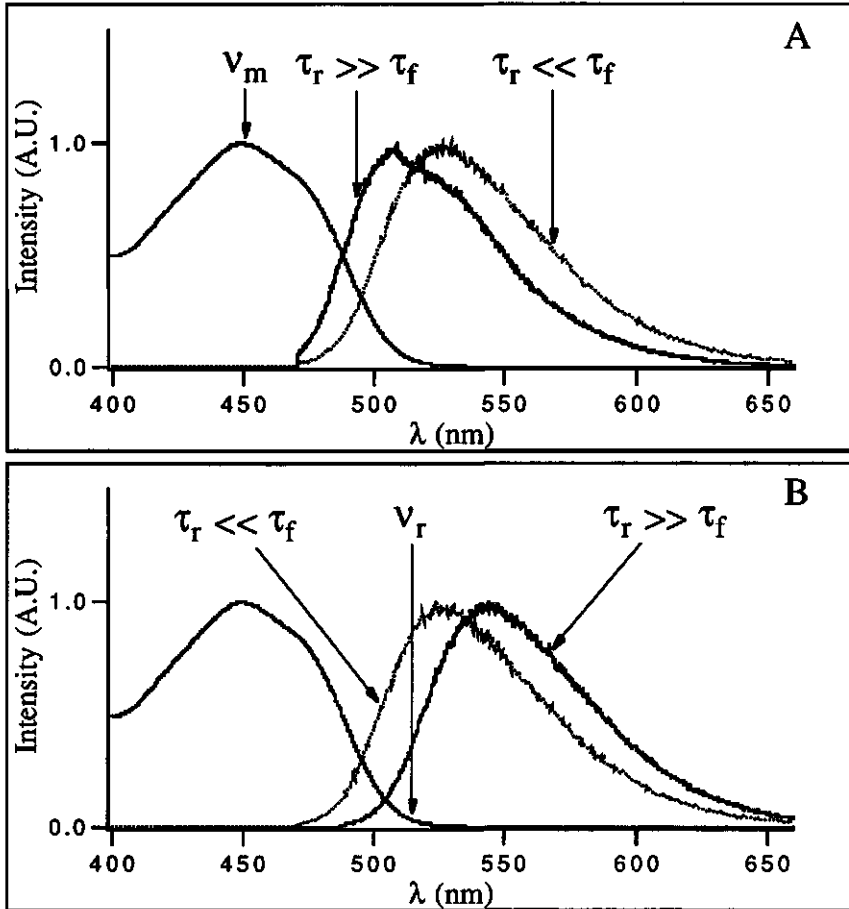


Fig.4: Effect of dipolar relaxation on overlap integral. Panel A: main-band excitation (ν_m), spectral overlap in the limit of slow ($\tau_r \gg \tau_f$) and rapid ($\tau_r \ll \tau_f$) relaxation. Panel B: red-edge excitation (ν_r), spectral overlap in the limit of slow and rapid relaxation. Absorption and emission spectra are normalized to unity.

Upon red-edge excitation a population of fluorophores is photoselected which have transition energies much smaller than the average one. The occurrence of fluorophores with this small transition energy is infrequent. A fraction of these excited

molecules is then not able to transfer energy to an acceptor since the most probable transition energy is larger. Nonetheless, there is a finite chance that a molecule is in a proper energy configuration to act as acceptor. Both fractional populations (transferring and nontransferring) can be determined by fitting edge- and main-band excited anisotropy decays to eq.8. The ratio of the pre-exponential amplitudes (β_1) in both cases yields the fractional population of transferring molecules (Chapter 4 of this thesis). Energy transfer in the edge-excited dimers is less efficient than transfer in the main-band excited ones because of the smaller overlap integral (Fig.4). This will result in a longer correlation time of transfer ($\phi_T = 1/(2k_T)$). Both the red shift of the emission spectrum and the decrease of the transferring fraction upon edge excitation, give rise to the Weber red-edge failure of energy transfer [65]. In a dynamic inhomogeneously broadened system ($\tau_r \ll \tau_f$) all energy configurations are sampled during energy transfer and the observed overlap integral (and thus k_T) is a dynamic average. [66]. The system behaves as if a single energy configuration is present in all dimers. The rate of transfer k_T has then a discrete value independent of excitation energy and the model described by eq.8 is exact. The transfer rate in this dynamic regime is smaller than in the static regime because in the latter case the overlap integral is larger (Fig.4). Upon increase of temperature the transfer correlation time (ϕ_T) will become longer. This temperature behavior is opposite to that of reorientational dynamics providing a diagnostic tool to distinguish between both sources of depolarization.

1.4 Aim of this thesis

The goal of this thesis is to further develop fluorescence spectroscopic methods in order to obtain quantitative information on structural and dynamic properties of dimeric flavoproteins in solution. In chapter 2 the conformational dynamics of glutathione reductase and of lipoamide dehydrogenase in aqueous solution are compared. The controversy about the mechanism of fluorescence depolarization (reorientational dynamics versus energy transfer) of the flavins is investigated [32, 33]. A coupling between the time-resolved fluorescence results of the enzymes and the catalytic aspects is proposed.

The dipolar relaxational properties of the flavin environment are compared in lipoamide dehydrogenase and a mutant lacking 14 C-terminal amino acids by excitation-frequency dependent steady-state fluorescence spectroscopy (chapter 3). Structural information is obtained on the C-terminal polypeptide of lipoamide dehydrogenase. Chapter 3 forms the basis of chapter

4 which deals with the role of dipolar relaxation and excitation energy on homo-energy transfer between the flavins in lipomide dehydrogenase. In addition, thermodynamic parameters of conformational dynamics are extracted from time-resolved fluorescence decays.

In chapter 5 we apply red- and blue-edge spectroscopy to obtain structural information on an "unknown" flavoprotein containing two FAD prosthetic groups in one subunit.

1.5 References

1. Müller, F. (1983) *Top. Curr. Chem.*, 108, 71-107.
2. Beechem, J.M. and Brand, L. (1985) *Ann. Rev. Biochem.*, 54, 43-71.
3. Burstein, E.A., Vedenkina, N.S. and Ivkova, M.N. (1973) *Photochem. Photobiol.*, 18, 263-279.
4. Creed, D. (1984) *Photochem. Photobiol.*, 39, 537-562.
5. Valeur, B. and Weber, G. (1977) *Photochem. Photobiol.*, 25, 441-444.
6. Cross, A.J., Waldeck, D.H. and Fleming, G.R. (1983) *J. Chem. Phys.*, 78, 6455-6467.
7. Ruggiero, A.J., Todd, D.C. and Fleming, G.R. (1990) *J. Am. Chem. Soc.*, 112, 1003-1014.
8. Penzer, G.R. and Radda, G.K. (1967) *Quart. Rev. Chem. Soc. (London)*, 21, 43-65.
9. Johansson, L.B.-Å., Davidsson, Å., Lindblom, G. and Razi Naqvi, K. (1979) *Biochemistry*, 18, 4249-4253.
10. Weber, G. (1950) *Biochem. J.*, 47, 114-121.
11. Visser, A.J.W.G. (1984) *Photochem. Photobiol.*, 40, 703-706.
12. Visser, A.J.W.G., van Hoek, A., Kulinski, T. and LeGall, J. (1987) *FEBS Lett.*, 224, 406-410.
13. van Hoek, A., Vos, K. and Visser, A.J.W.G. (1987) *IEEE J. Quantum Electron.*, QE-23, 1812-1820.
14. Worthington, D.J. and Rosemeyer, M.A. (1975) *Eur. J. Biochem.*, 60, 459-466.
15. Worthington, D.J. and Rosemeyer, M.A. (1976) *Eur. J. Biochem.*, 60, 231-238.
16. Nakashima, K., Miwa, S. and Yamauchi, K. (1976) *Biochim. Biophys. Acta.*, 445, 309-323.
17. Schulz, G.E., Zappa, H., Worthington, D.J. and Rosemeyer, M.A. (1975) *FEBS Lett.*, 54, 86-88.
18. Williams Jr, C.H. (1976) *The Enzymes*, 13, 89-173.
19. de Kok, A. and Visser, A.J.W.G. (1984) in: *Flavins and Flavoproteins* (Bray, R.C., Engel, P.C. and Mayhew S.G. eds.) pp. 149-152. Walter de Gruyter, Berlin.

20. de Kok, A., Bosma, H.J., Westphal, A.H. and Veeger, C. (1988) *Thiamine Pyrophosphate Biochemistry*, 2, 19-36.
21. Reed, L.J. (1974) *Acc. Chem. Res.*, 7, 40-46.
22. Karplus, P.A. and Schulz, G.E. (1987) *J. Mol. Biol.*, 195, 701-729.
23. Schierbeek, A.J., Swarte, M.B.A., Dijkstra, B.W., Vriend, G., Read, R.J., Hol, W.G.J., Drenth, J. and Betzel, C. (1989) *J. Mol. Biol.*, 206, 365-379.
24. Mattevi, A., Schierbeek, A.J. and Hol, W.G.J. (1991) *J. Mol. Biol.*, 220, 975-994.
25. Westphal, A.H. and de Kok, A. (1988) *Eur. J. Biochem.*, 172, 299-305.
26. Berry, A., Scrutton, N.S. and Perham, R.N. (1989) *Biochemistry*, 28, 1264-1269.
27. Schulze, E., Benen, J.A.E., Westphal, A.H. and de Kok, A. (1991) *Eur. J. Biochem.*, 200, 29-34.
28. Frauenfelder, H. (1985) in: *Structure and Motion: Membranes, Nucleic Acids and Proteins* (Clementi, E. and Chin, S. eds.), pp. 169-177. Plenum Press, New York.
29. Nemkovich, N.A., Rubinov, A.N. and Tomin, V.I. (1991) *Inhomogeneous Broadening of Electronic Spectra of Dye Molecules in: Topics in Fluorescence Spectroscopy* (Lakowicz, J.R. ed.) Vol 2, pp 367-428, Plenum Press, New York.
30. Demchenko, A.P. (1986) *Essays Biochem.* pp. 120-157. Academic Press, London .
31. Bastiaens, P.I.H., Bonants, P.J.M., Müller, F. and Visser, A.J.W.G. (1989) *Biochemistry*, 28, 8416-8425.
32. de Kok, A. and Visser, A.J.W.G. (1987) *FEBS Lett.*, 218, 135-138.
33. Kalman, B., Sandström, A., Johansson, L.B.-Å. and Lindskog, S. (1991) *Biochemistry*, 30, 111-117.
34. Tomin, V.I. and Rubinov, A.N. (1981) *J. Appl. Spectrosc. (USSR)*, 35, 237-251.
35. Demchenko, A.P. (1987) *Ultraviolet Spectroscopy of Proteins*, pp. 145-172. Springer-Verlag, Berlin.
36. Galley, W.C. and Purkey, R.M. (1970) *Proc. Natl. Acad. Sci USA*, 67, 1116-1121.
37. Rubinov, A.N. and Tomin, V.I. (1970) *Optics Spectrosc. (USSR)*, 29, 1082-1086.
38. Mazurenko, Y.T. and Bakhshiev, N.G. (1970) *Optics Spectrosc. (USSR)*, 28, 905-913.
39. Demchenko, A.P. (1982) *Biophys. Chem.*, 15, 101-109.
40. Demchenko, A.P. (1985) *FEBS Lett.*, 182, 99-102.
41. Demchenko, A.P. (1988) *Eur. Biophys. J.*, 16, 121-129.
42. Demchenko, A.P. and Ladokhin, A.S. (1988) *Biochim. Biophys. Acta*, 955, 352-360.

43. Frauenfelder, H. and Gratton, E. (1986) *Methods Enzymol.*, 127, 207-216.
44. Frauenfelder, H., Parak, F. and Young, R.D. (1988) *Ann. Rev. Biophys. Biophys. Chem.*, 17, 451-479.
45. Alcalá, R.J., Gratton, E. and Prendergast, F.G. (1987) *Biophys. J.*, 51, 587-596.
46. Alcalá, R.J., Gratton, E. and Prendergast, F.G. (1987) *Biophys. J.*, 51, 597-604.
47. Alcalá, R.J., Gratton, E. and Prendergast, F.G. (1987) *Biophys. J.*, 51, 925-936.
48. Livesey, A.K. and Brochon, J.C. (1987) *Biophys. J.*, 52, 693-706.
49. Jablonski, A. (1960) *Bull. Acad. Pol. Sci., Ser. Sci. Math. Astron. Phys.*, 8, 259-264.
50. Zannoni, C. (1981) *Mol. Phys.*, 42, 1303-1320.
51. Szabo, A. (1984) *J. Chem. Phys.*, 81, 150-167.
52. Small, E.W. and Isenberg, I. (1977) *Biopolymers*, 16, 1907-1928.
53. Dale, R.E., Chen, L.A. and Brand, L. (1977) *J. Biol. Chem.*, 252, 7500-7510.
54. Kinosita, K., Kawato, S. and Ikegami, A. (1977) *Biophys. J.*, 20, 289-305.
55. Nordio, P.L. and Segre, U. (1979) in: *Molecular Physics of Liquid Crystals* (Luckhurst, G.R. and Gray, G.W. eds.), pp. 411-426. Academic Press, London.
56. Lipari, G. and Szabo, A. (1980) *Biophys. J.*, 30, 489-506.
57. Zannoni, C., Arconi, A. and Cavatorta, P. (1983) *Chem Phys. Lipids*, 32, 179-250.
58. van der Meer, W., Pottel, H., Herreman, W., Ameloot, M., Hendrickx, H. and Schröder, H. (1984) *Biophys. J.*, 46, 515-523.
59. Bastiaens, P.I.H., Bonants, P.J.M., van Hoek, A., Müller, F. and Visser, A.J.W.G. (1988) *Proc. SPIE*, 909, 257-262.
60. Tanaka, F. and Mataga, N. (1979) *Photochem. Photobiol.*, 29, 1091-1097.
61. Weber, G. (1989) *J. Phys. Chem.*, 93, 6069-6073.
62. Bastiaens, P.I.H., Mayhew, S.G., O'Nualláin, E.M., van Hoek, A. and Visser, A.J.W.G. (1991) *J. of Fluorescence*, 1, 95-103.
63. Förster, T. (1948) *Ann. Physik.*, 2, 55-75.
64. Steinberg, I.Z. (1971) *Ann. Rev. Biochem.*, 40, 83-114.
65. Weber, G. and Shinitzky, M. (1970) *Proc. Natl. Acad. Sci. USA*, 65, 823-830.
66. Dale, R.E., Eisinger, J. and Blumberg, W.E. (1979) *Biophys. J.*, 26, 161-194.

Chapter 2

Comparison of the Dynamical Structures of Lipoamide Dehydrogenase and Glutathione Reductase by Time-Resolved Polarized Flavin Fluorescence

Bastiaens, P.I.H., van Hoek, A., Wolkers, W.F., Brochon, J.C. and Visser, A.J.W.G.

Abstract

Time-resolved polarized fluorescence spectroscopy has been applied to the bound FAD in the structurally related flavoproteins lipoamide dehydrogenase from *Azotobacter vinelandii* (LipDH-AV) and glutathione reductase (GR) from human erythrocytes. The fluorescence parameters as obtained from the maximum entropy analysis differ considerably in both enzymes, reflecting the unique properties of the flavin microenvironment. Three conformational substates are revealed in LipDH-AV and five in GR. Almost 90% of the population of GR molecules has a fluorescence lifetime in the order of 30 ps which originates from efficient exciplex formation with Tyr197. Equilibrium fluctuations between conformational substates are observed for LipDH-AV on a nanosecond time-scale in the temperature range 277-313 K. Interconversion between conformational substates in GR is slow indicating that large activation barriers exist between the states. In agreement with these results a model is postulated which ascribes a role in catalysis to equilibrium fluctuations between conformational substates in GR and LipDH-AV. From time-resolved fluorescence anisotropy as function of temperature distinction can be made between flavin reorientational motion and interflavin energy transfer. In both proteins intersubunit energy transfer between the prosthetic groups is observed. Furthermore, it is revealed that only the flavin in glutathione reductase exhibits rapid restricted reorientational motion. Geometric information concerning the relative orientation and distance of the flavins can be extracted from the parameters describing the energy transfer process. The obtained spatial arrangement of the flavins is in excellent agreement with crystallographic data.

2.1 Introduction

Lipoamide dehydrogenase (LipDH) and glutathione reductase (GR) are both members of the family of disulfide oxidoreductases. These flavoproteins have FAD as a prosthetic group and a redox active disulfide in common [1]. The proteins

with a molecular mass of 100 kDa have a dimeric quaternary structure [2, 3]. The catalytic site comprises amino acid residues from both subunits which explains that the physiological enzymatic activity is abolished upon monomerization of the enzymes [4-8]. LipDH is part of the multienzyme pyruvate dehydrogenase and 2-oxoglutarate dehydrogenase complexes catalyzing the oxidation of covalently bound dihydrolipoamide coupled to the reduction of NAD⁺ [9]:



GR operates as a dimer in erythrocytes where it maintains a high value for the ratio of reduced to oxidized glutathione concentrations which is, among others, essential for proper function of erythrocytes by stabilizing thiols in the cell membrane. The enzyme utilizes NADPH instead of NADH and, in contrast to LipDH, irreversibly oxidizes the cofactor under physiological conditions [1]:



The genes of lipoamide dehydrogenase from *Azotobacter vinelandii* (LipDH-AV) and glutathione reductase from *E.coli* have been cloned and brought to expression [10-12]. Relatively large quantities of the enzymes can be made available and the active site can be modified by site-directed mutagenesis. The crystal structure of GR from human erythrocytes has been refined to 1.54 Å and, recently, the structure of LipDH-AV to 2.2 Å, enabling detailed comparison of both structures [5, 7]. Small differences in tertiary and quaternary structure were revealed. The relative orientations of the NAD(P)⁺-and FAD-binding domains differ by a tilt angle of 7-8°. Furthermore, the relative position of the subunits differs by a translational shift of 4.4 Å which results in a much narrower binding cleft for lipoamide as compared to the glutathione binding site. It was postulated that this narrow binding cleft facilitates binding of the long aliphatic arm of the covalently bound substrate which is able to move between the catalytic centers of the different enzymes of the multienzyme complex [7].

LipDH-AV contains a C-terminal extension of 15 amino acids which is not present in GR. The last 10 amino acids residues are not visible in the electron density map indicating that this polypeptide is highly flexible or disordered [7]. Removal of the last 14 amino acids by site-directed mutagenesis results in inactivation of the enzyme. In addition, the deletion mutant

(LipDH- Δ 14) has a tendency to dissociate into monomers ($K_d = 2.5$ - $5.0 \mu\text{M}$ instead of 1 nM for wild type enzyme) which demonstrates that the C-terminal polypeptide is essential for interaction between the subunits [11]. From steady-state fluorescence spectroscopy it was shown that LipDH- Δ 14 has enhanced solvent accessibility of the isoalloxazines in comparison to LipDH-AV (chapter 3 of this thesis). From these studies it was concluded that the "disordered" C-terminal polypeptide interacts with the Lip(SH₂) binding site.

The fluorescence properties of FAD bound to GR and LipDH differ considerably [13]. The fluorescence quantum yield of FAD bound to GR is 7.7% of that of FAD bound to LipDH. Time-resolved fluorescence studies of the flavin in GR at 20° revealed a highly inhomogeneous fluorescence decay. At least 4 different lifetimes were needed to describe the fluorescence decay ranging from 50 ps to 5.5 ns. The fluorescence decay of LipDH could be fitted to a sum of three exponentials. Most remarkably was the difference in time-resolved fluorescence anisotropy in both proteins. Almost complete depolarization of the fluorescence was attained in GR with a correlation time of 3.6 ns. A predominantly long correlation time reflecting protein tumbling, was found for LipDH. In addition, a small amplitude process with a correlation time in the order of 10 ns could be resolved. These results were interpreted to arise from different dynamic behavior of the flavin in GR and LipDH. The shorter correlation time with a large amplitude support a highly mobile prosthetic group in GR whereas the flavin is apparently more rigidly bound in LipDH.

In this paper we report on a detailed time-resolved fluorescence and fluorescence anisotropy study of FAD in GR and LipDH-AV. Our purpose was to obtain insight into the structural and dynamic properties of these proteins as monitored by the polarized fluorescence decay at different temperatures. The basis of this approach was that inhomogeneity in the environment of the chromophore will lead to a range of excited-state processes and therefore will give rise to nonexponential fluorescence decay [14]. Due to this property it is in principle possible to monitor conformational substates in proteins and their dynamic exchange [15-17]. In mult flavin-containing proteins it can be expected that homo-energy transfer takes place. It is then of importance to be able to separate this contribution to the depolarization of the fluorescence from that arising from reorientational dynamics [18-21].

The classical description of the fluorescence decay by a discrete set of lifetimes has both mathematical and physical disadvantages [22]. The inverse Laplace transform of the fluorescence decay is recovered in the maximum entropy method

(MEM) by fitting the decay to a function composed of a large number (up to 200) of exponentials [22-24]. The advantage of this method is that one obtains a unique solution and that no *a priori* knowledge of the distribution model is needed. This type of analysis is well suited for complex decays encountered in biological molecules where multiple conformations of different tiers give rise to semi-continuous sets of lifetime distributions [16, 25].

2.2 Materials

LipDH-AV was expressed in *E. coli* TG2 and purified according to published procedures [10]. The enzyme preparations were frozen in liquid nitrogen and stored at -70 °C in 100 mM potassium phosphate buffer, 0.5 mM EDTA, pH 7.0. GR was isolated from erythrocytes obtained from 7.5 l of human blood according to the procedure of Krohne-Ehrich *et al.* [26]. The final preparation had a specific activity of 147 U/mg at 20°C and a 280/460 ratio of 6.0. The enzyme was pure as judged by SDS-PAGE. The preparation was stored in 50 mM potassium phosphate buffer, 200 mM KCl, 1 mM EDTA, 14 mM 2-mercaptoethanol, pH 7.0 at 4°C. In the morning of an experiment, the samples were brought to room temperature and chromatographed on a Biogel PGD-6 column (1 x 6 cm, Biorad) equilibrated with 50 mM potassium phosphate buffer, pH 7.0 in nanopure-grade water. In that way unbound FAD is removed from the samples. The enzyme preparations were brought to 80% (v/v) glycerol by gently mixing 100 μ l from the eluted sample with 400 μ l of 100% glycerol (Merck, fluorescence microscopy grade) until a homogeneous solution was obtained. All final preparations had a concentration of 10-15 μ M on the basis of FAD light absorption at 457 nm [10]. Upon freezing the samples down to 203 K a clear transparent glass was formed with no indications of any precipitate.

2.3 Methods

2.3.1 Time-resolved fluorescence

Fluorescence decay- and fluorescence anisotropy decay curves were measured by the time-correlated single photon counting (TCSPC) technique [27]. The TCSPC apparatus, consisting of an argon-ion laser and associated optics and detection electronics has been described elsewhere [28, 29]. The excitation wavelength was 457.9 nm, close to the absorption maximum of the first electronic transition of the bound flavin. Emission was passed through a combination of a KV 550 cut-off and 557.9

interference filter of 10 nm bandpass (Schott). The temperature in the sample housing was controlled by a liquid nitrogen flow set-up with a temperature controller (Oxford model ITC4) as described elsewhere [29]. The instrumental function, corresponding to the laser pulse convoluted with the detection response, was determined by measuring the fluorescence decay of a fast reference compound (erythrosine B in water). The lifetime of this compound is slightly dependent on temperature and amounts to approximately 80 ps. The exact value of the reference lifetime at a certain temperature was determined by iterative reconvolution with a compound having a longer fluorescence lifetime (erythrosine B in methanol, lifetime \approx 500 ps). Flavin fluorescence was sampled during 10 cycles of 10 seconds in each polarization direction where the detection frequency of the parallel polarized component was set to 30 kHz to prevent pulse pile-up. The pulse mimic was sampled 2 or 3 cycles of 10 seconds in each polarization direction until a approximate peak count of 20-30 kcounts was reached in the parallel component. One complete measurement consisted of measuring the polarized fluorescence decays of the reference compound, the sample, the background and again the reference compound. Background fluorescence was sampled at one fifth of the sample acquisition time and was always below 2% of the fluorescence intensity of the LipDH samples but amounted to 2-5% in the GR samples due to the lower quantum yield of this protein.

2.3.2 Data analysis

Analysis of total fluorescence decay $I(t)$ and anisotropy decay $r(t)$ was performed using the commercially available maximum entropy method (Maximum Entropy Data Consultants Ltd., Cambridge England). The principle of MEM has been described in the literature [22] and will be shortly outlined below in relation to our application. In all the experiments the parallel $I_{||}(t)$ and perpendicular $I_{\perp}(t)$ fluorescence intensity components were acquired after excitation with vertically polarized light. The image $\alpha(\tau)$ of the total fluorescence intensity $i(t)$, after δ -pulse excitation, is given by the inverse Laplace transform:

$$i(t) = i_{||}(t) + 2gi_{\perp}(t) = \int_0^{\infty} \alpha(\tau) e^{-t/\tau} d\tau \quad (1)$$

The g -factor was found to be equal to one in our TCSPC apparatus [28]. The image $\alpha(\tau)$ is recovered by maximizing the Shannon-Jaynes entropy function S_{SJ} [22]:

$$S_{SJ} = \int_0^{\infty} \alpha(\tau) - m(\tau) - \alpha(\tau) \log \frac{\alpha(\tau)}{m(\tau)} d\tau \quad (2)$$

and minimizing the χ^2 data fit criterium:

$$\chi^2 = \frac{1}{M} \sum_{k=1}^M \left(\frac{I_k^{\text{calc}} - I_k^{\text{obs}}}{\sigma_k} \right)^2 \quad (3)$$

where $m(\tau)$ is the starting model of the distribution chosen to be flat in $\log(\tau)$ space when there is no *a priori* knowledge about the system, as this introduces the least correlation between the parameters $\alpha(\tau)$. The superscripts "calc" and "obs" on I denote the observed and calculated intensity in channel k of the multichannel analyzer. M is the total amount of channels used in the analysis of the fluorescence decay (typically 1024 channels) and σ_k^2 is the variance in channel k . For an optimal fit of the data χ^2 should approach unity.

In practice 150 equally spaced values on a $\log(\tau)$ scale (between 0.01 and 10 ns) were used in the analysis of $i(t)$. In order to recover the proper lifetime image of GR in aqueous solution we had to introduce a negative shift of -0.5 channel in the analysis corresponding to a delay of about 10 ps in the excitation pulse (relative to the fluorescence profile). This shift can be rationalized by the fact that neutral density filters had to be introduced in the measurement of the pulse profile, which were absent in the measurement of the fluorescence decay of the sample. These additional filters give rise to a time delay owing to the increase of the refractive index relative to air. Because of the low fluorescence quantum yield of GR, neutral density filters were omitted in order to achieve a higher excitation intensity to reach a detection frequency of 30 kHz. In the LipDH samples the optical path of reference and sample were identical and no shift was introduced in the analysis.

One is able to recover from fluorescence anisotropy experiments the complete 3-dimensional image given by $\gamma(\tau, \phi, r_0)$ representing the number of fluorophores with lifetime τ , rotational correlation time ϕ and initial anisotropy r_0 . This image is related to the parallel $i_{||}(t)$ and perpendicular $i_{\perp}(t)$ polarized components of the fluorescence after deconvolution by [22]:

$$i_{||}(t) = \frac{1}{3} \int_0^{\infty} \int_0^{\infty} \int_{-0.2}^{0.4} \gamma(\tau, \phi, r_0) e^{-t/\tau} (1 + 2r_0 e^{-t/\phi}) d\tau d\phi dr_0 \quad (4)$$

$$i_{\perp}(t) = \frac{1}{3} \int_0^{\infty} \int_0^{\infty} \int_{-0.2}^{0.4} \gamma(\tau, \phi, r_0) e^{-t/\tau} (1 - r_0 e^{-t/\phi}) d\tau d\phi dr_0 \quad (5)$$

The Shannon-Jaynes entropy function S_{SJ} has the same form as in equation 2 except that $\alpha(\tau)$ is replaced by $\gamma(\tau, \phi, r_0)$ and integration is performed over the three dimensions τ , ϕ and r_0 . If one assumes *a priori* that there is no correlation between τ and ϕ (non-associative modeling) the images $\alpha(\tau)$ and $\beta(\phi)$ can be separated in equations 4 and 5 as shown for the parallel fluorescence intensity component:

$$i_{||}(t) = \frac{1}{3} \int_0^{\infty} \alpha(\tau) e^{-t/\tau} d\tau \int_0^{\infty} (1 + 2\beta(\phi)) e^{-t/\phi} d\phi \quad (6)$$

The integrated amplitude $\beta(\phi)$ corresponds to the fundamental anisotropy r_0 . From this type of one-dimensional anisotropy analysis one obtains a spectrum of amplitudes β against correlation times ϕ . Similar considerations regarding the starting model in the recovery of $\alpha(\tau)$ apply to the recovery of $\beta(\phi)$, *i.e.* if there is no *a priori* knowledge of the distribution one should start with a flat spectrum in $\log(\phi)$ space.

In the global fit of $i_{||}(t)$ and $i_{\perp}(t)$, a fixed image of the fluorescence decay consisting of 150 equally spaced values in $\log(\tau)$ space was introduced in the analysis. The starting model of $\beta(\phi)$ consisted of 100 uniform and equally spaced values on a $\log(\phi)$ scale (from 0.1 to 100 ns).

The fluorescence parameters as calculated from the images $\alpha(\tau)$ and $\beta(\phi)$ have been obtained as follows. The average fluorescence lifetime of a sample $\langle \tau \rangle$ is defined as:

$$\langle \tau \rangle = \frac{\sum_i^N \alpha_i \tau_i}{\sum_i^N \alpha_i} \quad (7)$$

where the summation is carried out over the whole range (N) of τ_i values of an $\alpha(\tau)$ spectrum. The barycenter of a peak in the

spectrum is determined in a similar fashion except that the summation is carried out over a limited range of τ_i values encompassing a local peak [23]. A peak is defined as a range of $\alpha(\tau)$ values containing a local maximum and delimited by two minima. The fractional area of a peak is the ratio between the integrated peak intensity and the total intensity of the spectrum. Similar parameters can be determined from the $\beta(\phi)$ image where the axes are replaced by ϕ and β instead of τ and α .

The time-resolved fluorescence anisotropy of the proteins at different temperatures was also analyzed with the commercially available global analysis software package (Globals UnlimitedTM, Urbana, IL). The parallel and perpendicular polarized fluorescence decays at the different temperatures were simultaneously analyzed to a single decay model encompassing temperature invariant parameters. These parameters were linked as given in the Results section. Errors in the parameters were determined at a 67% confidence interval by a rigorous error analysis [30, 31].

2.4 Results

2.4.1 Total fluorescence decay analysis.

In Fig.1 the time-resolved fluorescence profiles are shown for LipDH-AV and GR in aqueous solution at room temperature. Both decays are entirely different and have a strong heterogeneous character.

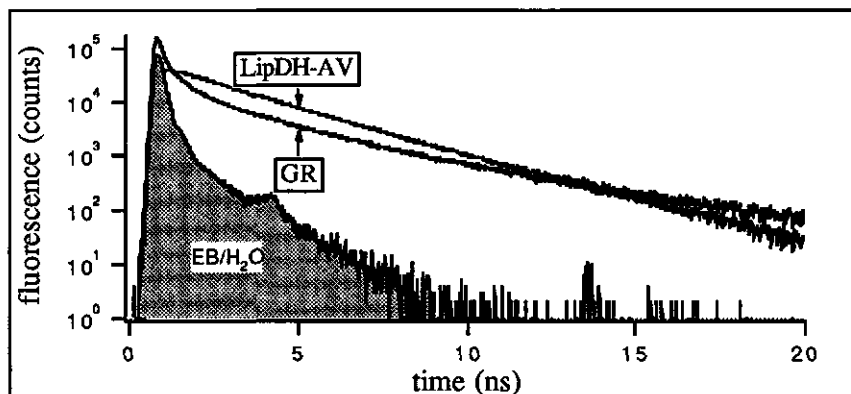


Fig.1: Experimental total fluorescence decay of lipoamide dehydrogenase (LipDH-AV) and glutathione reductase (GR) in 50 mM potassium phosphate buffer at pH 7.0 and 293 K. Excitation at 457.9 nm, emission at 550 nm. The fluorescence response of the pulse mimic erythrosine B in water (EB/H₂O) is also shown.

The inverse Laplace transform of the fluorescence decay of FAD bound to LipDH-AV in aqueous solution consists of three peaks (Fig.2A).

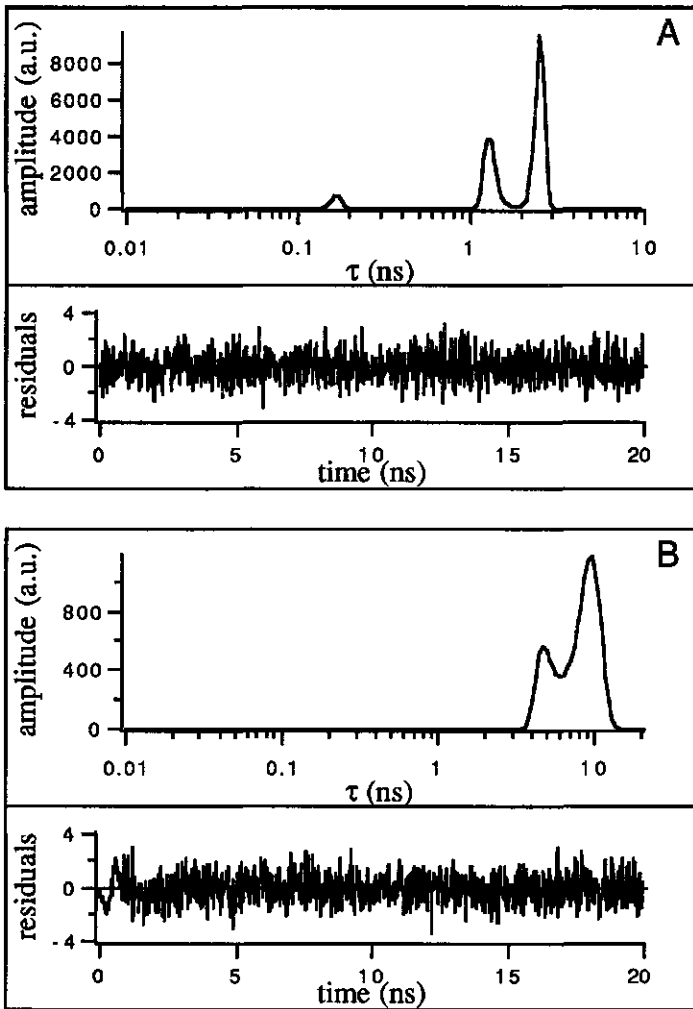


Fig.2: Inverse Laplace transform of fluorescence decay of LipDH-AV in 50 mM potassium phosphate buffer at pH 7.0 at 293 K (panel A) and in 80% glycerol 50 mM potassium phosphate buffer at pH 7.0 at 243 K (panel B). The weighted residuals of the fit are placed in the boxes under the lifetime spectra.

At 277 K the image is dominated by a peak with a barycenter at 3.2 ns. Above 283 K, the relative contributions of the shorter lifetime classes increase at the expense of the longer one (Fig.3B). The increase of the fractional contribution of the two shorter

components implies that states of the protein with higher conformational energy are populated. Since the barycenters of the lifetime classes converge (Fig.3A), interconversion between conformational states takes place on a time scale comparable to the excited-state lifetime. The amplitudes and lifetimes are then eigenvectors and eigenvalues of a system of three coupled linear differential equations [25]. In that case, the fractional contributions of the lifetime classes cannot be used to calculate the fractional population of the conformational states.

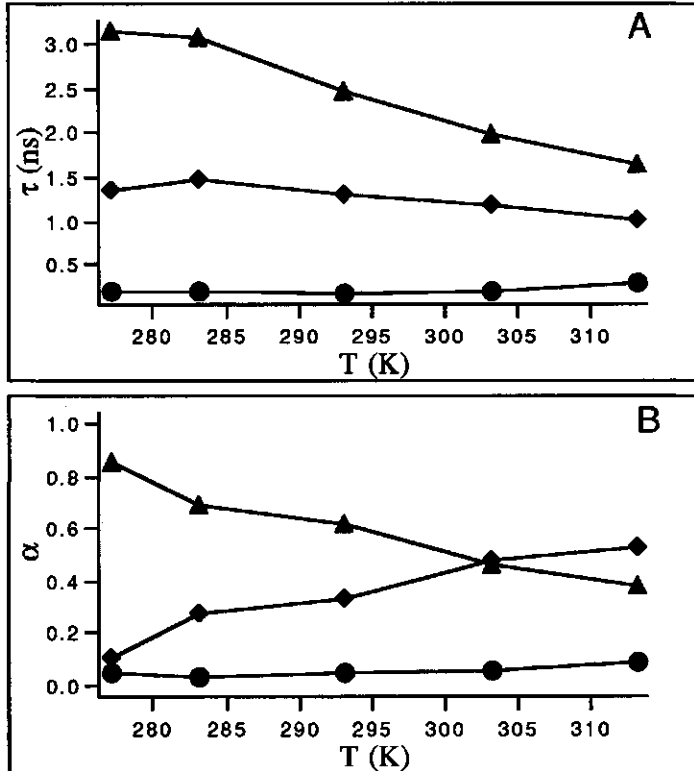


Fig.3: Temperature dependence of barycenters (panel A) and fractional contributions (panel B) of the lifetime classes in LipDH-AV in 50 mM potassium phosphate buffer at pH 7.0.

A bimodal instead of a trimodal distribution is recovered for the protein in 80% glycerol at 243 K (Fig.2B). The conformation associated with the short lifetime class (0.15 ns) is not populated at this temperature in 80% glycerol suggesting that this state of the protein has the highest conformational energy. The barycenters of the two observed states in 80% glycerol are shifted to longer lifetimes as compared to the lifetime classes in aqueous

solution. Since rapid protein fluctuations are damped in cryogenic solvents at low temperature [32], it is expected that the fluorescence lifetime of protein-bound flavin is longer due to diminished collisional quenching by neighboring amino acid residues.

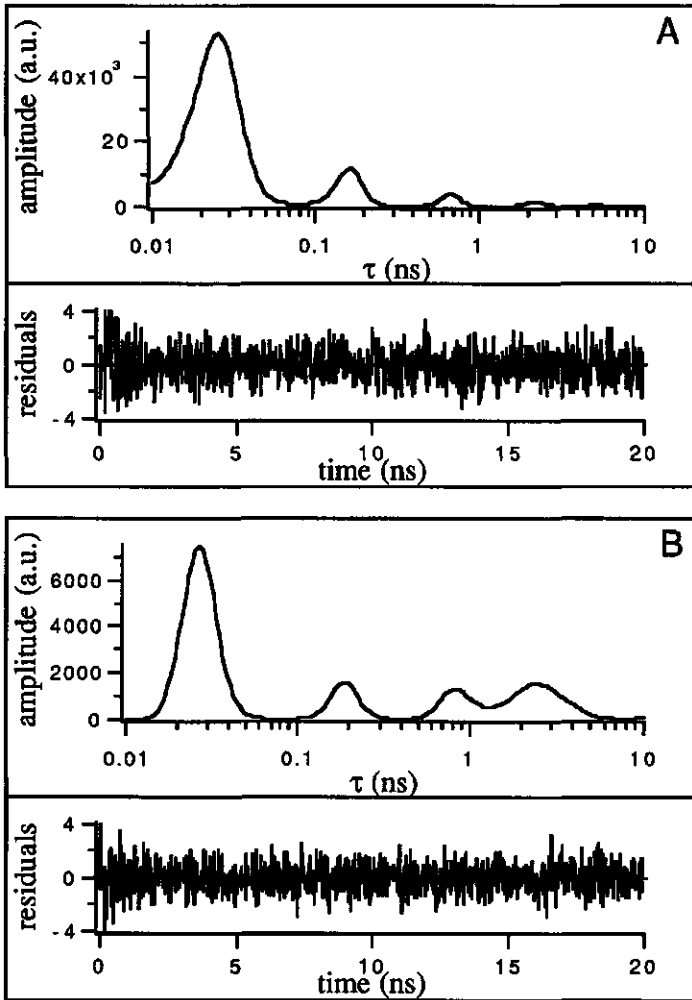


Fig.4: Inverse Laplace transform of fluorescence decay of GR in 50 mM potassium phosphate buffer at pH 7.0 at 293 K (panel A) and in 80% glycerol 50 mM potassium phosphate buffer at pH 7.0 at 243 K (panel B). The weighted residuals of the fit are placed in the boxes under the lifetime spectra.

The temperature dependence of the lifetime classes is then determined by two factors:

- i) the activation barrier between conformational states
- ii) the effective activation energy of collisional quenching.

The activation energies of the two processes differ by at least an order of magnitude and can be ascribed to equilibrium fluctuations of different tiers [16, 17]. The interplay of both mechanisms makes the system too complex to analyze using quantitative global analytical methods which are able to extract the activation energies [33, 34].

Up to five peaks could be distinguished in the spectrum of GR which is dominated by a short lifetime component with a barycenter positioned at 30 ps (Fig.4A).

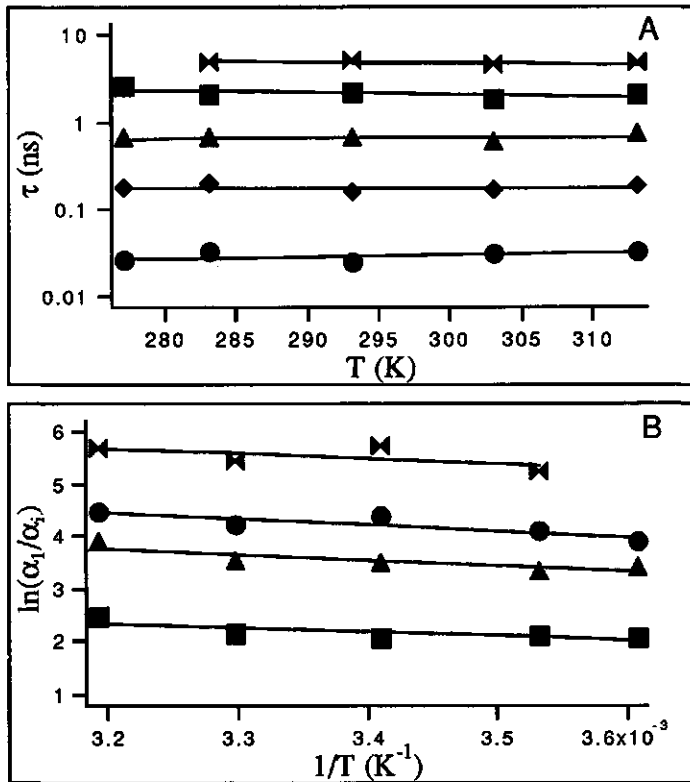


Fig.5: Temperature dependence of barycenters and relative populations of GR molecules in 50 mM potassium phosphate buffer at pH 7.0. Panel A: semi-logarithmic plot of barycenters of the lifetime classes as function of temperature. Panel B: van 't Hoff plot of conformational transition equilibrium constants ($K=\alpha_1/\alpha_i$).

The barycenters of the different lifetime classes were invariant to temperature (Fig.5A), implying that exchange between conformational states is slow in this temperature range in contrast to LipDH-AV. The normalized integrated amplitudes then correspond to the fractional population of the protein substates. From the fractional populations of the lifetime classes the standard enthalpy difference ΔH_i^0 between states can be estimated with van 't Hoff's law:

$$\frac{\Delta H_i^0}{R} = \frac{d \ln(\alpha_i/\alpha_1)}{d(1/T)} \quad (8)$$

where α_1 is the integrated amplitude of the shortest lifetime component (30 ps), α_i is the integrated amplitude of another component i , R is the gas constant ($8.31 \text{ JK}^{-1}\text{mol}^{-1}$) and T the temperature in Kelvin. So the enthalpy of the conformational states can then be calculated relative to the most populated state (30 ps) which we assigned a relative value of 0 kJ/mol (Fig.5B). In this way, part of the protein energy landscape can be drawn (Fig.6).

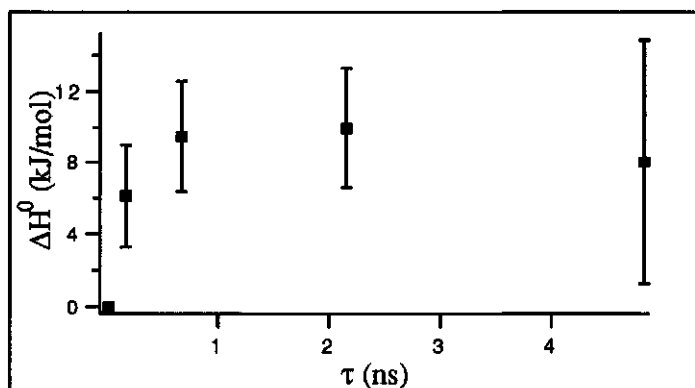


Fig.6: Standard free enthalpy of conformational transition in GR. The conformational coordinate is replaced by the barycenter of the lifetime classes on the x-axis. The enthalpy is relative to the conformational state associated with the smallest lifetime class (30 ps) which was assigned a value of 0 kJ/mol.

The large error bars on the enthalpies are due to the small values of the fractional populations with longer lifetimes. The activation barriers between conformational substates could not be determined but should be at least an order of magnitude larger than the enthalpy differences between states (slow exchange). The temperature invariance of the barycenter of the shortest lifetime component favors an interpretation based on an excited-state

reaction, such as electron transfer from Tyr197 to the flavin in the first excited singlet [21, 35], over a dynamic quenching process caused by collision with the redox-active disulfide bridge [13]. This is also supported by the lifetime spectrum of the protein in 80% glycerol at 243 K (Fig.4B). If the origin of a short lifetime component is due to dynamic quenching one would expect that the barycenter would shift towards longer lifetimes at decreasing temperature and/or increase of viscosity since in these experimental conditions the frequency of protein fluctuations decreases. Such an effect is not observed.

2.4.2 Fluorescence anisotropy analysis.

The fluorescence anisotropy decays of LipDH-AV and GR in aqueous solution at 293 K are shown in Fig.7. The rapid fluorescence anisotropy decline for GR, in contrast to LipDH-AV, is in agreement with previous results [13].

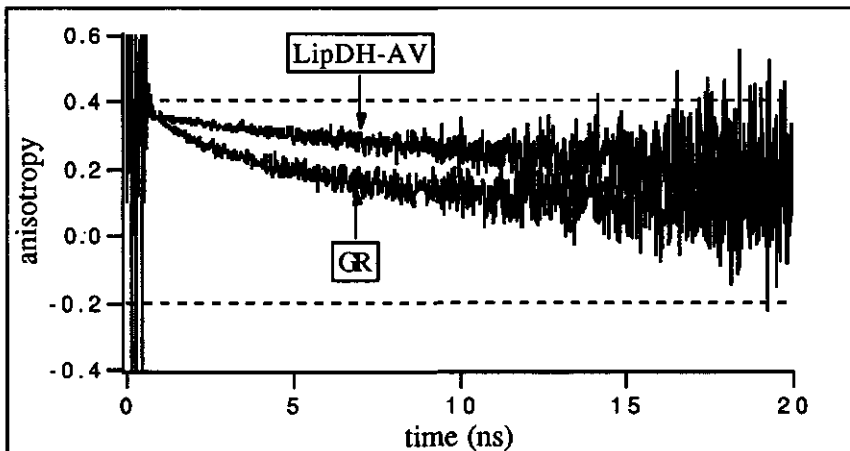


Fig.7: Experimental fluorescence anisotropy decays of lipamide dehydrogenase (LipDH-AV) and glutathione reductase (GR) in 50 mM potassium phosphate buffer at pH 7.0 and 293 K. Excitation at 457.9 nm, emission at 550 nm. The broken lines indicate the theoretically possible values of the fluorescence anisotropy.

In the one-dimensional correlation-time image of the fluorescence anisotropy decay of FAD bound to LipDH-AV one can distinguish three regions of interest (Fig.8). At the flank of the spectrum with the highest ϕ values an unresolved peak is apparent which indicates that the anisotropy levels to a constant value in the measured time window. From the size of the protein (100 kDa) one can calculate that the expected rotational

correlation time from a modified Stokes-Einstein relation [36] is 38 ns at 20°C. At all measured temperatures this correlation time exceeds the fluorescence lifetimes by more than a factor of ten. In this case the intensity of the carrier signal (fluorescence decay) is too low on the time scale where protein rotation takes place. In the region between 6 and 9 ns a peak could be resolved with a temperature-invariant barycenter and area (Fig.9A-B). The temperature invariance of this depolarizing process strongly suggests that it is not due to restricted reorientation of the flavins but to another depolarizing mechanism. The only other process which can then contribute to the depolarization of the fluorescence is intersubunit energy transfer between the flavins. As the overlap integral (J) was found to be temperature invariant between 277-313 K ($J = 3.514 \pm 0.088 \cdot 10^{-15} \text{ M}^{-1}\text{cm}^3$) we also expect that the rate of this process will be invariant with temperature.

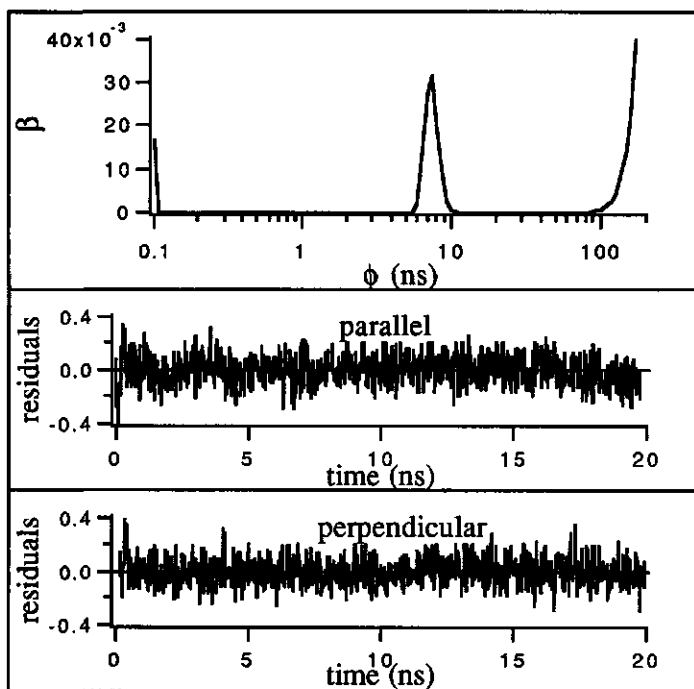


Fig.8: Correlation-time spectrum of LipDH-AV in 50 mM potassium phosphate buffer at pH 7.0 and 283 K with the residuals of the fit to the parallel and perpendicular polarized fluorescence intensities.

At the extremely short correlation-time flank of the spectrum an unresolved peak is observed at all temperatures. The area under this peak has a value smaller than 0.02 at the measured

temperature interval and corresponds to an ultrafast depolarizing process not resolvable by our experimental system. We assign this process to rapid reorientational fluctuations with small amplitude ($< 5^\circ$) of the isoalloxazines within the protein matrix.

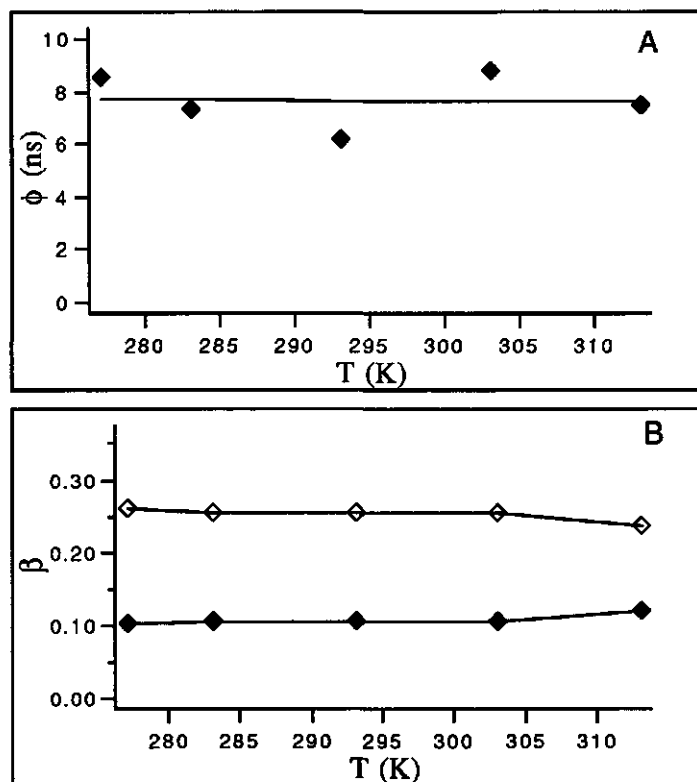


Fig.9: Temperature dependence of barycenters (panel A) and integrated amplitudes (panel B) as obtained from the correlation time spectra of LipDH-AV in 50 mM potassium phosphate buffer at pH 7.0. \blacklozenge : integrated amplitude and barycenter of process associated with energy transfer, \circ : integrated amplitude of limiting anisotropy.

In the correlation-time spectrum of GR an additional peak is revealed at approximately 1.5 ns at 283 K which is not present in the spectrum of LipDH-AV (Fig.10). The barycenter of this peak shifts towards shorter correlation times upon increase of temperature (Fig.11A). This temperature dependence is an indication that the depolarizing process associated with this peak corresponds to restricted reorientational motion of the flavins. Similar to the spectrum of LipDH-AV, a temperature-invariant peak is present with a barycenter around 6 ns which again is associated with energy transfer between the flavins. At 313 K,

protein tumbling and energy transfer cannot be distinguished. The peak associated with energy transfer is then recovered as a shoulder in the spectrum. In this particular case the relative amplitudes of both processes (energy transfer and protein tumbling) cannot be recovered. At the extreme short correlation-time edge of the spectrum an ultrarapid depolarization is recovered at all temperatures (Fig.10).

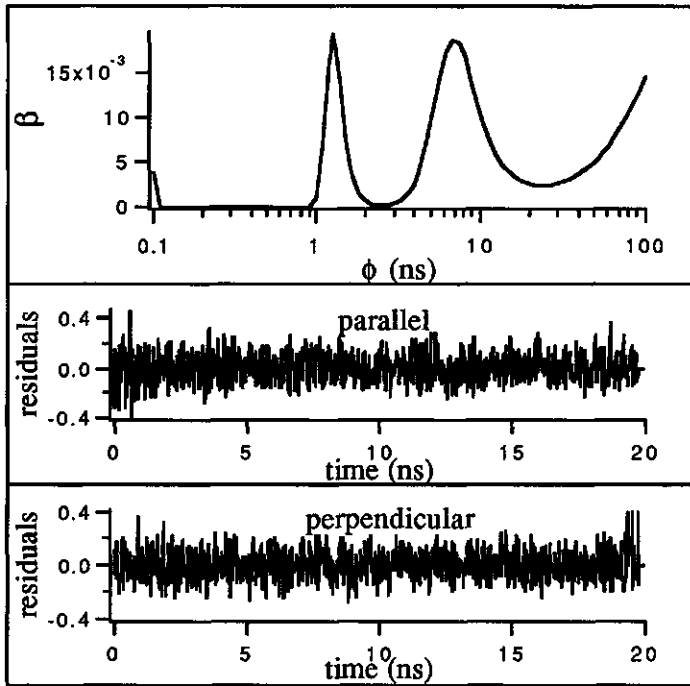


Fig.10: Correlation-time spectrum of GR in 50 mM potassium phosphate buffer at pH 7.0 and 283 K with the residuals of the fit to the parallel and perpendicular polarized fluorescence intensities.

This process is not resolvable by our measuring system and probably corresponds to small amplitude rapid reorientational fluctuations of the flavins like in LipDH-AV. The areas of the different peaks remained constant within the measured temperature interval (Fig.11B) which shows that the angular parameters associated with different depolarizing processes (*vide infra*) are invariant.

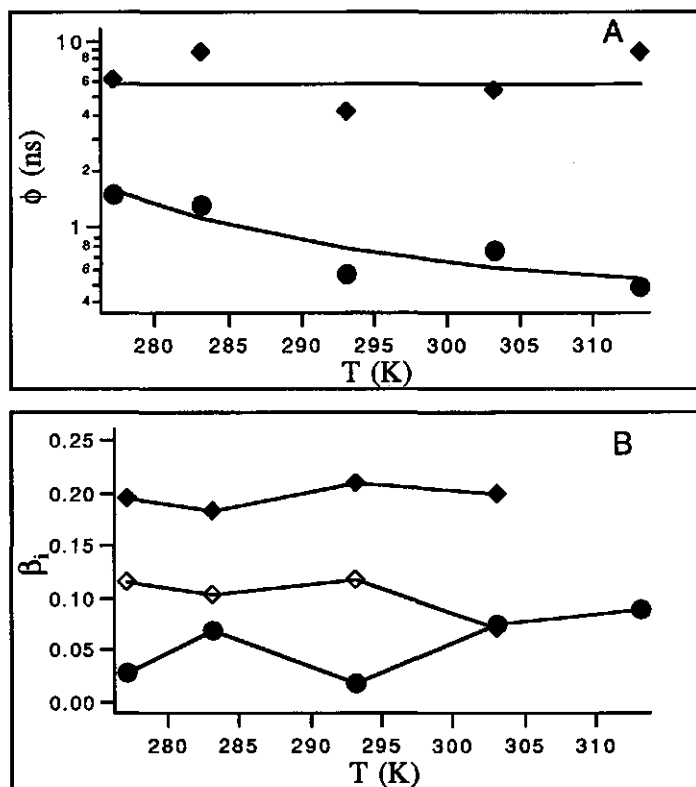


Fig.11: Temperature dependence of barycenters (panel A) and integrated amplitudes (panel B) as obtained from the correlation-time spectra of GR in 50 mM potassium phosphate buffer at pH 7.0. \blacklozenge : integrated amplitude and barycenter of process associated with energy transfer, \bullet : integrated amplitude and barycenter of process associated with restricted motion, \diamond : limiting anisotropy.

The temperature invariance of the parameters describing the anisotropy decays of LipDH-AV and GR can be exploited by a global analysis. The temperature invariant parameters can then be linked in the simultaneous analysis of the parallel and perpendicular polarized fluorescence decays at different temperatures. Since the inverse Laplace transform of the anisotropy decay of LipDH consisted of two peaks (energy transfer and protein tumbling), the anisotropy decays were modeled by a double exponential function ($N=2$):

$$r(t) = \sum_{i=1}^N \beta_i \exp(-t/\phi_i) \quad (9)$$

The pre-exponential amplitudes β_i were assumed to be invariant over the experimental temperature range and subsequently linked in the simultaneous analysis of the temperature dependent polarized fluorescence decays. The temperature invariant correlation time associated with energy transfer was also linked over all experiments. In the global analysis of the polarized fluorescence of GR the anisotropy decays were modeled by a triple exponential function (eq.9, N=3). The β_i were assumed invariant to temperature and linked over all experiments. The correlation time associated with energy-transfer was again interlinked but not the correlation time associated with restricted motion. The values of the temperature invariant parameters obtained after global and MEM analysis of the polarized fluorescence decays are collected in Table 1 together with the error estimates at 67% confidence.

Table 1: Temperature invariant parameters of fluorescence anisotropy decays of LipDH-AV and GR.

	β_1	β_2	β_3	ϕ_T (ns)	global χ^2
LipDH-AV		0.13† (0.11-0.17) 0.11* (0.01)	0.23† (0.18-0.25) 0.25* (0.01)	8.6† (6.2-14.8) 7.7* (1.1)	1.10
GR	0.10† (0.078-0.14) 0.06* (0.03)	0.19† (0.14-0.21) 0.20* (0.01)	0.08† (0.07-0.11) 0.10* (0.02)	9.4† (8.0-14.0) 6.5* (2.0)	1.25

† : Values as obtained from the global analysis of the parallel and perpendicular polarized fluorescence decays between 277 and 313 K. The numbers between brackets are the errors at 67% confidence as determined from a rigorous error analysis.

* : Average values as obtained from the MEM analysis of the individual decay curves. The average was taken from the inverse Laplace transforms of the decays at 5 temperatures (277-313 K). The numbers between brackets are the standard deviations.

The global fit of the polarized fluorescence decays of the proteins at five temperatures (277-313 K) was satisfactory as judged by the random distribution of residuals around zero except for a small non-random deviation at short times (Fig.12). This ultra-rapid depolarization observed both in GR and LipDH-AV which was resolved by MEM could not be fitted by the global analysis program even by addition of an extra exponential term in the decay model (eq.9, N=4). Since this process has a small amplitude and is outside the time-domain (few picoseconds) of our interest, it was further neglected in the analysis of the anisotropy decays.

It should be noted, however, that the global χ^2 is somewhat higher than unity by exclusion of this ultrarapid process in the analysis.

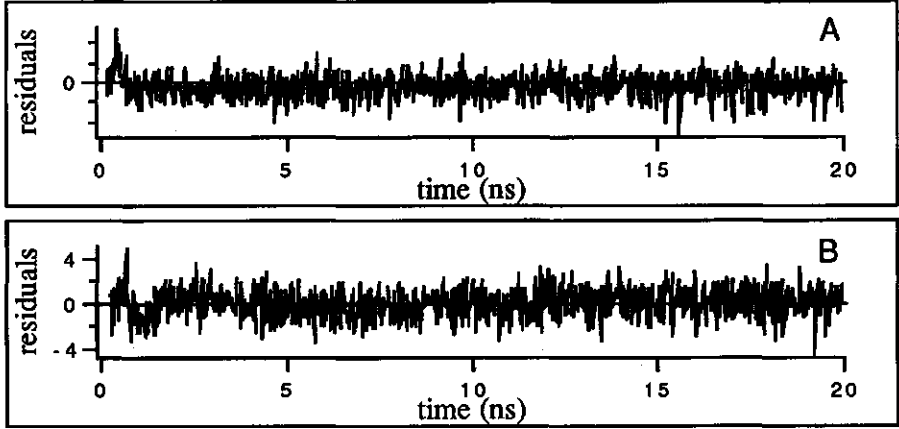


Fig.12: Residuals of global fit of anisotropy decays of LipDH-AV (A) and GR (B). Mark the deviations at short times due to an unresolvable ultrafast depolarization process. Only the residuals of the fit of the anisotropy decays at 293 K are shown.

With eq.A5 of the appendix we can relate the empirical parameters (ϕ_i, β_i) of the anisotropy decay model of GR to geometrical parameters of the protein. The integral of amplitudes associated with restricted reorientational motion is β_1 , the integral of amplitudes associated with energy transfer is β_2 and the integral of peak amplitudes associated with protein tumbling is β_3 (limiting anisotropy). By expanding the Legendre polynomials in eq.A5 and by algebraic manipulation of the pre-exponential amplitudes we obtain:

$$\beta_1 + \beta_2 + \beta_3 = \frac{3}{5} \cos^2 \delta - \frac{1}{5} \quad (10)$$

$$\frac{\beta_2 + \beta_3}{\beta_1 + \beta_2 + \beta_3} = 1 - \frac{\beta_1}{\beta_1 + \beta_2 + \beta_3} = S^2 \quad (11)$$

$$\frac{\beta_3 - \beta_2}{\beta_2 + \beta_3} = \frac{3}{2} \cos^2 \theta - \frac{1}{2} \quad (12)$$

where δ is the intramolecular angle between absorption and emission transition moments and θ is the intermolecular angle between the symmetry axes of the potential wells. The second

rank order parameter S can be related to a maximal cone semi-angle of reorientation (ψ) following the *a priori* solution of Kinoshita *et al.* [37]:

$$S = \sqrt{\frac{1}{2} \cos \psi (\cos \psi + 1)} \quad (13)$$

From the correlation time of restricted motion (ϕ_M) one obtains the diffusion coefficient (D_{\perp}) at temperature T :

$$D_{\perp} = \frac{1 - S^2}{6\phi_M} \quad (14)$$

and from the correlation time associated with energy transfer (ϕ_T) the rate of transfer (k_T):

$$k_T = \frac{1}{2\phi_T} \quad (15)$$

The pre-exponential amplitudes of the anisotropy-decay model of LipDH-AV can only be related to geometrical parameters describing the relative isoalloxazine orientation in both subunits. By expanding the Legendre polynomials in eq.A6 of the appendix and after addition and subtraction of the pre-exponential amplitudes we obtain:

$$\beta_2 + \beta_3 = \frac{3}{5} \cos^2 \delta - \frac{1}{5} \quad (16)$$

$$\beta_3 - \beta_2 = \frac{3}{5} \langle \cos^2 \theta \rangle - \frac{1}{5} \quad (17)$$

θ is now the intermolecular angle between absorption and emission transition moments. In eq.17 the brackets denote an average over two angles which are not necessarily the same; θ_1 : angle between emission transition moment in isoalloxazine 1 and absorption transition moment in isoalloxazine 2, θ_2 : angle between emission transition moment in isoalloxazine 2 and absorption transition moment in isoalloxazine 1. As we cannot distinguish the direction of transfer in the correlation-time spectrum of LipDH-AV (unimodal peak) θ_1 and θ_2 are taken as approximately equal. The geometrical parameters and the rate of transfer as calculated from the anisotropy decay parameters obtained after global and MEM analyses of the anisotropy decays are collected in Table 2. From eq.17 one obtains two solutions for the intermolecular

angle (θ) between transition moments. In Table 2 the solutions are collected which are in agreement with the C_2 symmetry of LipDH-AV and GR.

Table2: Geometrical parameters and interflavin energy transfer rate constant of LipDH-AV and GR.

	S	ψ (deg)	θ (deg)	δ (deg)	k_T (MHz)	R (nm)
LipDH-AV			134† (125-139) 139* (2)	15† (15-16) 15* (1)	58† (36-81) 65* (9)	3.7† (3.5-4.0) 3.6* (0.1)
GR	0.85† (0.79-0.91) 0.92* (0.05)	36† (28-44) 27* (9)	104† (101-120) 111* (8)	13† (10-14) 16* (2)	53† (36-63) 77* (23)	3.7† (3.6-4.0) 3.5* (0.2)

† : Values as calculated from the parameters obtained after a global analysis of the parallel and perpendicular polarized fluorescence decays between 277 and 313 K. The numbers between brackets are the errors at 67% confidence as determined from a rigorous error analysis.

* : Average values as calculated from the average parameters of a MEM analysis of the individual decay curves. The average was taken from the inverse Laplace transforms of the decays at 5 temperatures (277-313 K). The numbers between brackets are the standard deviations.

In GR we found evidence for reorientational motion of the flavins. When this motion is modelled as diffusive motion within a box with infinitely high potential walls, we found a cone semiangle between 28° and 44° .

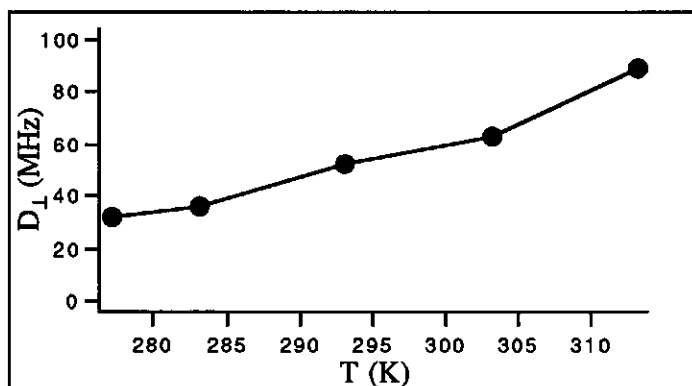


Fig.13: Perpendicular diffusion constant of reorientational motion of flavins bound to GR as function of temperature

The diffusion constant (D_{\perp}) as calculated with eq.14 increases with temperature as expected for a temperature dependent process

such as reorientational motion (Fig.13). Since reorientational motion of the flavins takes place in GR, the intermolecular angle (θ) is the angle between the symmetry axes of the potential wells. It is reasonable to assume that in the crystal structure the flavins are immobilized in an energy state corresponding to the minimum of a potential well. In that case the flavins are oriented with their pseudo-symmetry axes parallel to the symmetry axes of the potentials. The angle θ as obtained from crystallographic coordinates [5] is then 102° which is also agreement with the angle as obtained from fluorescence depolarization (Table 2).

The intermolecular angle between absorption and emission transition moments in the immobilized isoalloxazines (θ) of LipDH-AV is in accordance with the value as calculated from crystallographic coordinates (138°) [7]. The intermolecular distances between the isoalloxazines as obtained from the Förster equation with the orientation factor κ^2 as calculated from crystallographic data (Table 2) are in excellent agreement with those directly calculated from the crystal structures (3.9 nm both for GR and LipDH-AV). The correspondence between crystallographic geometry and that derived from optical spectroscopy shows that our interpretation of the fluorescence anisotropy is correct in both proteins.

A single peak with a limiting anisotropy was obtained for the proteins at 243 K in 80% glycerol (Fig.14). Restricted reorientational motion is then completely inhibited in the proteins and the sole mechanism responsible for fluorescence depolarization is energy transfer. It should be noted that the integrated amplitude of the energy transfer peak for GR in 80% glycerol is much lower than in aqueous solution (see Discussion)

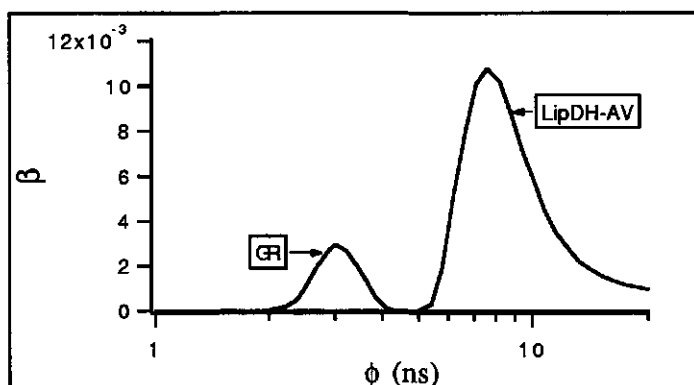


Fig.14: Correlation-time spectrum of LipDH-AV and GR in 80% glycerol 50 mM potassium phosphate buffer at pH 7.0 at 243 K. For clarity only the region between 1 and 20 ns is shown.

The angles θ and δ and the interflavin distance as calculated from the parameters obtained from a global analysis of the anisotropy decays of LipDH-AV in 80% glycerol at different temperatures ($\theta=139^\circ$, $\delta=17^\circ$, $R=3.8-4.2$ nm) correspond well with those obtained in aqueous solution (Table 2), which confirms that energy transfer is indeed the major cause for the depolarization of the fluorescence in LipDH-AV. Details of this analysis are presented in chapter 4 of this thesis. Restricted motion of the flavins in GR is completely abolished in 80%(v/v) glycerol at 243 K. The sole mechanism of depolarization is then energy transfer between the cofactors. The model of energy transfer has to be modified as compared to the one in aqueous solution. The recovered angle θ is now the intermolecular angle between transition moments instead of the intermolecular angle between symmetry axes of the potential wells. The angle θ , as obtained from the fluorescence depolarization experiment ($\theta=158^\circ$), is larger than the angle found in LipDH-AV. The subunits possibly have different mutual orientations in both proteins. The angle θ as obtained from crystallographic data [5] ($\theta=148^\circ$ for GR instead of 138° for LipDH-AV) corroborates this finding. The fluorimetric θ is comparable to the intermolecular angle between absorption transition moments (163°). The question then arises if the intramolecular angle δ is not overestimated because of rapid reorientational fluctuations of the flavins on a time scale beyond the resolution of the experimental system.

2.5 Discussion

Comparison of the thermal behavior of the fluorescence kinetics of GR and LipDH-AV shows that the conformational dynamics differ to a large extent. The temperature invariance of the lifetimes in GR indicates that the activation energies between conformational substates are larger than in LipDH-AV. Almost 90% of GR is in a state with an extremely short fluorescence lifetime (30 ps) of the flavin. The rapid depopulation of the flavin excited-state arises from exciplex formation with Tyr197, a residue absent in LipDH-AV. The other (minor) components probably originate from conformational substates where the relative positioning of Tyr197 and isoalloxazine is unfavorable for efficient electron transfer. It has been proposed that Tyr197 functions as a lid to protect the two-electron reduced enzyme against oxidation [38]. It is possible that equilibrium fluctuations between conformations with different orientations of the "lid" correspond to the observed five lifetime classes. The increase in relative populations associated with the longer lifetime

components, observed in 80% glycerol GR solution, can be accounted for by a decreased stacking interaction between the isoalloxazine and tyrosine rings. The "open" conformation of the enzyme is thus more stabilized in 80% glycerol. Since the activation barriers between conformational substates are large in GR (in the order of 100 kJ/mol or larger) the transitions between states, with different orientations of Tyr197, correspond to gross structural changes in the protein. Confirmation that large structural changes are involved in closing the active site came from site-directed mutagenesis on GR from *E. coli* [12]. In these studies the tyrosine had been replaced by glycine with maintenance of the protection against oxidation of the two-electron reduced enzyme. It was concluded that the flavin is buried within the protein in the "closed" form.

We can propose a role in catalysis of equilibrium fluctuations between conformational states in GR and LipDH-AV. With time-resolved fluorescence spectroscopy 90% of GR was found to exist in a conformation where the flavin has a tight interaction with Tyr197 (closed lid conformation [38]). In this conformation the prosthetic group is not accessible for NADPH and cannot form a productive binary complex. In the remaining fraction (<10%), the tyrosine is displaced and the enzyme is in a proper state to bind NADPH (open conformation). The protein in this conformation (without coenzyme) has the same spatial structure as the binary complex. When NADPH binds to this "open conformation" the equilibrium is shifted to the enzyme-substrate complex. Equilibrium between conformational substates is then re-established to repeat the binding cycle. In this model, binding of the coenzyme is only possible when the appropriate open enzyme conformation is pre-existing. Such a mechanism is in contrast to a model where a conformational change is induced by binding of the coenzyme to the closed form of the enzyme. Since large activation barriers prevail between conformational substates, the rate limiting step of cofactor binding could well be the conformational transition from "closed" to "open" enzyme forms.

From fluorescence quenching and solvent relaxation experiments, we obtained evidence that the flavin is not accessible to solvent in the majority of LipDH-AV molecules (chapter 3 of this thesis). In contrast, in a deletion mutant lacking 14 amino acids at the C-terminus the flavins are partly exposed to the solvent. It can be envisioned that this terminal peptide has a "lid" function preventing electrons to enter the flavin site in most of the enzymes. A minor fraction of LipDH-AV molecules possibly exists in an open conformation ready to bind substrate (Lip(SH)₂). The shortest component (150 ps) in the lifetime spectrum is a

possible manifestation for this more open protein conformation since it has the lowest contribution. Additional time-resolved fluorescence quenching experiments should be carried out to prove this point. We can then tentatively assign a similar role in catalysis to equilibrium fluctuations between conformational substates in LipDH-AV as in GR. In LipDH-AV, however, the interconversion between substates at 293 K is much more rapid than in GR ruling out that this transition is the rate limiting step in substrate binding.

In previous studies, the anisotropy decay of LipDH was fitted to double exponential decay functions. The two correlation times were interpreted as arising from restricted hinge motion of the subunits and protein tumbling [13, 39, 40]. From the analysis of the anisotropy decay with the one-dimensional version of MEM we obtained a unimodal distribution of correlation times with a limiting anisotropy. The information on the rotational correlation time of protein tumbling is thus highly uncertain and cannot be extracted from the data (Figs.8 and 10). The temperature invariance of the barycenter and of the integrated amplitude of the unimodal peak in the correlation-time spectrum firmly establishes that the underlying physical mechanism of depolarization is intersubunit energy transfer between the flavins. Additional evidence for this mechanism is obtained from the correlation-time spectrum of LipDH-AV in 80% glycerol at 243 K. The unimodal peak is also present with similar barycenter and amplitude. The geometrical parameters as derived from the global analysis of the fluorescence anisotropy decays at five temperatures according to an energy transfer model, are in agreement with crystallographic data. The flavins are thus rigidly bound and only ultrarapid reorientational fluctuations of small amplitude ($\psi < 5^\circ$) can be detected. The rapid exchange between conformational substates at temperatures above 283 K is then not associated with an angular displacement of the flavins. The equilibrium fluctuations of the conformational substate correspond to a rearrangement of the flavin environment without changing their relative orientation.

A bimodal correlation-time distribution and a limiting anisotropy is found for GR instead of the reported mono-exponential decay function [13]. By the temperature invariance of the peak located at around 6 ns we could demonstrate that a considerable contribution to the depolarization originates from energy transfer between the flavins. In addition to energy transfer, restricted reorientational motion of the flavins is observed in contrast to the situation in LipDH-AV. Despite the small angular displacement of the flavins (22° – 44°) almost complete depolarization of the fluorescence is observed for this

protein. Energy transfer is then the major contributor to the depolarization. The large peak amplitude of this process has two origins:

- i) the second rank order parameter contributes to the amplitude of the peak (eq.A5)
- ii) the angle between symmetry axes of the flavin potential wells is smaller than the angle between the transition moments in the immobilized state (104° instead of 158°).

The latter point is exemplified by the fluorescence depolarization of GR in 80% glycerol at 243 K. Restricted motion is then abolished and the sole mechanism of depolarization is energy transfer. The integrated amplitude of the peak associated with energy transfer is in that case about a factor of 6-7 smaller than in aqueous solution.

The flexibility of the flavins in GR is in sharp contrast with the highly immobilized isoalloxazines as found in the crystal structure [5]. The majority of the ensemble of enzymes (90%) have a conformation where the lifetime of the flavins is about 30 ps. The excited state of the flavin in this (large) fraction of molecules is depopulated before any depolarization due to restricted motion or energy transfer can take place. Because of this short lifetime one can not decide on the dynamic properties of this population. This conformational substate could thus be highly rigid, as observed in the crystal structure. The carrier signal for depolarization comes from the longer lived components which correspond to protein populations with an unfavorable conformation for the formation of the flavin-tyrosine exciplex. As can be envisioned the flavin is flexible in these conformations because of the alleviation of the spatial constraints of the proximal tyrosine.

Owing to the high dynamic range and nanosecond observation window in time-resolved fluorescence, in conjunction with the unequivocal lifetime distribution analysis, it is possible to monitor minor fractions of protein conformational substates. Temperature-dependent fluorescence relaxation spectroscopy provides us therefore with a powerful tool to investigate the role of conformational dynamics in flavoprotein catalysis. In addition, the factors contributing to the depolarization of the fluorescence can be quantitatively separated. In this way reliable geometric information in multichromophoric proteins in solution can be obtained.

2.6 Appendix

Quantitative interpretation of fluorescence anisotropy decay

The proteins have distinct structural and dynamic properties. In LipDH-AV energy transfer is the main cause for fluorescence depolarization whereas additional restricted reorientational motion takes place in GR. In order to find useful expressions which relate the inverse Laplace transform of the anisotropy decays to physical parameters one has to adopt reasonable assumptions about the system under investigation. Our first assumption is that the decay of the excited state is independent on the orientation of the molecules in the protein matrix. In this case, the electronic and orientational state of a molecule are uncoupled (non-associative modeling). The master equation relating the anisotropy decay $r(t)$ to the orientational correlation function is then [41, 42]:

$$r(t) = \langle\langle P_2[\vec{u}_a \cdot \vec{u}_e(t)] \rangle\rangle \quad (\text{A1})$$

where \vec{u}_a and \vec{u}_e are unit vectors pointing along the absorption and emission transition moments of the flavin molecule, respectively. P_2 denotes a second order Legendre polynomial and the brackets ($\langle\langle \dots \rangle\rangle$) indicate a molecular ensemble average. In a system where restricted reorientational motion takes place together with energy transfer (*e.g.* in GR), the contributions of the individual processes to the depolarization can be factorized into a Soleillet product when restricted motion takes place on a faster time scale than energy transfer [43]:

$$r(t) = \frac{2}{5} P_2(\cos \delta) C_M \cdot C_T \quad (\text{A2})$$

where C_M and C_T are the correlation functions of (restricted) motion and (energy) transfer, respectively, and δ is the angle between the absorption and emission transition moments within a flavin molecule. In order to obtain an analytical expression for the reorientational correlation function one has to consider:

- i) the potential well in which the flavin reorients
- ii) the type of dynamics (strong collision- or diffusion model).

In order to quantify our data we have chosen a simple model based on a uniaxial potential with diffusive dynamics for flavin

reorientation. The single exponential approximation of van der Meer *et al.* [44] describes such a system:

$$C_M = [1-S^2]\exp[-6D_{\perp}t/(1-S^2)] + S^2 \quad (\text{A } 3)$$

where S is the second rank order parameter and D_{\perp} (ns^{-1}) the diffusion coefficient perpendicular to the symmetry axis of the potential well. It is to be noted that this expression can be replaced by another type of model describing reorientational dynamics (*e.g.* jump [41] or more refined diffusion models [42, 44]). In eq.A3, the position of the emission transition moment is assumed to be approximately parallel to the flavin (pseudo) symmetry axis. The analytical expression for the transfer correlation function has been derived and is exact [45]:

$$C_T = \frac{1}{2} \{ [1 - P_2(\vec{D}_1, \vec{D}_2)] \exp[-2k_T t] + P_2(\vec{D}_1, \vec{D}_2) + 1 \} \quad (\text{A } 4)$$

where k_T is the rate of intermolecular Förster energy transfer. Since the transition moments are completely randomized within the potential well, this expression does not contain the angular parameters describing the mutual orientation of the absorption and emission transition moments. The angular parameter which is contained in the pre-exponential amplitudes in eq.A4 is the angle between the symmetry axes (\vec{D}_i) of the potentials. After substitution of eqs.A3 and A4 into eq.A2 an expression for the time-dependent anisotropy for a system where restricted motion and energy transfer contribute to the depolarization of the fluorescence is obtained:

$$r(t) = \frac{2}{5} P_2(\cos(\delta)) \left\{ [1-S^2] \exp\left[\frac{-6D_{\perp}t}{1-S^2}\right] + \frac{1}{2} S^2 [1 - P_2(\vec{D}_1, \vec{D}_2)] \exp[-2k_T t] + \frac{1}{2} S^2 [1 + P_2(\vec{D}_1, \vec{D}_2)] \right\} \quad (\text{A } 5)$$

For a system of two chromophores with fixed unique orientation interacting by the Förster mechanism (as in LipDH-AV), the time-dependent anisotropy is described by [45]:

$$r(t) = \frac{1}{10} \{ 2P_2(\vec{\mu}_a, \vec{\mu}_c) + P_2(\vec{\mu}_a, \vec{\mu}_c) + P_2(\vec{\mu}_a, \vec{\mu}_c) + [2P_2(\vec{\mu}_a, \vec{\mu}_c) - P_2(\vec{\mu}_a, \vec{\mu}_c) - P_2(\vec{\mu}_a, \vec{\mu}_c)] \exp[-2k_T t] \} \quad (\text{A } 6)$$

The pre-exponential amplitudes now contain information on the inter- and intra-molecular angles between absorption and

emission transition moments in the dimeric homo-transfer system.

2.7 References

1. Williams, C.H.J. (1976) *The Enzymes*, 13, 89-173.
2. Worthington, D.J. and Rosemeyer, M.A. (1974) *Eur. J. Biochem.*, 48, 167-177.
3. Schulz, G.E., Zappa, H., Worthington, D.J. and Rosemeyer, M.A. (1975) *FEBS Lett*, 54, 86-88.
4. Kalse, J.F. and Veeger, C. (1968) *Biochim. Biophys. Acta* 159, 244-256
5. Karplus, P.A. and Schulz, G.E. (1987) *J. Mol. Biol.*, 195, 701-729.
6. Schierbeek, A.J., Swarte, M.B.A., Dijkstra, B.W., Vriend, G., Read, R.J., Hol, W.G.J., Drenth, J. and Betzel, C. (1989) *J. Mol. Biol.*, 206, 365-379.
7. Mattevi, A., Schierbeek, J.A. and Hol, W.G.J. (1991) *J. Mol. Biol.*, 220, 975-994.
8. van Berkel, W.J.H., Benen, J.A.E. and Snoek, M.C. (1991) *Eur. J. Biochem.*, 197, 769-779.
9. Reed, L.J. (1974) *Acc. Chem. Res.*, 7, 40-46.
10. Westphal, A.H. and de Kok, A. (1988) *Eur. J. Biochem.*, 172, 299-305.
11. Schulze, E., Benen, J.A.E., Westphal, A.H. and de Kok, A. (1991) *Eur. J. Biochem*, 200, 29-34.
12. Berry, A., Scrutton, N.S. and Perham, R.N. (1989) *Biochemistry*, 28, 1264-1269
13. de Kok, A. and Visser, A.J.W.G. (1987) *FEBS Lett.*, 218, 135-138.
14. Beechem, J.M. and Brand, L. (1985) *Ann. Rev. Biochem.*, 54, 43-71.
15. Austin, R.H., Beeson, K.W., Eisenstein, L., Frauenfelder, H. and Gunsalus, I.C. (1975) *Biochemistry*, 14, 5355-5373.
16. Frauenfelder, H. and Gratton, E. (1986) *Methods Enzymol.*, 127, 207-216.
17. Frauenfelder, H., Parak, F. and Young, R.D. (1988) *Ann. Rev. Biophys. Biophys Chem.*, 17, 451-479.
18. Bastiaens, P.I.H., Bonants, P.J.M., van Hoek, A., Müller, F. and Visser, A.J.W.G. (1988) *Proc. SPIE*, 909, 257-262.
19. Bastiaens, P.I.H., Bonants, P.J.M., Müller, F. and Visser, A.J.W.G. (1989) *Biochemistry*, 28, 8416-8425.
20. Bastiaens, P.I.H., Mayhew, S.G., O'Nualláin, E.M., van Hoek, A. and Visser, A.J.W.G. (1991) *J. of Fluorescence*, 1, 95-103.
21. Kalman, B., Sandström, A., Johansson, L.B.-Å. and Lindskog, S. (1991) *Biochemistry*, 30, 111-117.

22. Livesey, A.K. and Brochon, J.C. (1987) *Biophys. J.*, 52, 693-706.
23. Mérola, F., Rigler, R., Holmgren, A. and Brochon, J.C. (1989) *Biochemistry*, 28, 3383-3398.
24. Gentin, M., Vincent, M., Brochon, J.C., Livesey, A.K., Cittanova, N. and Gallay, J. (1990) *Biochemistry*, 29, 10405-10412.
25. Alcalá, R.J., Gratton, E. and Prendergast, F.G. (1987) *Biophys. J.*, 51, 597-604.
26. Krohne-Ehrich, G., Schirmer, R.H. and Untucht-Grau, R. (1971) *Eur. J. Biochem.*, 80, 65-71.
27. O'Connor, D.V. and Phillips, D. (1984) *Time-Correlated Single Photon Counting*, Academic Press, London.
28. van Hoek, A., Vos, K. and Visser, A.J.W.G. (1987) *IEEE J. Quantum Electron.*, QE-23, 1812-1820.
29. Bastiaens, P.I.H., van Hoek, A., Benen, J.A.E., Brochon, J.C. and Visser, A.J.W.G. (1992) Chapter 4 of this thesis
30. Beechem, J.M. and Gratton, E. (1988) *Proc. SPIE*, 909, 70-81.
31. Beechem, J.M., Gratton, E., Ameloot, M., Knutson, J.R. and Brand, L. (1991) *The global analysis of fluorescence intensity and anisotropy decay data in: Topics in Fluorescence Spectroscopy (Lakowicz, J.R. ed.) Vol 2*, pp 241-305, Plenum Press, New York.
32. Gavish, B. and Werber, M.M. (1979) *Biochemistry*, 18, 1269-1275.
33. Ameloot, M., Beechem, J.M. and Brand, L. (1986) *Chem. Phys. Lett.*, 129, 211-219.
34. Boens, N., Janssens, L.D. and de Schryver, F.C. (1989) *Biophys. Chem.*, 33, 77-90.
35. Visser, A.J.W.G., van Hoek, A., Kulinski, T. and LeGall, J. (1987) *FEBS Lett.*, 224, 406-410.
36. Visser, A.J.W.G. and Lee, J. (1980) *Biochemistry*, 19, 4366-4372.
37. Kinoshita, K., Kawato, S. and Ikegami, A. (1977) *Biophys. J.*, 20, 289-305.
38. Pai, E.F. and Schulz, E. (1983) *J. Biol. Chem.*, 258, 1752-1757.
39. Bosma, H.J., de Graaf-Hess, A.C., de Kok, A., Veeger, C., Visser, A.J.W.G. and Voordouw, G. (1982) *Ann. NY Acad. Sci.*, 378, 265-286.
40. de Kok, A. and Visser, A.J.W.G. (1984) in: *Flavins and Flavoproteins (Bray, R.C., Engel, P.C. and Mayhew S.G. eds.)*, pp. 149-152, Walter de Gruyter, Berlin.
41. Zannoni, C. (1981) *Mol. Phys.*, 42, 1303-1320.
42. Szabo, A. (1984) *J. Chem. Phys.*, 81, 150-167.
43. Soleillet, P. (1929) *Ann. Phys. X.*, 12, 23-97.

44. van der Meer, W., Pottel, H., Herreman, W., Ameloot, M., Hendrickx, H. and Schröder, H. (1984) *Biophys. J.*, 46, 515-523.
45. Tanaka, F. and Mataga, N. (1979) *Photochem. Photobiol.*, 29, 1091-1097.

Chapter 3

Molecular Relaxation Spectroscopy of Flavin Adenine Dinucleotide in Wild Type and Mutant Lipoamide Dehydrogenase from *Azotobacter vinelandii*

Bastiaens, P.I.H., van Hoek, A., van Berkel, W.J.H., de Kok, A. and Visser, A.J.W.G.

Abstract

The temperature dependence of the fluorescence emission spectra of flavin adenine dinucleotide (FAD) bound to lipoamide dehydrogenase from *Azotobacter vinelandii* shows that the protein matrix in the vicinity of the prosthetic group is rigid on a nanosecond time scale in a medium of high viscosity (80% glycerol). The active site of a deletion mutant of this enzyme, which lacks 14 C-terminal amino acids, is converted from a solid state environment (on the nanosecond time scale of fluorescence) into a state where efficient dipolar relaxation takes place at temperatures between 203-303 K. In aqueous solution fast dipolar fluctuations are observed in both proteins. From fluorescence quenching of the flavin by iodide ions it is shown that the prosthetic groups of the mutant protein are partially iodide accessible in contrast to the wild type enzyme. A detailed analysis of the temperature dependence of spectral energies according to continuous relaxation models reveals two distinct relaxation processes in the deletion mutant which were assigned to solvent and protein dipoles, respectively. From the long-wave shifts of the emission spectra upon red-edge excitation it is demonstrated that the active site of the wild type enzyme has high structural homogeneity in comparison to the deletion mutant. In combination with results obtained by x-ray diffraction studies on crystals of the wild type enzyme it can be concluded that the C-terminal polypeptide of the *A.vinelandii* enzyme interacts with the dehydrolipoamide binding site thereby shielding the flavins from the solvent.

3.1 Introduction

Steady-state fluorescence spectroscopy has been extensively used to obtain information on structural and dynamical properties of biological macromolecules, since the spectral parameters of fluorescence emission such as position, shape and intensity are dependent on the electronic and dynamic properties of the

chromophore environment [1-4]. During the last decade a new approach has evolved to observe dipolar relaxational dynamics in the vicinity of fluorophores in proteins [5-9]. This technique exploits the possibility to photoselect nonequilibrium solvates (solvate: fluorescent molecule and its immediate surrounding) by site-selective excitation at the red-edge of the absorption band. The spectral parameters of the fluorescence emission are then dependent on the inhomogeneity of the electric field surrounding the fluorophores and on its relaxational properties as caused by temperature-dependent structural fluctuations of protein and solvent dipoles. This technique has been applied to obtain information on dipolar relaxation in the vicinity of the intrinsically fluorescent tryptophan residue in proteins [10]. It was found that proteins containing a tryptophan with either an extreme short- or long-wave emission spectrum did not exhibit a long-wave shift upon red-edge excitation in contrast to proteins with an emission spectrum in the intermediate spectral region. The apolar nature of the chromophore environment in the short-wave emitting class of proteins results in a narrow distribution of interaction energies. The absence of a long-wave shift in this class of proteins indicated a negligible photoselection of nonequilibrium excited states. In the long-wave emitting class, the absence of a spectral shift was explained because the chromophores were accessible to the rapidly fluctuating solvent dipoles causing fluorescence emission to take place from the equilibrium excited state irrespective of excitation wavelength. In the mid-range emitting proteins, temperature- and excitation frequency-dependent shifts of the emission spectra were associated with dipolar relaxation with a characteristic time constant in the same order as the lifetime of the excited state. From the average dipolar relaxation time obtained from such experiments, the protein matrix surrounding a chromophore can be ranked from fluid to solid state on the time scale of fluorescence emission. These experiments, among others, demonstrate the potential of molecular relaxation spectroscopy to obtain information on dynamical properties near an extrinsic or intrinsic fluorophore in proteins.

No attempts have been made thus far to study dipolar relaxational properties in flavoproteins by investigating the fluorescence spectral emission characteristics of the intrinsically fluorescent prosthetic group FAD or FMN. These fluorescent nucleotides exhibit different spectral characteristics in different flavoproteins, reflecting the specific environmental properties of the isoalloxazine, which is the relevant chromophore [11-15]. In this study we present the structural and dynamic properties of the active sites in the flavoprotein lipoamide dehydrogenase from

Azotobacter vinelandii (LipDH-AV) as inferred from temperature-dependent laser-induced site-selective fluorescence emission spectroscopy. Lipoamide dehydrogenase belongs to the class of disulfide-oxidoreductases and catalyses the NAD⁺-dependent oxidation of the covalently attached dihydrolipoyl groups of lipoate-acyltransferase in different multienzyme complexes [16-18]. The dimeric 100 kDa protein possesses an $\alpha\alpha$ -quaternary structure where each subunit contains one highly fluorescent FAD cofactor (quantum yield 240% of that of free FAD). The gene encoding lipoamide dehydrogenase from *Azotobacter vinelandii* has been cloned and expressed in *Escherichia coli* TG2 which provides means to modify the active site near the isoalloxazine of FAD by site-directed mutagenesis [19]. The last ten C-terminal amino acids of the *A. vinelandii* enzyme are not visible in the electron density map of the high resolution crystal structure indicating that they are disordered [20, 21]. From biochemical studies on a deletion mutant of the *A. vinelandii* enzyme, lacking the C-terminal 14 amino acids, it was concluded that the C-terminus has an important function in catalytic activity and stability of the dimer [22]. It is then possible that the C-terminal tail interacts with the lipoamide binding site, which comprises amino acid residues from both subunits thereby stabilizing the dimer. In this respect we compared the solvent accessibility and the dipolar relaxational properties near the flavins of the deletion mutant (LipDH- Δ 14) and the wild type enzyme.

3.2 Theory

Chromophores in an unstructured dipolar environment, such as a polar solvent, exhibit a statistical deviation of dipolar interaction energies around the equilibrium minimal interaction energy due to thermal motions of solvent molecules. This holds true for both ground and excited states of the chromophore resulting in a distribution of singlet-singlet transition frequencies and inhomogeneous broadening of spectra [23, 24]. Excitation at the main-band or red-edge of the absorption spectrum results in the population of nonequilibrium Franck-Condon excited states. Site-selective excitation at the red-edge of the absorption band photoselects chromophores with minimal electronic transition frequencies [7, 8]. The corresponding instantaneous emission spectrum will be shifted to long wavelengths relative to the spectrum obtained at main-band excitation [23, 25]. In both excitation regimes (red-edge and main-band) the excited solvates will have a tendency to relax to the minimal energy configuration with a characteristic dipolar relaxation time τ_r . According to the time-integrated continuous relaxation model of Bakshiev and

Mazurenko, the relation between the mean wavenumber of the steady-state emission spectrum ($\bar{\nu}$), dipolar relaxation time (τ_r) and average fluorescence lifetime ($\bar{\tau}_f$) is [26]:

$$\frac{\bar{\nu} - \bar{\nu}_\infty}{\nu_0 - \bar{\nu}_\infty} = \frac{\Delta\nu}{\Delta\nu_0} = \frac{\tau_r}{\tau_r + \bar{\tau}_f} \quad (1)$$

When there is no motion of the dipoles of the chromophore environment on the time scale of fluorescence, τ_r is much longer than $\bar{\tau}_f$ and the unrelaxed spectrum is obtained with mean frequency $\bar{\nu}_0$. This spectrum is typically observed at low temperatures. In the reverse situation where $\bar{\tau}_f$ is much longer than τ_r , practically all emission takes place from the equilibrium excited state and the relaxed spectrum with mean frequency $\bar{\nu}_\infty$ is obtained. This spectrum, typically observed at elevated temperatures, is difficult to obtain for proteins due to temperature-induced denaturation and subsequent loss of tertiary structure. A useful expression was derived which does not contain $\bar{\nu}_\infty$ by assuming that τ_r , $\bar{\tau}_f$ and $\bar{\nu}_\infty$ are independent of excitation wavelength [5-8]:

$$\frac{\bar{\nu} - \bar{\nu}^{\text{edge}}}{\nu_0 - \nu_0^{\text{edge}}} = \frac{\Delta\nu^{\text{edge}}}{\Delta\nu_0^{\text{edge}}} = \frac{\tau_r}{\tau_r + \bar{\tau}_f} \quad (2)$$

where $\bar{\nu}^{\text{edge}}$ is the mean wavenumber of the spectrum obtained upon red-edge excitation. From this expression the dipolar relaxation time in biological molecules can be estimated from the ratio of the difference in mean frequency of the spectra upon main-band- and edge excitation at a certain temperature. Maximal difference in mean frequency is obtained at low temperatures where the dipolar relaxation is much slower than the fluorescence emission.

3.3 Materials

LipDH-AV and the mutant LipDH- Δ 14 expressed in *E. coli* TG4 were purified as described before [19, 22]. The enzyme preparations were frozen in liquid nitrogen and stored at -70°C in 100 mM K_2HPO_4 , pH 7.0, 0.5 mM EDTA. The samples were defrosted at room temperature and 300 μl aliquots were chromatographed on a Biogel PGD-6 column (Biorad, 1 x 6 cm) equilibrated with 50 mM K_2HPO_4 , pH 7.0 to eliminate unbound

FAD. All buffers were made with nanopure water prepared on a millipore water purification system. The enzyme preparations to be brought to 80% (v/v) glycerol were chromatographed as above except that the column was equilibrated with 250 mM K_2HPO_4 , pH 7.0. From the eluted sample 100 μl was gently mixed with 400 μl of 100% glycerol (Merck, fluorescent microscopy grade) until a homogeneous solution was obtained. Enzyme concentrations were determined with a molar extinction coefficient of $\epsilon_{457} = 11.3 \text{ mM}^{-1} \text{ cm}^{-1}$ [19]. Care was taken that all final preparations had a concentration of 10-15 μM to ensure that the enzymes are in the dimeric form. FAD was purified on a Biogel P-2 (Biorad). 100 μl aliquots of this preparation were mixed with 400 μl glycerol to a final concentration of 10 μM . Upon freezing the samples down to 203 K a clear transparent glass was formed with no indications of any precipitate.

3.4 Instrumentation

Emission spectra at different temperatures were obtained by excitation with light of 514.5 or 457.9 nm wavelength of a mode-locked cw argon-ion laser (Coherent Radiation model CR 18) emitting light pulses at a rate of 76 MHz. Samples were 0.5 cm^3 in volume in 1 cm lightpath cuvetts, placed in a thermostated holder. This holder was placed in a sample housing also containing the optics.

For sample temperatures down to 203 K a liquid nitrogen flow set-up was used with a temperature controller (Oxford model ITC4). At these low temperatures experiments can be easily disturbed by the condensation of water from the surrounding air on the cuvet. Therefore the sample housing was extended in height and filled with a steady stream of the relatively heavy argon gas onto the cuvet walls. The final temperature of the sample appeared to be in balance with different heat sources (cold nitrogen, room temperature argon gas, the heater of the controller and heat radiation), and care was taken to control the true sample temperature. Furthermore the cuvetts were exchanged wearing surgical gloves. In this way experiments could be performed over a period of a few hours without dew and ice problems. At the front of the sample housing a Glan-laser polarizer was mounted, optimizing the already vertical polarization of the input light beam. Between sample and photomultiplier (microchannel-plate, Hamamatsu model 1645U) a single fast lens (uncoated fused silica), a rotatable sheet polarizer and a computer controlled monochromator (two tandemized 0.25 m monochromators, f/3.5 Jarrel Ash model 82.410) were placed. The sheet type polarizer in

the detection pathway was placed under magic angle with respect to the polarization of the excitation light. Emission photons (via a constant fraction discriminator, Canberra model 1428A) were directly fed to the multichannel scaling (MCS) input of the multichannel analyzer (MCA, Nuclear Data model ND66 equipped with both a ND582 ADC and a zero dead time multichannel scaling unit). The channel stepping of the MCS was time-synchronized by the controller of stepper motor of the monochromator. The bandwidth of the monochromator was 6 nm for the spectra with 457.9 nm excitation and 2 nm for the spectra with 514.5 nm excitation. Four spectra were acquired at every temperature and excitation wavelength in the range of 470 to 662 nm over 1024 channels. The emission spectra were converted from technical to molecular spectra in a computer program containing the transmission characteristics of the monochromator and photomultiplier.

Fluorescence quenching experiments were performed on a SLM-Aminco SPF-500C fluorometer. The excitation wavelength was set at 450 nm and the emission at 550 nm. Both excitation and emission slits were set at 4 nm bandpass.

Time-resolved fluorescence measurements and analysis were performed as described in chapters 2 and 4 of this thesis

3.5 Computational methods

All emission spectra contained 1024 points and were linear on a wavelength scale (470-662 nm). The spectra were converted to a wavenumber scale by taking the reciprocal of the vector $\vec{\lambda}$ where each element λ_i is the discrete value of the corresponding wavelength in channel i of the MCA:

$$\vec{\nu} = \frac{1}{\vec{\lambda}} \quad (3)$$

The center of gravity or mean wavenumber of a spectrum is then calculated by:

$$\bar{\nu} = \frac{(\vec{\nu} \cdot \vec{I})}{|\vec{I}|} \quad (4)$$

where each element I_i of the vector \vec{I} contains the number of counts in channel i of the MCA. Upon excitation at 514.5 nm (red-edge excitation) the spectra contained a peak of large amplitude spanning the channels 224-264 of the MCA (512-519 nm) which could be attributed to scattered light. Both in the main-band and

red-edge excited emission spectra these channels were omitted in the calculation of the center of gravity to obtain comparable results. Manipulation of the excitation and emission spectra (such as correction for instrumental distortions, calculation of the center of gravity of the fluorescence bands and fitting to quenching and relaxation models) were performed on a Apple Macintosh SE/30 computer equipped with the program IGOR (wavemetrics™).

3.6 Results

3.6.1 Fluorescence quenching by iodide

The solvent accessibility of the isoalloxazines in the wild type (LipDH-AV) and deletion mutant (LipDH-Δ14) of lipoamide dehydrogenase were compared to that of the free chromophore by measuring the extent of collisional quenching of the flavin fluorescence by iodide ions. The data is represented in a Stern-Volmer plot (Fig.1) where the relative flavin fluorescence is plotted against the iodide concentration ([I]).

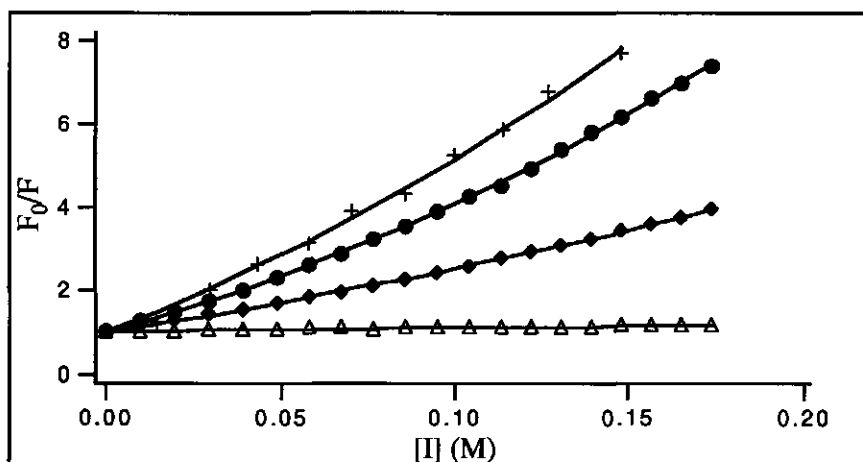


Fig.1: Stern-Volmer plot of iodide quenching of flavin fluorescence in LipDH-AV (Δ), LipDH- Δ 14 (\blacklozenge), free FAD (\bullet) and free FMN (+) in 50 mM KPi pH 7.0 at 293 K. The solid lines are the optimized fits of the data to the modified Stern-Volmer equation.

The data were fitted to a modified Stern-Volmer equation to account for static quenching due to the presence of ions at the moment of excitation in the quenching sphere of action (V) [27]:

$$\frac{F_0}{F} = (1 + K_{sv}[I]) \exp([I]V) \quad (5)$$

where F_0 and F are the fluorescence intensity in absence and presence of quencher, respectively. The Stern-Volmer quenching constant (K_{sv} in M^{-1}) is the product of the bimolecular dynamic quenching constant (k_q in $M^{-1}ns^{-1}$) and the lifetime of the chromophore ($\bar{\tau}_f$ in ns) in absence of quencher. V is the effective volume around the chromophore in dm^3 at which static quenching occurs per mol of fluorophore. The optimized parameters as obtained from the fit of the data are gathered in Table 1 and the curves described by these parameters are represented in Fig.1 by the solid lines.

Table 1: Fluorescence quenching parameters

sample:	K_{sv} (M^{-1})	$\bar{\tau}_f$ (ns)	k_q ($M^{-1}.ns^{-1}$)	V (M^{-1})
LipDH-AV	0.86 ± 0.06	2.0	0.43 ± 0.03	-
LipDH- Δ 14	11.7 ± 0.2	1.1	9.9 ± 0.2	1.12 ± 0.04
FAD	20.9 ± 0.2	2.5*	8.4 ± 0.1	2.74 ± 0.06
FMN	31.1 ± 2.0	4.7*	6.6 ± 0.4	2.24 ± 0.41

* Value obtained from ref [28]

Visual inspection of the Stern-Volmer plots as well as the larger bimolecular quenching constant indicate the increased iodide accessibility of the isoalloxazines in LipDH- Δ 14 in comparison with that in LipDH-AV. From the decreased effective volume of static quenching in LipDH- Δ 14 as compared to that of the free chromophore one can conclude that flavin is partly shielded from iodide ions by the protein matrix. In the deletion mutant protein we thus expect an enhanced interaction of the flavin with solvent dipoles and in this way the relaxational properties of the excited state of a chromophore inside a protein in distinct environments can be compared.

3.6.2 Spectral Shifts

We examined the emission spectra of free FAD and bound to LipDH-AV and LipDH- Δ 14 in 80% glycerol and in aqueous solution as function of temperature upon main-band (457.9 nm) and red-edge (514.5 nm) excitation. As can be seen in Fig.2A the spectrum of FAD in 80% glycerol exhibits a considerable shift ($\Delta\nu = 600 \text{ cm}^{-1}$) in the temperature region from 203 K to 303 K at main-band excitation. A similar longwave shift of the spectrum is observed at 203 K at red-edge excitation (Fig.2B) which is

completely abolished above 280 K. In aqueous solution no substantial shifts were observed with temperature or upon red-edge excitation. The temperature dependence of the center of gravity of the emission spectra is represented in Fig.2C on a wavenumber scale. From Fig.2C it is clear that:

- i) site-selective excitation of nonequilibrium solvates takes place upon excitation at 514.5 nm at low temperature
- ii) the energy of the emitted photons is dependent on the dipolar relaxational properties of the solvent.

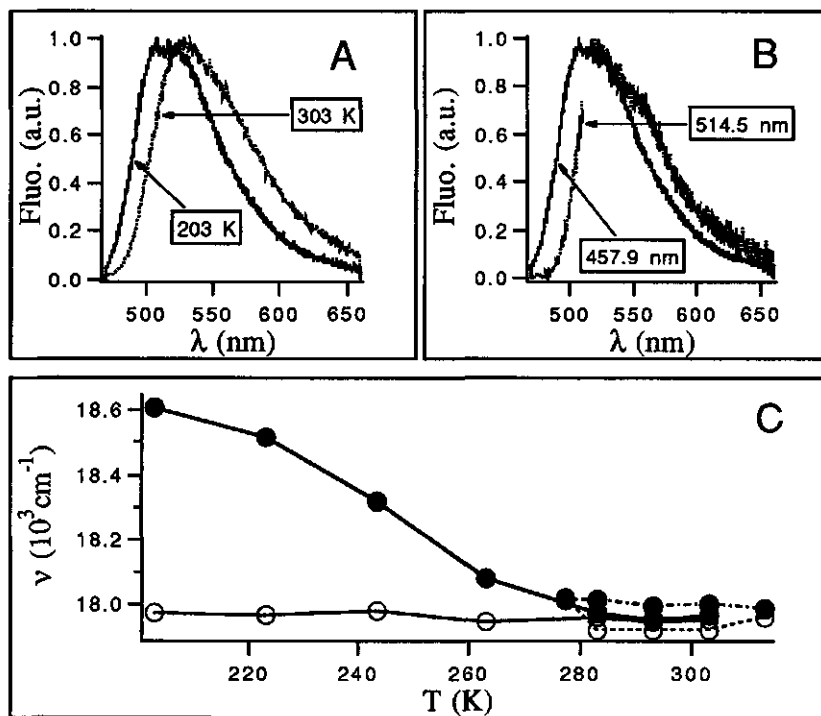


Fig.2: Temperature- and excitation-wavelength dependence of fluorescence spectra of free FAD. A) temperature-dependent shift of emission spectra of free FAD in 80% glycerol 50 mM KPi pH 7.0. upon 457.9 nm excitation. B) excitation wavelength dependent shift of emission spectra at 203 K in same solvent as in A. The points between 512 and 519 nm contain a considerable amount of 514.5 nm laser scattering and were therefore omitted in the spectrum obtained after red-edge excitation. C) center of gravity expressed on a wavenumber scale as function of temperature and excitation wavelength. Open symbols: 514.5 nm excitation, closed symbols: 457.9 nm excitation, solid lines: data obtained in 80% glycerol 50 mM KPi pH 7.0, broken lines: data obtained in 50 mM KPi pH 7.0. Error bars are within the thickness of the experimental points.

The spectral dependence of bound FAD in the wild type enzyme on temperature and excitation wavelength was completely different to that of the free chromophore. With an increase in temperature the emission spectra of LipDH-AV in 80% glycerol hardly shifts to longer wavelengths upon main-band excitation (Fig.3A). A small bathochromic shift of the emission spectra could be detected upon red-edge excitation (Fig.3B). In Fig.3C the center of gravity of the emission spectrum on wavenumber scale has been plotted as function of temperature.

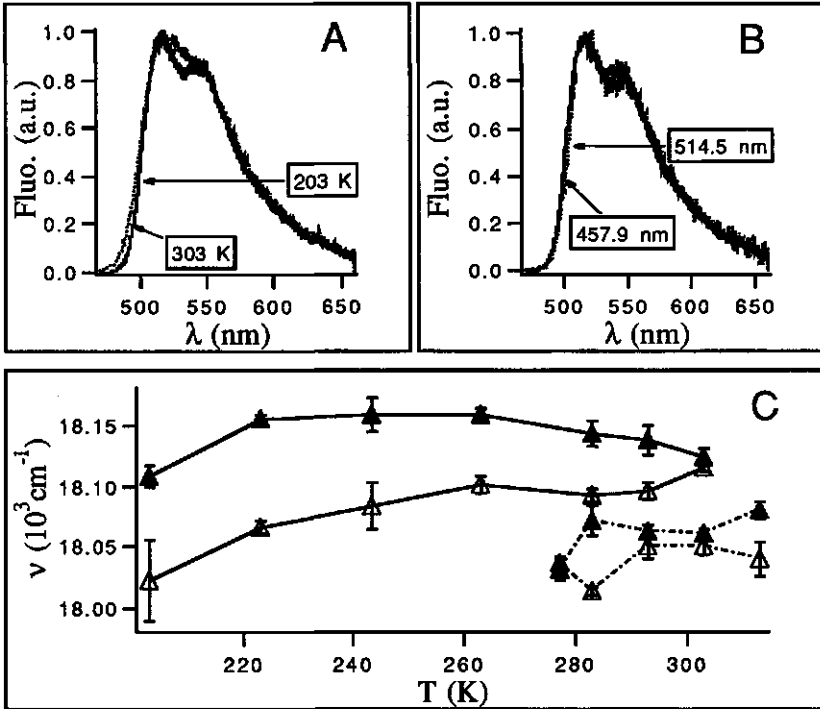


Fig.3: Temperature- and excitation-wavelength dependence of emission spectra of wild type lipoamide dehydrogenase. A) temperature dependent shift of emission spectra of FAD bound to LipDH-AV in 80% glycerol 50 mM KPi pH 7.0 upon 457.9 nm excitation. B) excitation wavelength-dependent shift of emission spectra at 203 K for same sample as in A. The points between 512 and 519 nm contain a considerable amount of 514.5 nm laser scattering and were therefore omitted in the spectrum obtained after red-edge excitation. C) center of gravity expressed on a wavenumber scale as function of temperature and excitation wavelength. Open symbols: 514.5 nm excitation, closed symbols: 457.9 nm excitation, solid lines: data obtained in 80% glycerol 50 mM KPi pH 7.0, broken lines: data obtained in 50 mM KPi pH 7.0.

In aqueous solution the spectra were shifted longwave relative to the spectra in 80% glycerol and did not show either a substantial

temperature- or edge excitation-induced shift (see symbols connected by broken lines in Fig.3C).

For LipDH- $\Delta 14$ we found a clear temperature- and excitation wavelength-dependence of the emission spectra. Upon main-band excitation, a red-shift of the emission spectra was apparent with increase of temperature (Fig.4A). Upon red-edge excitation at 203 K the emission spectrum is shifted longwave relative to the spectrum obtained upon main-band excitation (Fig.4B).

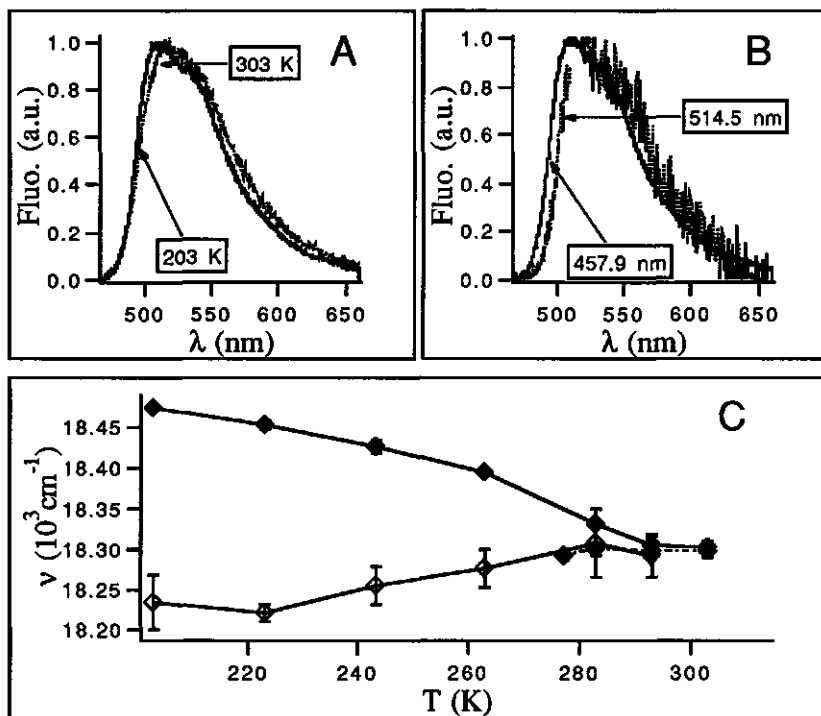


Fig.4: Temperature- and excitation-wavelength dependence of emission spectra of the $\Delta 14$ deletion mutant of lipoamide dehydrogenase from *Azotobacter vinelandii*. A) temperature-dependent shift of emission spectra in 80% glycerol 50 mM KPi pH 7.0 upon 457.9 nm excitation. B) excitation wavelength-dependent shift of emission spectra at 203 K. The points between 512 and 519 nm contain a considerable amount of 514.5 nm laser scattering and were therefore omitted in the spectrum obtained after red-edge excitation. C) center of gravity of fluorescence spectrum expressed on a wavenumber scale as function of temperature and excitation wavelength. Open symbols: 514.5 nm excitation, closed symbols: 457.9 nm excitation, solid lines: data obtained in 80% glycerol 50 mM KPi pH 7.0, broken lines: data obtained in 50 mM KPi pH 7.0.

With an increase of temperature the center of gravity of main-band and red-edge excited fluorescence spectra converge to the same wavenumber (Fig.4C) which shows that the active site of the

protein is converted from a solid-state environment (on a fluorescence time scale) at low temperature, to a state with efficient dipolar relaxation ($\tau_r \ll \bar{\tau}_f$). Comparison of these results with the temperature- and excitation-wavelength dependence of the wild type enzyme clearly shows that the deletion of the 14 C-terminal amino acids has a drastic effect on the dipolar relaxational properties of the active site.

3.6.3 Interpretation of the data according to continuous relaxation models

Upon red-edge excitation a significant bathochromic shift of the emission spectra was observed in 80% glycerol at 203 K in the wild type enzyme whereas no clear shift could be detected in aqueous solution between 277 and 313 K. Furthermore, the spectra of the protein in aqueous solution were red-shifted relative to the spectra obtained in 80% glycerol at all measured temperatures. Since there is practically no interaction of the solvent dipoles with the isoalloxazines in this protein, the results indicate rapid dipolar relaxation in aqueous solution on the time scale of fluorescence emission ($\tau_r \ll \bar{\tau}_f$). Protein dynamics are considerably damped in 80% glycerol at 203 K and dipolar relaxation is slowed down to a time scale beyond that of fluorescence emission. In this situation, the emission is observed from the nonequilibrium Franck-Condon excited states and the bathochromic shift upon edge-excitation is related to the inhomogeneous bandwidth of the spectra reflecting the structural disorder of the dipoles in the neighbourhood of the isoalloxazines. From the plot of $\Delta\nu^{\text{edge}}$ as a function of temperature (Fig.5) it can be seen that the edge-shift at 203 K in LipDH-AV amounts to 100 cm^{-1} whereas 250 cm^{-1} and 650 cm^{-1} were obtained for LipDH- $\Delta 14$ and free FAD, respectively. In the wild type enzyme the isoalloxazine thus exists in a highly ordered dipolar environment which exhibits small amplitude fluctuations in a medium of low viscosity. In the absence of the 14 C-terminal amino acids of LipDH-AV, the solvent dipoles interact with isoalloxazine causing an increased disorder of the dipolar environment with a concomitant increase of the inhomogeneous bandwidth.

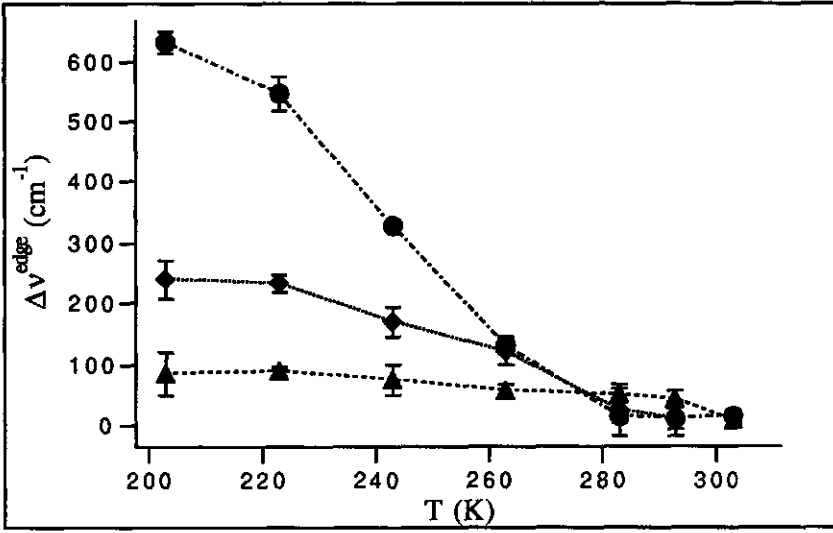


Fig.5: Difference between center of gravity of emission spectra obtained upon main-band and red-edge excitation as function of temperature in 80% glycerol. ●: FAD, ◆: LipDH-Δ14, ▲: LipDH-AV.

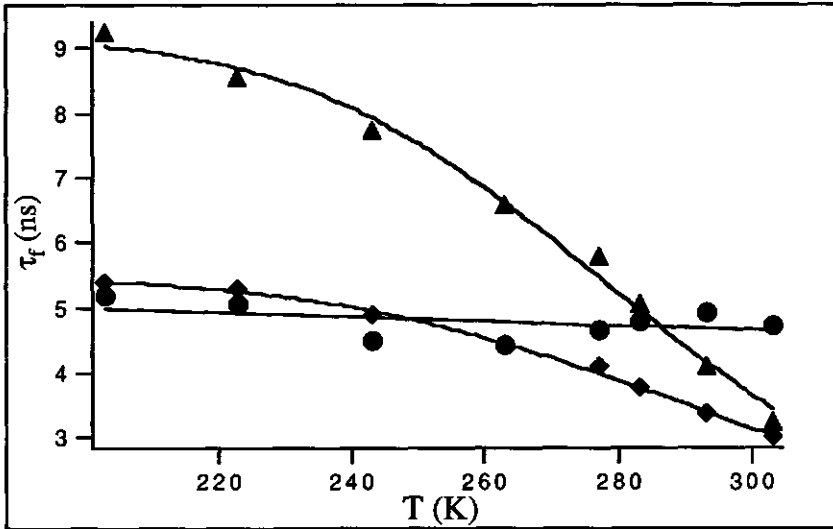


Fig.6: Average fluorescence lifetimes as function of temperature, ▲: LipDH-AV, ◆: LipDH-Δ14, ●: FAD. Solid lines: best fit of data to eq.7.

From the ratio of Δv^{edge} to its limiting value at low temperature (Fig.5), the dipolar relaxation time can be estimated by eq.2 when the average fluorescence lifetime ($\bar{\tau}_f$) as function of temperature is known. The average fluorescence lifetime are obtained from analysis of the fluorescence decays and are presented in Fig.6. The results and details of the analysis are presented elsewhere (chapter 4 of this thesis). In 80% glycerol, both for free FAD and that bound to LipDH- Δ 14 fast dipolar relaxation ($\tau_r \ll \bar{\tau}_f$) is found at temperatures above 263 K whereas rapid relaxation is only found at 303 K for the wild type enzyme (Fig.7A). As mentioned in the preceding section, dipolar relaxation is fast ($\tau_r \ll \bar{\tau}_f$) in aqueous solution for both proteins. In this particular case, the center of gravity of the emission spectra must then coincide with the relaxed energy state (v_∞ of the Bakshiev-Mazurenko model). The dipolar relaxation time of the proteins in 80% glycerol can then be estimated from the time-integrated continuous relaxation model of Bakshiev and Mazurenko (eq.1). Results of this procedure are displayed in Fig.7B. Comparison of the dipolar relaxation times as obtained by the two methods (Figs.7A and 7B), shows that the results are comparable for FAD and LipDH- Δ 14 but not for the wild type enzyme. In this enzyme the values of τ_r determined from eq.1 exceed those of the calculation based on eq.2.

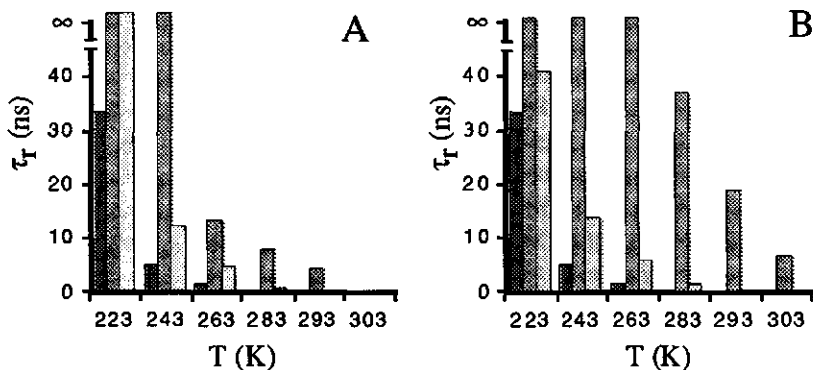


Fig.7: Dipolar relaxation times of free and protein-bound FAD in 80% glycerol. A) Dipolar relaxation times as obtained from the modified Bakshiev-Mazurenko relation applying red-edge excitation (eq.2). B) Dipolar relaxation times as obtained from the Bakshiev-Mazurenko relation (eq.1). From dark- to light-shaded columns or from left to right, FAD, LipDH-AV, LipDH- Δ 14. Each set of 3 columns refers to the temperature indicated at the abscissa.

A possible cause for the discrepancy in the calculation of τ_r by the two methods is a temperature-dependent change of the selection

function S [24]. This parameter is a measure for the photoselection of nonequilibrium solvates, defined as the ratio of the number of nonequilibrium- to the number of equilibrium excited states, immediately after excitation. S will decrease with an increase of the homogeneous bandwidth ($\delta\nu$) relative to the inhomogeneous bandwidth ($\Delta\nu$). The increase of $\delta\nu$ is caused by the increase of Boltzmann population of vibronic energy levels with temperature. With a decrease of S , the photoselection of nonequilibrium solvates will be less favored than that of equilibrium solvates resulting in a smaller apparent magnitude of $\Delta\nu^{edge}$. This decrease will result in an underestimation of the dipolar relaxation time as calculated from eq.2. When $\Delta\nu \ll \delta\nu$ (as for the wild type enzyme), the error in the estimation of τ_r by eq.2 due to a change of S with temperature becomes considerable and τ_r cannot be determined. In this case the Bakshiev-Mazurenko model (eq.1) will lead to a better estimation of τ_r provided that the value of the relaxed energy state is known.

The activation energies of dipolar relaxation as determined from τ_r calculated by eq.1 on Arrhenius coordinates (Fig.8) was 62 ± 10 kJ/mol for LipDH-AV (3 points) and 47 ± 3 kJ/mol for free FAD in 80% glycerol. In an Arrhenius plot of the dipolar relaxation times of LipDH- Δ 14 a breakpoint is observed which is not present for free FAD (Fig.8).

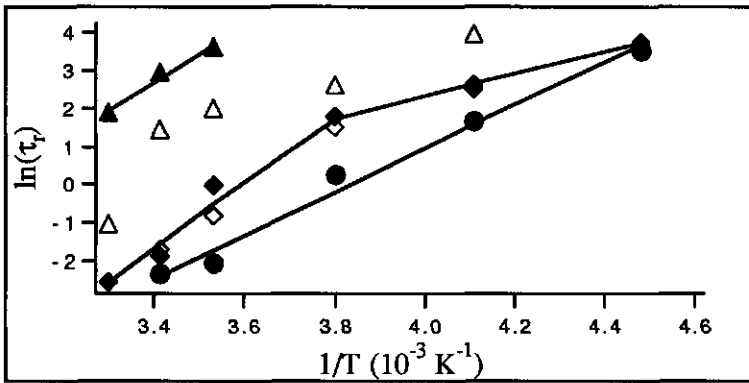


Fig.8: Dipolar relaxation times on Arrhenius coordinates. Open symbols: τ_r as obtained from eq.2, closed symbols τ_r as obtained from eq.1. ▲: LipDH-AV, ◆: LipDH- Δ 14 and ●: free FAD in 80% glycerol 50 mM KPi pH 7.0, solid lines: linear fit of the data.

This nonlinearity can be interpreted as originating from a temperature-induced conformational change, but a more probable interpretation is that the isoalloxazines interact with two types of (dipolar) environments with different relaxational properties. To

each of the environments (i) one can attribute a characteristic dipolar relaxation time τ_i^i whose dependence on temperature (T) is governed by an Arrhenius relation:

$$\frac{1}{\tau_i^i} = k_f^i \exp\left(\frac{-E_i^i}{RT}\right) \quad (6)$$

where k_f^i is the frequency factor (ns^{-1}), E_i^i the activation energy of relaxation of environment i (kJ/mol) and R the gas constant ($8.31 \text{ J mol}^{-1} \text{ K}^{-1}$). The thermal quenching of the fluorescence can be described by a temperature-dependent and a temperature-independent rate process [29]:

$$\frac{1}{\tau_f} = k_f^0 + k_f^1 \exp\left(\frac{-E_f}{RT}\right) \quad (7)$$

where τ_f is the average fluorescence lifetime of the chromophore, k_f^0 the temperature-independent rate constant (ns^{-1}), k_f^1 the frequency factor (ns^{-1}) and E_f the activation energy of thermal quenching (kJ/mol).

Let us assume that the relative energy loss of the excited state ($\Delta v/\Delta v_0$ in the Bakshiev-Mazurenko relation) originates from several (N) independent relaxation processes of equal weight:

$$\frac{\Delta v}{\Delta v_0} = \sum_{i=1}^N \frac{1}{N} \left(\frac{\tau_i^i}{\tau_f + \tau_i^i} \right) \quad (8)$$

By substitution of relations 6 and 7 in to eq.8 one obtains:

$$\frac{\Delta v}{\Delta v_0} = \sum_{i=1}^N \frac{1}{N} \left[1 + \frac{k_f^i \exp\left[\frac{-E_i^i}{RT}\right]}{k_f^0 + k_f^1 \exp\left[\frac{-E_f}{RT}\right]} \right]^{-1} \quad (9)$$

The parameters k_f^0 , k_f^1 and E_f are obtained from a time-resolved fluorescence experiment (chapter 4 of this thesis) where the average fluorescence lifetime as function of temperature is fitted to eq.7 (Fig.6). These parameters are collected in Table 2. The average fluorescence lifetime of free FAD in 80% glycerol is temperature invariant in the measured temperature domain (Fig.6). In that case, only a temperature independent rate constant

is used to describe the thermal behavior of the fluorescence decay (Table 2).

Table 2: Thermal quenching of average fluorescence lifetime of free and bound FAD.

	k_f^0 (MHz)	k_f^1 (THz)	E_f (kJ/mol)
LipDH-AV	109 ± 3	2.7 ± 2.6	24.2 ± 2.4
LipDH-Δ14	183 ± 2	0.55 ± 0.33	20.7 ± 1.5
FAD	189 ± 25	-	-

The fluorescence decay parameters can be fixed in the subsequent analysis of the temperature-dependent energy loss of the excited state to a model describing a single ($N=1$) relaxation process (two parameters: k_f^1 , E_f^1) or a double ($N=2$) relaxation process (four parameters: k_f^1 , E_f^1 , k_f^2 , E_f^2).

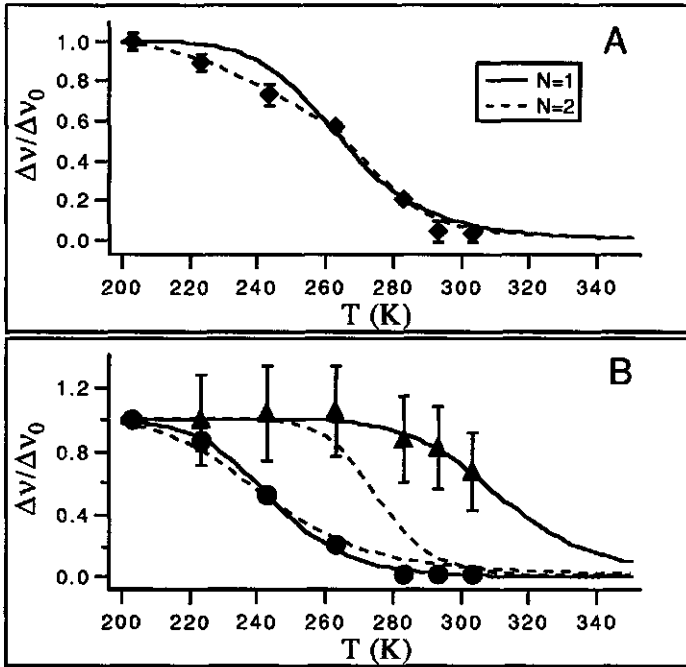


Fig.9: Relative energy loss ($\Delta v/\Delta v_0$) as function of temperature fitted to eq.9. A) \blacklozenge : LipDH-Δ14 in 80% glycerol 50 mM KPi pH 7.0, solid line: fit to a model with a single activation energy, broken line: fit to a model with two activation energies. B) free FAD (\bullet) and LipDH-AV (\blacktriangle) in 80% glycerol 50 mM KPi pH 7.0. Solid line: fit to a model with single activation energy, broken lines: calculated energy losses of the individual relaxational processes in LipDH-Δ14 as obtained from the parameters of the best fit to a $N=2$ model.

As can be seen in Fig.9A we obtained an improved fit by assuming that relaxation in LipDH- Δ 14 originates from two types of environments ($N=2$, $\chi^2 = 1.56$) instead of one ($N=1$, $\chi^2 = 15.6$). The recovered activation energies were 33 ± 14 kJ/mol (first environment) and 83 ± 7 kJ/mol (second environment). We performed a similar fit to the relative energy loss of free FAD in 80% glycerol assuming a single environment ($N=1$, $\chi^2 = 4.9$) and obtained an activation energy of 43 ± 3 kJ/mol. This value is in close agreement with the value obtained from the slope of the Arrhenius plot (47 ± 3 kJ/mol, Fig.8) which shows the validity of the method. The temperature dependence of the individual relative energy losses ($\Delta v/\Delta v_0$) due to the relaxation of the two distinct environments in LipDH- Δ 14 are plotted in Fig.9B together with data of the free chromophore and of the wild type enzyme in 80% glycerol. The similarity in shape of the curve and activation energy of the first environment with that of the free chromophore makes it tempting to assign the first type of relaxation in LipDH- Δ 14 to solvent dipoles and the second to protein dipoles. For LipDH-AV we found an activation energy of 73 kJ/mol assuming a single environment ($N=1$, $\chi^2 = 0.08$). However, the error in the activation energy was completely undetermined due to the small energy loss in the measured temperature region (Fig.9B). From these results we conclude that the activation energy of relaxation is relatively large (>70 kJ/mol) which indicates a rigid dipolar environment on a time scale of fluorescence in LipDH-AV in 80% glycerol.

3.7 Discussion

With the steady-state iodide quenching experiments in aqueous solution we demonstrated that the isoalloxazines in the wild type and deletion mutant of LipDH-AV are located in different environments. The larger bimolecular rate constant of quenching (k_q) in LipDH- Δ 14 points to an enhanced solvent accessible active site over the wild type enzyme. Although one may argue that a net negative charge in the vicinity of the isoalloxazines is the predominant factor which causes shielding of iodide ions in the wild type enzyme, this is contradicted by the temperature invariance of the emission spectra in 80% glycerol in contrast to LipDH- Δ 14. If indeed the active site would be solvent accessible, one would expect the solvent dipoles to interact with the flavins causing temperature-dependent relaxational shifts as observed in LipDH- Δ 14. Another possible cause which could lead to an apparent increase of k_q in the deletion mutant, is a larger

dissociation constant of the FAD-apo-enzyme complex. In that case a substantial fraction would be free in solution and accessible to iodide ions. This possibility can also be disregarded as:

- i) molecular sieve chromatography was applied prior to any measurement
- ii) the spectral parameters of the emission spectra of free FAD and that bound to LipDH- Δ 14 are different
- iii) the Stern-Volmer plot of the Δ -14 mutant does not exhibit concave upward behavior which is typical for two classes of fluorophores with different accessibility [30]
- iv) energy transfer between the cofactors in the mutant protein is observed indicating that FAD is still bound and the $\alpha\alpha$ -quaternary structure preserved (chapter 4 of this thesis).

The local electronic and relaxational properties of the flavins in the deletion mutant were shown to be different from the wild type enzyme although the gross structure is conserved [22]. By red-edge excitation at 203 K we found a small inhomogeneous bandwidth in the wild type enzyme (≈ 100 -150 cm^{-1}) which was substantially larger in LipDH- Δ 14 ($\approx 250 \text{ cm}^{-1}$). This observation reveals the highly structured character of the protein matrix in the vicinity of the flavins in the wild type enzyme. Exposure of the flavins to the isotropic dipole distribution of the solvent (as in the deletion mutant) creates an increase of the inhomogeneous bandwidth and a concomitant increase of the selection function upon red-edge excitation. Rapid dipolar relaxation between 203-303 K was only found in LipDH- Δ 14 where we could resolve two independent relaxational processes. One process with the lower activation energy (≈ 30 -45 kJ/mol) was assigned to solvent relaxation and the other with the larger activation energy (≈ 80 kJ/mol) to protein dipole relaxation. If dipolar relaxation is coupled to the dynamic properties of the protein, the latter higher activation energy reflects the ordered rigid protein structure in the vicinity of the active site. In LipDH-AV where the flavin is predominantly surrounded by protein dipoles, dipolar relaxation in 80% glycerol was ineffective ($\tau_r \gg \bar{\tau}_f$) in the measured temperature interval. The activation energy of relaxation (>70 kJ/mol) was in the same order as that found for one of the relaxational processes in LipDH- Δ 14 which is an indication that we are observing the same dynamic behavior of the protein matrix in both proteins in 80% glycerol. The removal of the 14 C-terminal

amino acids has a most drastic effect on the Lip(SH₂) binding site which comprises amino acid residues from both subunits [21, 22]. Since the Lip(SH₂) binding site is composed of amino acid residues of both subunits and removal of the 14 C-terminal amino acids destabilizes the dimer we expect that the C-terminal tail folds back into the Lip(SH₂) binding site thereby shielding the active site from the solvent. Both in the wild type enzyme and in the deletion mutant rapid small amplitude fluctuations of (protein) dipoles in the vicinity of the isoalloxazines take place in aqueous solution. It would then be of interest to investigate the coupling between enzyme catalysis and the dynamics of the active site by studying the effect of different viscosogens on enzyme kinetic parameters and dipolar relaxation in these systems [31].

Another experimental method by which the dipolar relaxational properties of the active site can be investigated is by monitoring energy transfer between the flavin cofactors. From crystallographic data it is known that the isoalloxazinic parts of the FAD's are separated by approximately 3.9 nm [21]. Calculation of the relevant parameters of the Förster equation shows that energy transfer between the cofactors is possible and measurable (chapters 2 and 4 of this thesis). Both the excitation energy and the dipolar relaxational properties of the active sites will have a large influence on the efficiency of this process [8, 24]. Upon main-band excitation the efficiency of energy transfer in the wild type enzyme in 80% glycerol should be practically temperature invariant as the S₀₋₁ transition energy of the flavins is approximately constant between 203-303 K (both absorption and emission spectra are indicative for that). In LipDH-Δ14, however, energy transfer should become less efficient with an increase of temperature due to long-wave shift of the emission spectra which causes a decrease in the overlap integral. The most drastic effects are expected upon red-edge excitation. Due to the small selection function in the wild type enzymes the probability of energy transfer will hardly decrease upon edge excitation. Furthermore, the slow relaxational properties of the protein matrix will again cause a temperature invariance of this process. In contrast, the probability of energy transfer in LipDH-Δ14 will drastically decrease upon edge excitation at low temperature (203 K) due to the substantial inhomogeneous broadening. Upon elevation of temperature, fast dipolar relaxation will cause both an increase and an excitation-energy invariance in the efficiency of energy transfer. Such experiments corroborate the findings on the dynamic properties of the active sites as reported in this study (chapter 4 of this thesis).

3.8 References

1. Teale, F.W.J. (1960) *Biochem. J.*, 76, 381-388.
2. Weber, G. (1960) *Biochem. J.*, 75, 335-345.
3. MacGregor, R.B. and Weber, G. (1981) *Ann. N.Y. Acad. Sci.*, 366, 140-154.
4. MacGregor, R.B. and Weber, G. (1986) *Nature*, 319, 70-73.
5. Demchenko, A.P. (1982) *Biophys. Chem.*, 15, 101-109.
6. Demchenko, A.P. (1985) *FEBS Lett.*, 182, 99-102.
7. Demchenko, A.P. (1986) *Essays in Biochemistry* 22, 120-157
8. Demchenko, A.P. (1987) *Ultraviolet Spectroscopy of Proteins* pp. 145-172, Springer-Verlag, Berlin.
9. Demchenko, A.P. (1988) *TIBS*, 13, 374-377.
10. Demchenko, A.P. (1988) *Eur. Biophys. J.*, 16, 121-129.
11. Weber, G. (1950) *Biochem. J.*, 47, 114-121.
12. Visser, A.J.W.G., Grande, H.J., Müller, F. and Veeger, C. (1974) *Eur. J. Biochem.*, 45, 99-107.
13. Visser, A.J.W.G. and Müller, F. (1979) *Helv. Chim. Acta*, 62, 593-608.
14. Visser, A.J.W.G., Penners, N.H.G., van Berkel, W.J.H. and Müller, F. (1984) *Eur. J. Biochem.*, 143, 189-197.
15. Visser, A.J.W.G. (1989) *Time-Resolved Fluorescence Studies of Flavins in: Fluorescent Biomolecules* (Jameson, D.M. and Reinhart, D. eds.) pp. 319-341. Plenum Press, New York.
16. Williams Jr, C.H. (1976) *The Enzymes*, 13, 89-173.
17. Reed, L.J. and Oliver, R.M. (1986) *Brookhaven Symp. Biol.*, 21, 397-412.
18. McCully, V., Burns, G. and Sokatch. (1986) *Biochem. J.*, 233, 737-742.
19. Westphal, A.H. and de Kok, A. (1988) *Eur. J. Biochem.*, 172, 299-305.
20. Schierbeek, A.J., Swarte, M.B.A., Dijkstra, B.W., Vriend, G., Read, R.J., Hol, W.G.J., Drenth, J. and Betzel, C. (1989) *J. Mol. Biol.*, 206, 365-379.
21. Mattevi, A., Schierbeek, A.J. and Hol, W.G.J. (1991) *J. Mol. Biol.*, 220, 975-994.
22. Schulze, E., Benen, J.A.E., Westphal, A.H. and de Kok, A. (1991) *Eur. J. Biochem.*, 200, 29-34.
23. Rubinov, A.N. and Tomin, V.I. (1970) *Optics Spectrosc. (USSR)*, 29, 1082-1086.
24. Nemkovich, N.A., Rubinov, A.N. and Tomin, V.I. (1991) *Inhomogeneous Broadening of Electronic Spectra of Dye Molecules in: Topics in Fluorescence Spectroscopy* (Lakowicz, J.R. ed.) Vol 2, pp 367-428, Plenum Press, New York.

25. Galley, W.C. and Purkey, R.M. (1970) *Proc. Natl. Acad. Sci USA*, 67, 1116-1121.
26. Mazurenko, Y.T. and Bakhshiev, N.G. (1970) *Optics Spectrosc. (USSR)*, 28, 905-913.
27. Eftink, M.R. and Ghiron, C.A. (1981) *Anal. Biochem.*, 114, 199-227.
28. Visser, A.J.W.G. (1984) *Photochem. Photobiol.*, 40, 703-706.
29. Bushueva, T.L., Busel, E.P. and Burstein, E.A. (1977) *Biochim. Biophys. Acta*, 534, 441-452.
30. Lehrer, S.S. (1971) *Biochemistry*, 10, 3254-3263.
31. Demchenko, A.P., Rusyn, O.I. and Saburova, E.A. (1989) *Biochim. Biophys. Acta*, 998, 196-203.

Chapter 4

Conformational Dynamics and Intersubunit Energy Transfer in Wild Type and Mutant Lipoamide Dehydrogenase from *Azotobacter vinelandii*.

A multidimensional time-resolved polarized fluorescence study.

Bastiaens, P.I.H., van Hoek, A., Benen, J.A.E., Brochon, J.C. and Visser, A.J.W.G.

Abstract

Time-resolved fluorescence and fluorescence anisotropy data surfaces of FAD bound to lipoamide dehydrogenase from *Azotobacter vinelandii* in 80% glycerol have been obtained by variation of excitation energy and temperature between 203-303 K. The fluorescence kinetics of a deletion mutant lacking 14 C-terminal amino acids was compared to the wild type enzyme in order to study a possible interaction of the C-terminal tail with the active site of the enzyme. The FAD fluorescence in both proteins exhibits a bimodal lifetime distribution as recovered by the maximum entropy method of data analysis. The difference in standard enthalpy and entropy of associated conformational substates was retrieved from the fractional contributions of the two lifetime classes. Activation energies of thermal quenching were obtained which confirm that the isoalloxazines in the deletion mutant are solvent accessible in contrast to the wild type enzyme. Red-edge spectroscopy in conjunction with variation of temperature provides the necessary experimental axes to interpret the fluorescence depolarization in terms of intersubunit energy transfer rather than reorientational dynamics of the flavins. The results can be explained by a compartmental model which describes the anisotropy decay of a binary, inhomogeneously broadened homo-energy transfer system. By using this model in a global analysis of the fluorescence anisotropy decay surface, the distance between and relative orientation of the two flavins are elucidated. For the wild type enzyme this geometrical information is in agreement with crystallographic data of the *A. vinelandii* enzyme whereas the mutual orientation of the subunits in the deletion mutant is slightly

altered. In addition, the ambiguity in the direction of the emission transition moment in the isoalloxazine ring is solved. The anisotropy decay parameters provide also information on electronic and dipolar relaxational properties of the flavin active site. The local environment of the prosthetic groups in the deletion mutant of the *A. vinelandii* enzyme is highly inhomogeneous and a transition from slow to rapid dipolar relaxation is observed over the measured temperature range. In the highly homogeneous active site of the wild type enzyme dipolar relaxation is slowed down beyond the time scale of fluorescence emission at any temperature studied. Our results are in favor of a C-terminal polypeptide interacting with the active site thereby shielding the isoalloxazines from the solvent. This biological system forms a very appropriate tool to test the validity of photophysical models describing homo-energy transfer.

4.1 Introduction

Flavoproteins belong to a class of proteins with appropriate photophysical properties to study protein dynamics and structure by time-resolved fluorometric methods. The intrinsically fluorescent prosthetic group of most of these proteins is either FAD or FMN which both have the spectroscopically relevant isoalloxazine in common. The fluorescence properties of the isoalloxazinic ring vary largely among different flavoproteins reflecting the variety in structure and dynamical properties of the active sites containing the flavin compounds [1-6].

The 100 kDa flavoprotein lipoamide dehydrogenase of the class of disulfide-oxidoreductases has a dimeric quaternary structure containing one FAD per subunit. The protein catalyses the NAD⁺-dependent oxidation of the covalently attached dihydrolipoyl groups of lipoate acyltransferase in different multienzyme complexes such as the pyruvate dehydrogenase- and 2-oxoglutarate complex [7-10]. This flavoprotein has several distinct advantages to study dynamics and structure by time-resolved fluorescence spectroscopy. First, it is a flavoprotein with an unusually high quantum yield of flavin fluorescence (240% of free FAD). Second, the gene encoding lipoamide dehydrogenase from *Azotobacter vinelandii* has been cloned and overexpressed in *Escherichia coli* [11] providing large quantities of protein and means to modify the physical properties of the active site near the fluorescent FAD. Third, the crystal structure of the *A. vinelandii* enzyme has been solved to 0.22 nm resolution which enables topological comparison with different spectroscopic methods [12].

Previously, fluorescence studies have been performed on lipoamide dehydrogenase from pig heart and from bacterial sources [4, 5, 13]. The fluorescence decay was shown to be slightly heterogeneous and could be fitted to a triple exponential decay model. The fluorescence anisotropy decay was composed of two components [4]. One correlation time was assigned to protein rotation in the solvent but the physical origin of the correlation time of about 12 ns with small amplitude was unclear and was tentatively assigned to restricted subunit motion.

In this study we have examined the time-resolved fluorescence of lipoamide dehydrogenase from *Azotobacter vinelandii* (LipDH-AV) and a deletion mutant of LipDH-AV, lacking 14 C-terminal amino acids (LipDH- Δ 14) [14]. 10 C-terminal amino acids of LipDH-AV are not visible on the electron density map from which it was concluded that they are disordered [12]. However, recently it was also proposed that a C-terminal polypeptide of 10 amino acids in lipoamide dehydrogenase from *Pseudomonas putida* is in interaction with the binding cleft of dehydrolipoamide [15]. This interaction possibly also occurs in LipDH-AV as is substantiated by the large influence of the solvent on the dielectric properties near the flavin in LipDH- Δ 14 in contrast to the wild type enzyme (chapter 3 of this thesis). This solvent effect causes an increased statistical spread in the electronic energy levels of ground and excited state (inhomogeneous broadening) reflecting the multiple solvent dipole configurations interacting with the chromophore [16, 17]. A comparative time-resolved polarized fluorescence study of both wild type and deletion mutant of lipoamide dehydrogenase will lead to insight in the dynamic structure surrounding the flavins and will assist in the verification of existing theories on spectral inhomogeneous broadening, dipolar relaxation and energy transfer.

In the last decade both time-correlated single-photon counting and multifrequency phase fluorometry became highly sophisticated, enabling data collection with a high signal to noise ratio and data density [18-21]. In conjunction with this development considerable improvements in data analysis emerged over the classical treatment of fitting fluorescence decays by a sum of discrete exponentials. Two main approaches have appeared. The inverse Laplace transform of the fluorescence or fluorescence anisotropy decay is obtained by fitting the data to a distribution of parameters in the maximum entropy method (MEM) [22-24]. The advantage of this method is that no *a priori* knowledge of the distribution model is needed. This type of analysis is well suited for complex fluorescence decay behavior

encountered in biological macromolecules where multiple interchanging conformations give rise to semicontinuous sets of lifetime distributions. When *a priori* knowledge of the system is present, multiple fluorescence decays as a function of different experimental independent variables (temperature, excitation wavelength) can be analyzed with global analytical procedures to a model encompassing multiple interrelated parameters. This computational method which exploits the physical invariants of a model allows for better model discrimination and parameter recovery than multiple single curve analysis [25, 26]. In this study both methods of data analysis are applied to the fluorescence and fluorescence anisotropy decays of lipoamide dehydrogenase in highly viscous media.

The goal of this investigation is threefold:

- i) To obtain insight in the kinetic and thermodynamic properties of conformational substates in lipoamide dehydrogenase
- ii) to ascertain whether the short component in the anisotropy decay may originate either from intersubunit energy-transfer between the FAD prosthetic groups or from restricted flavin motion
- iii) to investigate the influence of dipolar relaxation and site selective excitation on energy transfer.

To achieve this goal we have measured time-resolved polarized fluorescence of the enzymes in 80% glycerol as function of temperature and excitation energy.

4.2 Materials and Methods

4.2.1 Biochemical preparations

The plasmid-encoded LipDH-AV and deletion mutant LipDH- Δ 14 expressed in *E. coli* TG2 were purified as described before [11]. The enzyme preparations were stored at -70 °C in 100 mM potassium phosphate buffer, pH 7.0, 0.5 mM EDTA. The samples were defrosted at room temperature the morning before an experiment and 300 μ l aliquots were chromatographed on a Biogel PGD-6 (Biorad) column (1 x 6 cm) equilibrated with 250 mM potassium phosphate buffer, pH 7.0 to eliminate unbound FAD. All buffers were made with nanopure water prepared on a millipore water

purification system. The enzyme preparations were brought to 80% (v/v) glycerol by gently mixing 100 μ l from the eluted sample with 400 μ l of 100% glycerol (Merck fluorescent grade) until a homogeneous solution was obtained. Enzyme concentrations were determined with a molar extinction coefficient of $\epsilon_{457} = 11.3 \text{ mM}^{-1} \text{ cm}^{-1}$ [11]. Care was taken that all final preparations had a concentration of 10-15 μ M.

FAD was purified on a Biogel P-2 (Biorad). 100 μ l aliquots of this preparation were mixed with 400 μ l glycerol to a final concentration of 10 μ M.

4.2.2 Instrumental

Decays of fluorescence and fluorescence anisotropy were measured using the time-correlated single photon counting technique [18]. For excitation with light of either 514.5 or 457.9 nm a mode-locked cw argon-ion laser was used (Coherent Radiation model CR18). The rate of the light pulses was decreased from 76 MHz to 596 kHz by an electro-optic modulator set-up in a dual-pass configuration [27]. Excitation pulses were about 100 ps full width at half maximum with energies in the picojoule region.

Samples volumes were 0.5 cm^3 and 1 cm lightpath cuvetts, placed in a thermostated holder were used. This holder was placed in a sample housing also containing optics. Extreme care was taken to avoid artefacts from depolarizing effects. At the front of the sample housing a Glan-laser polarizer was mounted, optimizing the already vertical polarization of the input light beam. The fluorescence was collected at an angle of 90° with respect to the direction of the exciting light beam. Between sample and photomultiplier (MCP, Hamamatsu model 1645U) a single fast lens (uncoated fused silica), a rotatable sheet polarizer, a filter compartment and a single focussing lens (uncoated fused silica) were placed.

The polarizer sheet was in a dc motor-driven ball-bearing holder with mechanical stops allowing computer controlled rotation (0.2 s) to parallel and perpendicular polarized detection of emission. The sheet polarizer was a polaroid type HN38 for the green to red region. Filters used for wavelength selection of emission were a KV 550 cut-off and a 557.9 nm interference filter with 10 nm bandpass (Schott). The sample and photomultiplier housings were home built. Polarizers were aligned carefully and when measuring reference samples of known anisotropy it was found that no correction factor was necessary (g-factor = 1).

For sample temperatures down to 203 K a liquid nitrogen flow set-up was used with a temperature controller (Oxford model ITC4). At these low temperatures experiments can easily be disturbed by the depolarizing effect of condensation of water from the surrounding air on the cuvet. Therefore the sample housing was extended in height and filled with a steady stream of the relatively heavy argon gas onto the cuvet walls. The final temperature of the sample appeared to be in balance with different heat sources (cold nitrogen, room temperature argon gas, the heater of the controller and heat radiation), and care was taken to control the true sample temperature. Furthermore the cuvetts were exchanged wearing surgical gloves. In this way samples could be easily exchanged over a period of a few hours without dew and ice problems.

Detection electronics were standard time-correlated single photon counting modules [18]. A photon frequency of 30 kHz (5% of 596 kHz) was used [28] to prevent pile-up distortion. Also other instrumental sources for distortion of data were minimized [29] to below the noise level of normal photon statistics. Measurements consisted of a number of sequences of measuring 10 s parallel and 10 s perpendicular polarized emission until a content in the data sets of $3.5 \cdot 10^6$ counts for the reference compound and $5 \cdot 10^6$ counts for the sample was reached. The time-window consisted of 1024 channels at 20 ps per channel. For deconvolution of the data the reference convolution method was used [28]. The reference compound was erythrosine B in methanol. One complete measurement consisted of measuring the polarized fluorescence decays of the reference compound, the sample, the background and again the reference compound. Background fluorescence decay was sampled at one fifth of the time of the sample acquisition time and was always below 2% of the sample intensity. Manipulation and fitting of the data were performed on a microVAX computer.

Emission spectra at different temperatures were recorded using this same set-up by replacing the optical filters between the sample and the photomultiplier by a computer controlled monochromator (two tandemized 0.25m monochromators, F/3.5 Jarrel Ash model 82.410) and adapting lenses. The sheet type polarizer in the detection pathway was placed under magic angle with respect to the polarization of the excitation light. Furthermore emission photons (via a constant fraction discriminator, CFD, Canberra model 1428A) were not used now to trigger the start-stop sequence of the time to amplitude converter (Ortec model 457), but photon pulses via the CFD were directly fed to the multichannel scaling input of the multichannel analyzer (Nuclear Data model ND66

equipped with both a ND582 ADC and a ZDT-MCS zero dead time multichannel scaling unit). The channel stepping of the MCS was synchronized by the controller of stepper motor of the monochromator. The bandwidth of the monochromator was 6 nm for the spectra with 457.9 nm excitation and 1.5 nm for the spectra with 514.5 nm excitation. The emission spectra were converted from technical into molecular spectra using a computer program containing the transmission characteristics of the monochromator and the photomultiplier.

Temperature-dependent excitation spectra were recorded on a DMX-1000 (SLM Aminco, Urbana, IL). Spectra were recorded in the ratio mode to correct for the spectral output of excitation monochromator and lamp combination. The temperature in the sample holder was controlled by the same set-up as used in the acquisition of the emission spectra described above. Both the excitation and emission bandwidths were set at 4 nm, the emission detection wavelength was fixed at 580 nm. Overlap integrals between excitation and emission spectra were determined on a Macintosh SE/30 microcomputer using the program IGOR (wavemetricsTM).

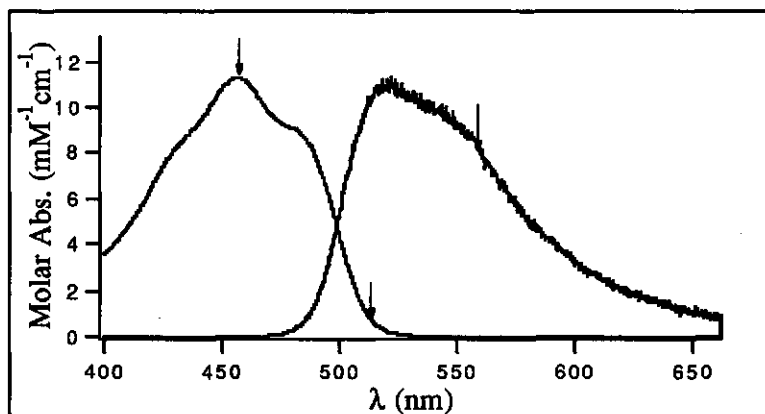


Fig.1: Absorption and emission spectra of LipDH-AV at 293 K in 80% glycerol, 50 mM KPi, pH 7.0. The arrows on the absorption spectrum indicate main band (457.9 nm) and red-edge (514.5 nm) excitation. The arrow on the emission spectrum is pointed at the maximal transmission of the interference filter used in the detection path. The emission spectrum was normalized to the maximum absorbance of LipDH-AV.

4.2.3 Generation of fluorescence data surface

In Fig.1 the normalized absorption and fluorescence spectra of LipDH-AV in 80% glycerol 50 mM K₂HPO₄, pH 7.0 at 293 K are shown. The data surface was generated by collecting the parallel and perpendicular polarized component of the time-resolved fluorescence upon separate excitations (457.9 nm and 514.5 nm) at 203, 223, 243, 263, 283, 293 and 303 K. Both polarized decays were collected in the 1024 channels of a multichannel analyzer, temporarily stored in a PC and transferred to the microVAX.

4.2.4 Data analysis

The data were analyzed with the commercially available second generation global analysis package (Globals UnlimitedTM, Urbana, IL) and with the maximum entropy method (FAME, Maximum Entropy Data Consultants Ltd., Cambridge U.K.). The principles of both analysis methods will be shortly outlined in relation to the protein system under investigation. The parallel $I_{\parallel}(t)$ and perpendicular $I_{\perp}(t)$ fluorescence intensity components were acquired after excitation with vertically polarized light. With the maximum entropy method (MEM) the image ($\alpha(\tau)$) of the total fluorescence intensity $i(t)$ after δ -pulse excitation is given by the Laplace transform [22]:

$$i(t) = i_{\parallel}(t) + 2 i_{\perp}(t) = \int_0^{\infty} \alpha(\tau) e^{-t/\tau} d\tau \quad (1)$$

The image $\alpha(\tau)$ is recovered by maximizing the Shannon-Jaynes entropy function S_{SJ} [22]:

$$S_{SJ} = \int_0^{\infty} \alpha(\tau) - m(\tau) - \alpha(\tau) \log \frac{\alpha(\tau)}{m(\tau)} d\tau \quad (2)$$

and minimizing the χ^2 (data) fitting criterium:

$$\chi^2 = \frac{1}{M} \sum_{k=1}^M \left(\frac{I_k^{\text{calc}} - I_k^{\text{obs}}}{\sigma_k} \right)^2 \quad (3)$$

where $m(\tau)$ is the starting model of the distribution chosen to be flat in $\log(\tau)$ space as this introduces the least correlations between the parameters $\alpha(\tau)$ [22]. The superscripts calc and obs on I denote the observed and calculated intensity in channel k of the multichannel analyzer, M is the total amount of channels used in the analysis of the fluorescence decay (typically 1024 channels) and σ_k^2 is the variance in channel k . For an optimal fit of the data χ^2 should approach unity [22]. In the analysis of the total fluorescence decay of protein bound FAD, 150 equally spaced values on a $\log(\tau)$ scale between 0.01 and 20 ns were used. The starting model $m(\tau)$ was chosen to be flat in $\log(\tau)$ space since no *a priori* knowledge about the system was present.

One is able to recover from fluorescence anisotropy experiments the complete 3-D image which is given by $\gamma(\tau, \phi, r_0)$ representing the number of fluorophores with lifetime τ , rotational correlation time ϕ and initial anisotropy r_0 [22]. If one assumes *a priori* that there is no correlation between τ and ϕ (non-associative modeling) the images $\alpha(\tau)$ and $\beta(\phi)$ are independent as shown for the parallel and perpendicular fluorescence intensity components:

$$i_{\parallel}(t) = \frac{1}{3} \int_0^{\infty} \alpha(\tau) e^{-t/\tau} d\tau \int_0^{\infty} (1 + 2\beta(\phi)) e^{-t/\phi} d\phi \quad (4)$$

$$i_{\perp}(t) = \frac{1}{3} \int_0^{\infty} \alpha(\tau) e^{-t/\tau} d\tau \int_0^{\infty} (1 - \beta(\phi)) e^{-t/\phi} d\phi \quad (5)$$

the integrated amplitude $\beta(\phi)$ corresponds to the fundamental anisotropy r_0 . In the (one-dimensional) anisotropy analysis one obtains a spectrum of amplitudes β against correlation times ϕ . Similar considerations regarding the starting model in the recovery of $\alpha(\tau)$ apply to the recovery of $\beta(\phi)$, *i.e.* if one has no *a priori* knowledge of the distribution one should start with a flat spectrum in $\log(\phi)$ space.

The final image $\alpha(\tau)$ of the fluorescence decay was introduced as a fixed image in the analysis of the anisotropy decay. As a starting model, 100 equally spaced values on a $\log(\phi)$ scale (from 0.1 to 100 ns) were used in the analysis and a limiting anisotropy was encoded since protein rotation is inhibited in 80% glycerol.

The following approach was used in the global analysis of the fluorescence and fluorescence anisotropy decay surfaces. The total fluorescence intensity curves were constructed from the parallel and perpendicular decay files (eq.1). Background fluorescence was subtracted from the data and weighting factors were calculated as described by Vos *et al.* [28]. Multiple experiments were simultaneously analyzed using the model and parameter link schemes given in the Results section. The obtained fluorescence decay parameters were fixed in the analysis of the fluorescence anisotropy. Parallel and perpendicular decay files were subsequently constructed from the raw data with appropriate correction for background fluorescence and weighting [28]. The fluorescence anisotropy surface was fitted to models described in the theory section by a global approach where all parameters of the individual parallel and perpendicular polarized components were completely linked and simultaneously analyzed [26]. In all cases non-associative modeling was used in the analysis of the fluorescence anisotropy decay. In the temperature- and excitation wavelength-dependent experiments the linking schemes of fluorescence anisotropy parameters are given in the Results section. All fits were subjected to rigorous error analysis based on an exhaustive search along each parameter axis allowing all other parameters to vary so as to find a minimum χ^2 . This method takes into account all higher order correlation which may exist between the recovered parameters. From this analysis the identifiability of a model and the standard error of the parameters can be determined [26].

4.3 Results

4.3.1 Total fluorescence decay

The inverse Laplace transforms of the fluorescence decays of LipDH-AV and LipDH- Δ 14 in 80% glycerol upon 457.9 nm excitation (main-band) are represented as function of temperature in 3-D plots in Fig.2. The residuals of the fits were randomly distributed around zero indicating that the parameters of the lifetime spectra were optimized (not shown). For both proteins a bimodal distribution in lifetime space was found with a tendency to collapse into a single broad distribution upon lowering the temperature.

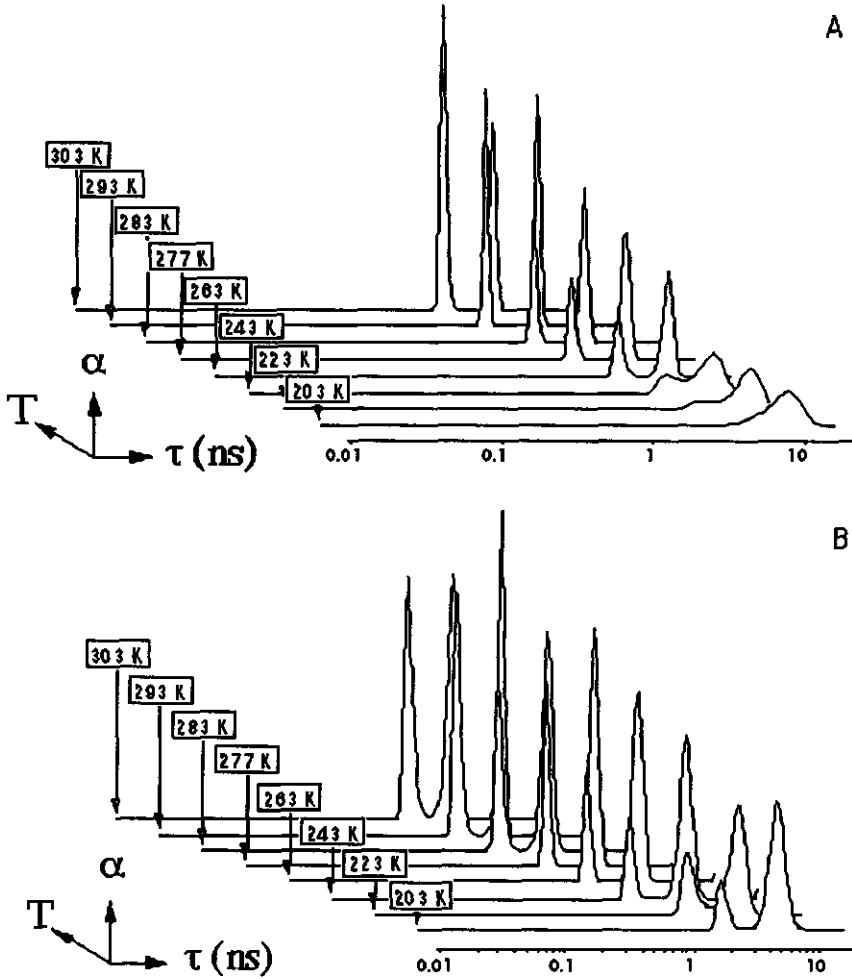


Fig.2: Temperature-dependence of fluorescence decay of lipoamide dehydrogenase upon 457.9 nm excitation in 80% glycerol, 50 mM KPi, pH 7.0. Panel A: inverse Laplace transforms of fluorescence decays of LipDH-AV. Panel B: inverse Laplace transforms of fluorescence decays of LipDH- $\Delta 14$.

The two lifetime classes of the protein-bound flavin cannot correspond to an equilibrium between "stacked" and "extended" FAD conformations [30] since they are bound in an extended conformation [12]. The possibility that the flavins have different lifetimes in each subunit of the protein can also be disregarded since a constant ratio of the integrated amplitudes would be expected at all temperatures. The two peaks in the lifetime spectrum can then be assigned to conformational substates of the protein. The fractional contributions of the peaks are proportional to the relative populations of these substates when the exchange between protein conformations (k_{exc}) is much slower than the depopulation of the excited state (k_f) [31].

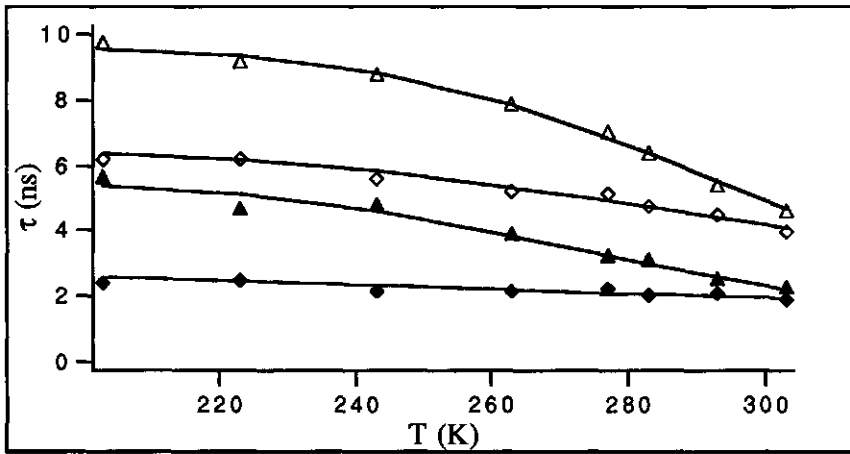


Fig.3: Temperature dependence of barycenters of the lifetime distributions. (\blacktriangle): LipDH-AV, (\blacklozenge) LipDH- Δ 14, open symbols: longest lifetime class, closed symbols: shortest lifetime class, solid lines: best fit of data to eq.8.

Examination of the barycenters of the peaks [23] as function of temperature (Fig.3) shows that these do not converge upon increase of temperature. Slow exchange between substates ($k_{exc} \ll k_f$) thus takes place in this temperature range.

From the ratio of the normalized fractional contribution of the peaks (α_1/α_2) the equilibrium constant (K) of conformational exchange is obtained. The standard enthalpy difference between states (ΔH^0) can then be calculated from the van 't Hoff equation:

$$\Delta H^0 = -R \frac{d \ln(\alpha_1/\alpha_2)}{d(1/T)} \quad (6)$$

where T is the temperature in Kelvin and R the gas constant ($8.31 \text{ JK}^{-1}\text{mol}^{-1}$). The van 't Hoff plots of the equilibrium constants of protein-bound FAD are presented in Fig.4. The plot of LipDH- $\Delta 14$ deviates from linearity below 263 K. At these temperatures, the conformational states in LipDH- $\Delta 14$ are not at equilibrium. The activation barrier between states is apparently smaller in LipDH-AV since the van 't Hoff plot is linear over the whole temperature range (equilibrium attained). In order to determine ΔH^0 the linear part of the plot was used (203-303 K for LipDH-AV and 243-303 K for LipDH- $\Delta 14$). From the slope we found a ΔH^0 of $13.2 \pm 1.5 \text{ kJ/mol}$ for LipDH- $\Delta 14$ and $11.4 \pm 1.5 \text{ kJ/mol}$ for LipDH-AV.

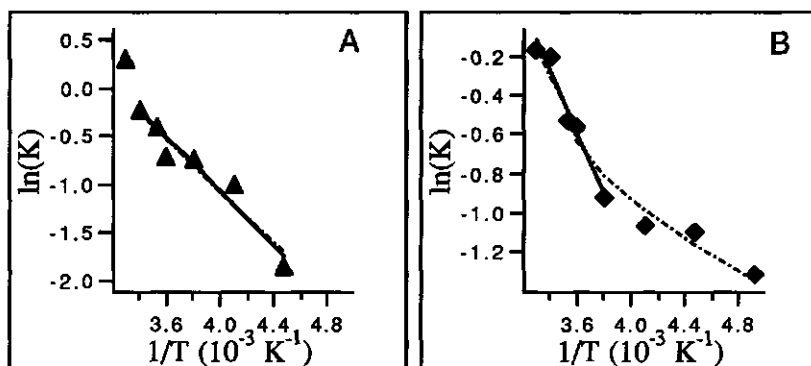


Fig.4: van 't Hoff plot of equilibrium constants of conformational transition. Panel A: data for LipDH-AV, panel B: data for LipDH- $\Delta 14$. Solid lines: linear fit to experimental data.

The standard entropy difference (ΔS^0) between states is obtained from the temperature dependence of the free energy (ΔG^0):

$$\frac{d\Delta G^0}{dT} = -\Delta S^0 \quad (7)$$

ΔG^0 for both proteins is plotted as function of temperature in Fig.5.

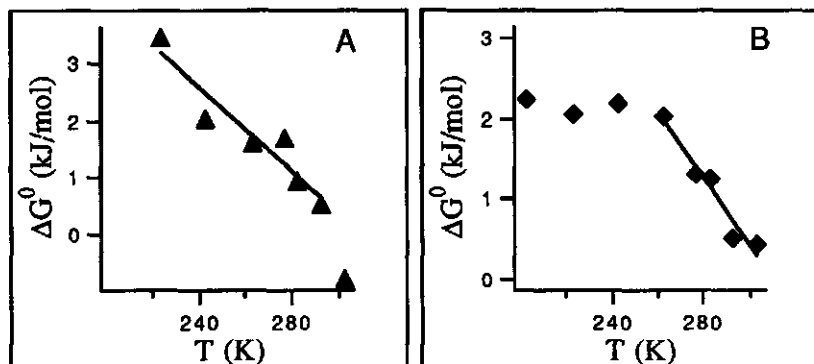


Fig.5: Free energy of conformational transition as function of temperature. Panel A: data for LipDH-AV, panel B: data for LipDH- $\Delta 14$. Solid lines: linear fit to experimental data.

From the slope of the plots we obtained a ΔS^0 of $36 \pm 6 \text{ JK}^{-1}\text{mol}^{-1}$ for LipDH-AV (fit region: 223-293 K) and $42 \pm 6 \text{ JK}^{-1}\text{mol}^{-1}$ for LipDH- $\Delta 14$ (fit region: 263-303 K). Entropy increase is thus the "driving force" for the population of the conformational state associated with the smallest average lifetime.

From the plot (Fig.3) of the barycenters as function of temperature it can be seen that the flavins are located in different environments in both proteins. The fluorescence rate constants were not linear on Arrhenius coordinates (not shown) and they approach to a constant value at low temperature. The deactivation of the excitation energy of the intrinsic fluorophores by adjacent residues is then governed by a thermally activated and temperature-independent radiative constants [32]:

$$\frac{1}{\tau_i(T)} = k_0^i + k_1^i \exp\left(\frac{-E_i^i}{RT}\right) \quad (8)$$

where $\tau_i(T)$ is the lifetime of the flavin in conformation i at temperature T in ns, k_0^i is the temperature-independent rate constant in ns^{-1} , k_1^i is the frequency factor in ns^{-1} , E_i^i the effective activation energy of thermal deactivation in J/mol . The barycenters were fitted to eq.8 with T as the independent variable (Fig.3). In addition, a global analysis of the fluorescence decay surface assuming two non-interacting compartments was performed where 8 fluorescence

decays (203-303 K) were analyzed simultaneously with the k_0^i , k_1^i and E_f^i ($i = 1, 2$) linked over all experiments. We obtained an optimized fit with global χ^2 of 1.08 and 1.09 for LipDH-AV and LipDH- $\Delta 14$, respectively. Both residual surfaces were randomized around zero indicating a correct implementation of the model to the system (not shown). Both types of analysis gave comparable results with the advantage of the global analysis that the error in the parameters can be estimated (Table 1). The two activation energies of thermal quenching in each individual conformation of both proteins are significantly different. The activation energy associated with the shortest lifetime class is smaller than the one associated with the longest lifetime class, indicating a more rigid local protein matrix surrounding the isoalloxazines in the conformation associated with the longer fluorescence lifetime. The difference in local amino acid residue dynamics in both states could account for the positive entropy difference as found from equilibrium thermodynamic considerations.

In the partially exposed isoalloxazine in LipDH- $\Delta 14$, interaction of the flavin with the solvent causes effective internal conversion to the ground state. This leads to an elevated temperature-independent rate constant, a smaller frequency factor and smaller activation energy of thermal quenching as compared to the shielded flavin in the wild type protein (Table 1).

Table 1: Fluorescence decay parameters

	k_0^1 (GHz)	k_1^1 (THz)	E_f^1 (kJ/mol)	k_0^2 (GHz)	k_1^2 (THz)	E_f^2 (kJ/mol)
LipDH-AV	0.18* 0.22† (0.13-0.26)	0.82* 1.1† (0.02-7)	20* 20† (13-23)	0.10* 0.10† (0.087-0.11)	3.2* 2.9† (2-20)	26* 25† (23-33)
LipDH- $\Delta 14$	0.35* 0.30† (0.27-0.33)	0.004* 0.017† (0.016-0.2)	7.5* 11† (6.6-24)	0.15* 0.14† (0.13-0.14)	0.063* 0.065† (0.050-0.35)	17* 16† (16-22)

*: Values obtained by fitting the barycenters of the fluorescence lifetime distributions as function of temperature to eq.8.

†: Values obtained from a simultaneous (global) analysis of 8 decay curves. The numbers between brackets are the errors obtained from a rigorous error analysis with 67% confidence.

The advantage of MEM in the analysis of the fluorescence data is that additional information can be extracted which is not *a priori*

encoded in the analysis. An example is the half width (FWHM) of the lifetime distributions which showed a trend with temperature (Fig.6). In all the experiments the total number of counted photons was approximately equal. In that case one can reasonably assign a physical meaning to the relative widths of the distributions as recovered by MEM, since the signal to noise ratio should be comparable in every experiment. The FWHM of a lifetime class at temperature T is related to two factors:

- i) the number of conformational substates
- ii) the relative rate of interconversion between states

At 203 K the interconversion is assumed to be slow on a fluorescence time scale and therefore the width is mainly determined by the number of conformational substates. This number can be ranked by the magnitude of the FWHM at the lowest temperature. By examining Fig.6 A-B it is clear that the population of conformational substates is largest in the wild type enzyme. A decrease in the FWHM with temperature can be interpreted as an increase in the rate of exchange between subconformations. The half widths of the two lifetime distributions of LipDH-AV on Arrhenius coordinates show a clear breakpoint at 243 K (Fig.6A inset). A similar transition at the same temperature is observed in the barycenters of the two lifetime distributions of LipDH-AV (Fig.3). The empirical activation energy determined from the slope of the Arrhenius plot of the FWHM between 243 and 303 K is 20 ± 2 kJ/mol for both distributions. This energy is comparable with the activation energy of thermal quenching (Table 1). For LipDH- Δ 14 the breakpoint at 243 K was less apparent but also present in the Arrhenius plot of the FWHM of the longer lifetime component (Fig.6B inset). The activation energies were 4 ± 1 kJ/mol for the shorter lifetime component and 7 ± 2 kJ/mol for the longer lifetime component. These activation energies are lower than those of thermal quenching (Table 1) but demonstrate the smaller temperature dependence of the lifetime distributions of FAD bound to LipDH- Δ 14. Quenching of flavin fluorescence is caused by collisional interaction with local amino acid residues which can be interpreted as a transition from one conformational coordinate to another. It can then be conceived that the transition between conformational substates, as reflected in the decrease of the FWHM, is the origin of the thermal quenching.

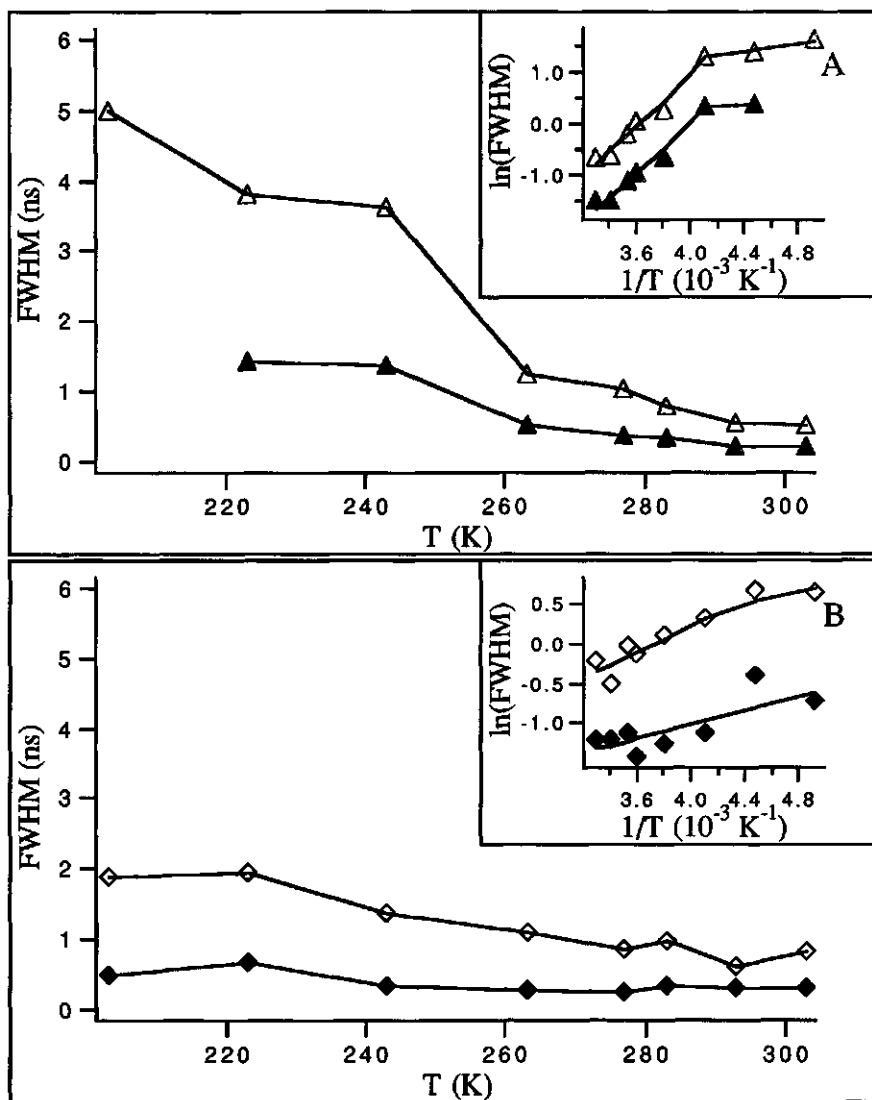


Fig.6: Full width at half maximum (FWHM) of lifetime distributions as function of temperature. Open symbols: longest lifetime class, closed symbols: shortest lifetime class. Panel A: LipDH-AV, Panel B: LipDH- $\Delta 14$. Figure insets: FWHM on Arrhenius coordinates.

4.3.2 Fluorescence anisotropy decay

To ascertain whether another process than protein tumbling alone causes depolarization of fluorescence in lipoamide dehydrogenase and to obtain a qualitative insight in the physical origin of this depolarizing mechanism we will focus on a few two-dimensional slices of the experimental anisotropy decay data surfaces of LipDH-AV and LipDH- Δ 14. In Fig.7 the fluorescence anisotropy decays of LipDH-AV in 80% glycerol at 203.15 (A) and 293 K (B) excited at 457.9 nm are depicted together with the anisotropy decays of free FAD under the same conditions. The fluorescence of the relatively small molecule FAD (596 Da) does not depolarize at 203.15 K in the experimental time window, whereas the fluorescence of FAD bound to the large macromolecule LipDH-AV (100 kDa) exhibits a clear depolarization. This shows that, because protein tumbling is effectively abolished under such conditions, that another process is causing depolarization of the fluorescence in LipDH-AV. At 293.15 K the fluorescence of free FAD depolarizes due to Brownian molecular rotation whereas in a first approximation the anisotropy decay of LipDH-AV can be superimposed to the one at 203 K. This lack of temperature variance is the first qualitative indication that the mechanism of depolarization is not due to restricted rotation but to intersubunit energy transfer between the flavins. The same phenomena were observed for LipDH- Δ 14 (not shown).

Failure of energy transfer between like molecules is known to occur in systems where the dipolar relaxation time (τ_r) exceeds the average fluorescence lifetime (τ_f) [17, 33]. Upon excitation of the proteins at 514.5 nm we found an increase in the anisotropy as compared to the samples excited at 457.9 nm (Fig.7C-D). We thus have a second indication that the depolarization of the fluorescence is caused by energy transfer between the flavins. The magnitude of this effect and the relaxation rate of the anisotropy is dependent on the properties of the dipolar surroundings of the chromophores as outlined below.

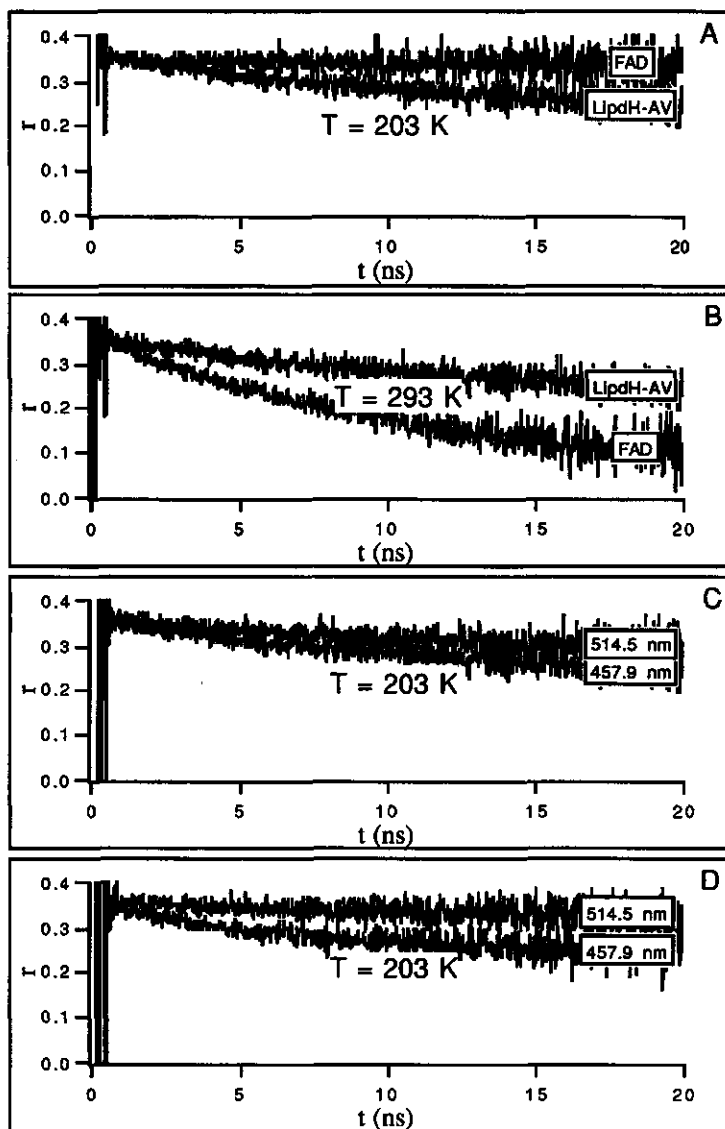


Fig.7: Temperature- and excitation wavelength-dependence of experimental time-dependent fluorescence anisotropy. Panels A and B: comparison of fluorescence anisotropy of free and protein-bound FAD at 203 K and 293 K upon main-band excitation (457.9 nm). Panels C and D: fluorescence anisotropy of LipDH-AV (C) and LipDH- Δ 14 (D) at 203 K upon main-band (457.9 nm) and red-edge (514.5 nm) excitation.

The inverse Laplace transform of the fluorescence anisotropy decays (Fig.8A) upon main-band excitation (457.9 nm) contains two regions of interest. At all measured temperatures (203-303 K), a peak is resolved for LipDH-AV with an integrated amplitude (scattered) around 0.08 ± 0.01 . The barycenter (7.7 ± 1.5 ns) of this peak does not show a significant trend with temperature. At the long-correlation time edge of the spectrum the amplitude continuously increases (Fig.8A). This limiting anisotropy of 0.28 ± 0.01 originates from the rotational immobilization of the protein in the highly viscous solvent on a time scale of fluorescence emission.

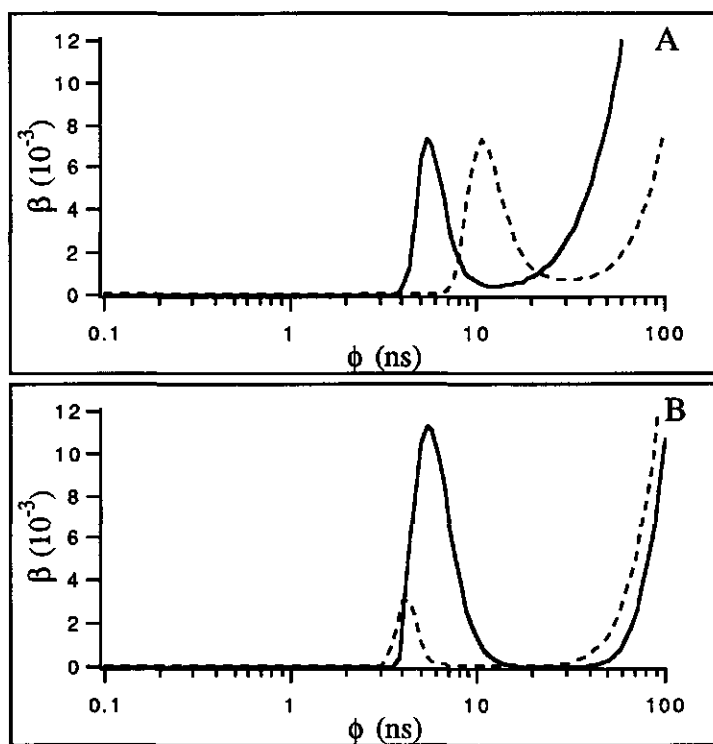


Fig.8: One-dimensional MEM analysis of fluorescence anisotropy decays of LipDH-AV (A) and LipDH- Δ 14 (B) at 203 K. Solid line: correlation-time spectrum obtained after 457.9 nm excitation, broken line: correlation time spectrum obtained after 514.5 nm excitation.

The anisotropy decay is thus composed of a single relaxation process (or unimodel relaxation distribution) with a constant term. A similar correlation-time spectrum was found for LipDH- Δ 14 with a

somewhat shorter value for the average of the barycenters (5.1 ± 1.2 ns) and similar average sum of amplitudes (0.07 ± 0.02), taken over the measured temperature domain (Fig.8B).

Upon red-edge excitation (514.5 nm), the correlation-time spectrum is again composed of a unimodal distribution and a limiting anisotropy in both proteins (Fig.8A, B). However, the integrated amplitude of the unimodal distribution around 5 ns in LipDH- Δ 14 is strongly diminished upon red-edge excitation at 203 K (Fig.8B) and only a slight decrease of total amplitude is observed for LipDH-AV.

In order to quantify these phenomena let us assume that intersubunit energy transfer between the flavins is the physical mechanism which causes the observed depolarization of the fluorescence in lipoamide dehydrogenase. For a homogeneous binary system where the independent states have equal rates of depopulation of the excited state, the time-dependent anisotropy $r(t)$ is given by [34] :

$$r(t) = \frac{3}{5(r_1+r_2)} \left[\frac{r_1 k_{21} + r_2 k_{12}}{k_{12} + k_{21}} (3\cos^2 \delta - 1) + \frac{r_1 k_{12} + r_2 k_{21}}{k_{12} + k_{21}} (3\cos^2 \theta - 1) \right. \\ \left. + \left(\frac{r_1 k_{21} + r_2 k_{12}}{k_{12} + k_{21}} (3\cos^2 \delta - 1) - \frac{r_1 k_{21} + r_2 k_{12}}{k_{12} + k_{21}} (3\cos^2 \theta - 1) \right) e^{-(k_{12} + k_{21})t} \right] \quad (9)$$

where r_1 and r_2 are the fractional absorptions at excitation wavelength λ of monomer 1 and 2 respectively and k_{12} and k_{21} are the rates of energy transfer from monomer 1 to 2 and *vice versa*. The parameters δ and θ in the pre-exponential amplitude and limiting anisotropy are the intramolecular and intermolecular angle, respectively, between absorption and emission transition moments in the binary system. The intermolecular angle of absorption and emission transition moments from monomer 1 to monomer 2 (θ_1) is equated to the intermolecular angle from monomer 2 to monomer 1 (θ_2) as these can not be separately resolved (three unknowns in a system of two linear equations). Note that in this expression the energy of transition from ground to excited state does not need to be the same in monomer 1 and 2. Upon main-band excitation of an inhomogeneously broadened system, the most probable energy configuration (Fig.9A) of monomer 1 and 2 is excited with equal probability so that $r_1 = r_2$ and $k_{12} = k_{21} = k_T$.

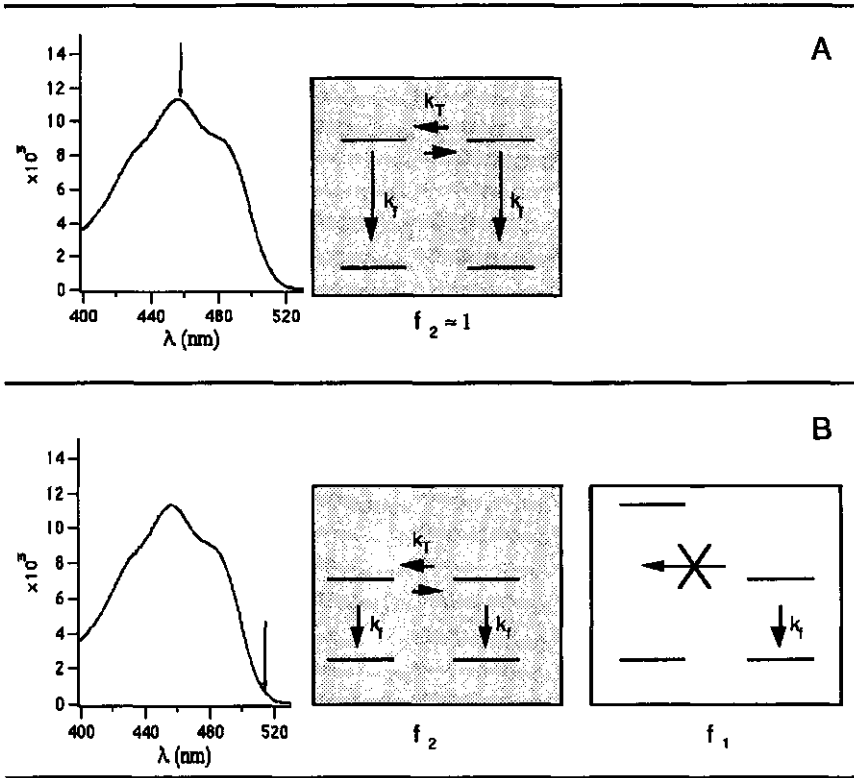


Fig.9: Compartmental model for excitation energy dependence of energy transfer. Absorption spectrum with an arrow on the excitation wavelength is shown together with a schematic energy diagram with ground and excited states in a dimer. k_T is the rate of energy transfer, k_f is the rate of fluorescence emission, f_1 is the fractional population of dimers in which energy transfer does not take place and f_2 is the fractional population of dimers in which energy transfer occurs. Panel A: Main-band excitation, the fractional population of dimers in unfavorable energy configuration for transfer is approximately zero ($f_1 \approx 0$). Panel B: Red-edge excitation, a considerable fraction of excited dimers is in an energy configuration unfavorable for transfer ($f_1 > 0$). Note that the energy separations between ground and excited states in the red-edge excited molecules, are smaller than in the case of main-band excitation.

Eq.9 reduces to the expression derived by Tanaka and Mataga [34] for a dimeric system with a unique spatial configuration:

$$r(t) = \frac{1}{10} [3\cos^2 \delta + 3\cos^2 \theta - 2 + \{3\cos^2 \delta - 3\cos^2 \theta\} e^{-2k_T t}] \quad (10)$$

The pre-exponential amplitude and the limiting anisotropy are functions of the relative geometrical arrangement of the transition moments of the interacting moieties. This geometrical arrangement is independent of temperature if there are no temperature-dependent conformational changes in the proteins. Consequently when the data surface obtained from main-band excitation is fitted to an exponential anisotropy decay function plus a constant term:

$$r(t) = \beta_1 e^{(-t/\phi_T)} + \beta_2 \quad (11)$$

the amplitudes β_i must be physical invariants along the temperature axis.

Upon red-edge excitation, photoselection of nonequilibrium solvate energy configurations can take place even in a situation where the homogeneous bandwidth exceeds the inhomogeneous one [33]. A solvate is in this case defined as a fluorophore and its immediate (protein) environment. In a system, with rapidly reorienting dipolar environment ($\tau_r < \tau_f$) in the high temperature regime, uprelaxation causes emission or weak dipole-dipole interaction to take place from a non-equilibrium energy state, irrespective of excitation wavelength [35, 36]. Consequently the system is analogous to the main-band excited case and the β_i should be physical invariants of excitation wavelength and temperature. When dipolar relaxation is much slower than fluorescence emission ($\tau_r \gg \tau_f$) up-relaxation is slowed down and energy transfer or emission of a photon will take place from a nonequilibrium excited state with minimal energy separation between ground and excited state [17, 35, 36]. In this case the most probable energy configuration of the dimer will be that of an unequilibrium excited state together with an acceptor in an equilibrium ground state energy configuration (Fig.9B). In this configuration, energy transfer will be endothermic and cannot take place. It will only take place in dimers where the acceptor-protein matrix system have equal or smaller magnitude of the transition energy than the excited donor. The system can be treated as consisting of two compartments. One compartment with a fractional population of f_1 which is not able to transfer energy and one compartment with fractional population of f_2 which is able to transfer energy ($f_1 + f_2 = 1$). The expression for the anisotropy decay is constructed from the Weber's addition law [37] assuming that both compartments have equal quantum yields:

$$r(t) = \frac{1}{10} [3(2 - f_2)\cos^2 \delta + 3f_2\cos^2 \theta - 2 + f_2(3\cos^2 \delta - 3\cos^2 \theta)] e^{-2k_T t} \quad (12)$$

The anisotropy is again described by an exponential and constant term analogous to eq.11. In case of red-edge excitation, the β_i are not physical invariants of temperature since f_2 is dependent on the dipolar relaxational properties of the protein matrix and on photoselection of unequilibrium solvates. From the anisotropy decay curves obtained after main-band excitation, the δ and θ can be determined so that the fractional populations (f_1, f_2) can be calculated from the amplitudes of the red-edge excited anisotropy decays.

The additional relation we can impose upon the parameters of eq.11 at different temperatures (T) and excitation wavelengths (λ) is between the correlation times of transfer $\phi_T(T, \lambda)$ which is reciprocally related to the rate of energy transfer k_T :

$$\phi_T = \frac{1}{2k_T} \quad (13)$$

The rate of energy transfer k_T is related to geometrical and spectral parameters by the Förster equation (chapter 1). The overlap integral J, which is a spectral parameter of the Förster equation, depends on the shape and relative position of the absorption and fluorescence emission spectrum of the interacting luminophores of the binary homotransfer system in question. J will be dependent on excitation wavelength and temperature since the emission spectrum is dependent on the dipolar relaxational properties of the protein matrix (Fig.10A). The $\phi_T(T_i, \lambda_j)$ are then related through the experimentally determined overlap integrals $J(T_i, \lambda_j)$:

$$\frac{\phi_T(T_i, \lambda_j)}{\phi_T(T_k, \lambda_l)} = \frac{J(T_k, \lambda_l)}{J(T_i, \lambda_j)} \quad (14)$$

The abovementioned relations between parameters of the energy transfer model (eq.11) can be introduced as *a priori* knowledge into a global analysis of the anisotropy decay surfaces. The parameter link schemes can be represented in matrix notation where one dimension represents the parameters of the model and the other dimension the experiment number [26]. Globally linked parameters will have the same logic number in the matrix. The large amount of experiments performed on the proteins made it

unpractical to list each experiment number separately in the global link matrix. Instead the experiments have been divided in two categories in Table 2. The division between categories is based on excitation energy. Two entries are presented in the matrix where the first numerical entry represents the intercategory linkage and the second alphabetical entry represents the intracategory linkage.

Table 2: Link matrix

TYPE OF EXPERIMENT:	parameters		
	β_1	β_2	ϕ_T^1
$\lambda_{ex}=457.9$ nm	1	3	5
80%glycerol T=203-303 K	a.l.	a.l.	a.l.
$\lambda_{ex}=514.5$ nm	2	4	5
80%glycerol T=203-303 K	n.l.	n.l.	a.l.

1) Transfer correlation time linked by a $1/J(T, \lambda_{ex})$ vector.

a.l.: all parameters within category linked
n.l.: all parameters within category not linked

Table 3: Fluorescence anisotropy fit parameters

Sample:	β_1	β_2	ϕ_T (ns)	global χ^2	
				linked	unlinked
LipDH-AV	0.106† (0.098-0.120) 0.0759* (0.014)	0.245† (0.228-0.252) 0.279* (0.015)	8.46† (6.8-11.2) 7.73* (1.52)	1.01	1.00
LipDH-Δ14	0.0909† (0.090-0.102) 0.0675* (0.023)	0.260† (0.248-0.263) 0.283* (0.022)	5.43† (4.5-7.2) 5.12* (1.21)	1.04	1.02

† : Values as obtained from the global analysis of the data surface. The numbers between brackets are the errors as determined from a rigorous error analysis with a 67% confidence interval.

* : Average values as obtained from the MEM analysis of the individual decay curves. The average was taken from the inverse Laplace transforms of the decays at 7 temperatures (203-303 K). The numbers between brackets are the standard deviations.

The J-normalized transfer correlation time and amplitudes obtained from the global fit of the anisotropy data surfaces to eq.11 with the link scheme as in Table 2 are presented in Table 3 together with the global χ^2 when no linkages were imposed between the

parameters. The values of the global χ^2 are close to unity and comparable in the two cases indicating the correct implementation of the more stringent link scheme in Table 2. The residual surfaces were randomly scattered around a $z=0$ surface (Fig.12) which shows that eq.11 is a proper model to describe the anisotropy decay of LipDH-AV and LipDH- $\Delta 14$ in 80% glycerol.

By summation and subtraction of the amplitudes β_1 and β_2 , information on intra- and intermolecular angles of absorption and emission transition moments in the isoalloxazines of the FAD's in lipoamide dehydrogenase can be obtained:

$$\beta_2 + \beta_1 = \frac{3}{5} \cos^2 \delta - \frac{1}{5} \quad (15)$$

$$\beta_2 - \beta_1 = \frac{3}{5} \langle \cos^2 \theta \rangle - \frac{1}{5} \quad (16)$$

where the brackets in eq.16 denote an average of the two values ($\langle \cos^2 \theta \rangle = 1/2[\cos^2 \theta_1 + \cos^2 \theta_2]$). In the isoalloxazine ring the emission and absorption transition moments are not parallel which manifests itself experimentally in a value of the anisotropy of 0.35 at time $t=0$ which is lower than the fundamental anisotropy of 0.4. From eq.15 we obtained a value of 17° for δ . The direction of the absorption transition moment relative to the pseudo symmetry axis of the flavin is known ($\psi = -32^\circ$) [38] which gives two possibilities for the direction of the emission transition moment ($\zeta = -15^\circ$ or -49°), provided that it lies in the plane of the molecule. The crystallographic coordinates of the isoalloxazine rings in LipDH-AV together with the values of the anisotropy decay parameters β_1 and β_2 , allow us to calculate the absolute position of the emission transition moment in the isoalloxazine ring bound to the dimeric protein. The angles θ_1 and θ_2 can be calculated from crystallographic coordinates and the directions of the absorption and emission transition moments in the molecular planes of both isoalloxazines in the subunits. For the direction of the emission transition moment there are two possibilities giving two sets of angles θ_1 and θ_2 . From the direction of $\zeta = -47^\circ$ we obtained a value of 0.37 for $\beta_2 - \beta_1$ which is in disagreement with the experimentally obtained value (0.14 for LipDH-AV: Table 3) whereas the direction $\zeta = -15^\circ$ yielded $\beta_2 - \beta_1 = 0.13$ in closer agreement with experiment. With the directions of the transition moments known in the flavin structure we can calculate the orientation factor κ^2 [39] from crystallographic data. We obtained

the values $\kappa^2 = 3.23$ and $\kappa^2 = 3.35$ for both directions of energy transfer. An estimation of the distance between the centers of the isoalloxazines can be made by substituting the rate of transfer k_T and the experimental overlap integral $J(T, \lambda)$ in the Förster equation [40] with a value for the refractive index $n=1.4$ [41] and radiative rate $\lambda_d=0.056 \text{ ns}^{-1}$ [42].

Table 4: Geometric parameters

sample:	geometry from anisotropy decay parameters.			geometry from crystallographic data.		
	R(nm) ¹	δ (deg) ²	ϵ (deg) ³	R(nm) ⁴	ϵ_1 (deg) ⁵	ϵ_2 (deg) ⁵
LipDH-AV	4.0 (3.8-4.2)	16.6 (16.6-17.1)	138.7 (135.8-140.2)	3.9	138.4	137.9
LipDH- Δ 14	3.7 (3.6-3.9)	16.6 (16.3-16.8)	141.7 (139.4-142.0)	-	-	-

1) Interflavin distance as obtained from the Förster equation with $n=1.4$, $\lambda_d=0.0556 \text{ ns}^{-1}$ and $\kappa^2=3.29$.

2) Intramolecular angle between absorption and emission moments obtained from eq. 18.

3) Intermolecular angle between absorption and emission moments obtained from eq. 19.

4) Interflavin distance calculated from crystallographic coordinates where the center of the isoalloxazines has been taken in the middle of the N5 and N10 atoms

5) Intermolecular angle between absorption and emission from crystallographic coordinates in both directions of energy transfer.

Numbers between brackets are the errors as determined from the rigorous error analysis with a 67% confidence interval.

The calculated distances can be compared to the distance directly obtained from crystallographic coordinates in LipDH-AV. In case that the orientation factor would be an unknown, only an upper limit of the distance can be calculated [39]. The interflavin distance and angular parameter θ derived from fluorometric and crystallographic data are in excellent agreement for LipDH-AV (Table 4) which shows the validity of the used model. In comparison, the upper limit for the distance between the prosthetic groups is slightly smaller and the angle θ is slightly larger for LipDH- Δ 14. This result suggests that the geometric arrangement of the subunits in LipDH- Δ 14 is different to that of the wild type enzyme.

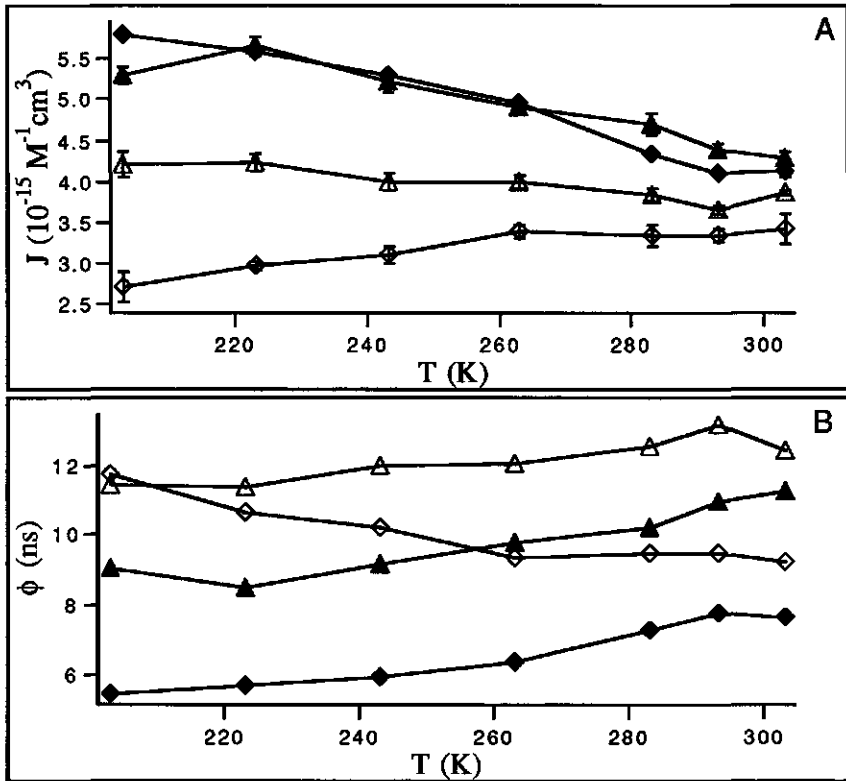


Fig.10: Temperature and excitation wavelength dependence of overlap integrals. (panel A) and transfer correlation-times (panel B) (▲): data for LipDH-AV, (◆): data for LipDH-Δ14, open symbols: red-edge excitation (514.5 nm), closed symbols: main-band excitation (457.9 nm).

The transfer correlation function $\phi_T(T, \lambda)$ as function of temperature is shown in Fig.10B. Due to the red-shift of the emission spectra upon 514.5 nm excitation with a concomitant decrease in J as compared to main-band excitation, an increase of the transfer correlation function is obtained upon red-edge excitation. The decrease of the probability of energy transfer upon edge excitation is not uniform for the wild type and mutant proteins. The values of $\phi_T(T, 514.5)$ of LipDH-Δ14 exhibit a much stronger temperature dependence and converge to the values of $\phi_T(T, 457.9)$ upon increase of temperature. The convergence of the $\phi_T(T, \lambda)$ in LipDH-Δ14 shows that the dipolar surroundings of the isoalloxazines is converted from a solid state environment ($\tau_r \gg \tau_f$) to an environment with efficient

dipolar relaxation ($\tau_r \ll \tau_f$). The $\phi_T(T, \lambda)$ values of LipDH-AV do not converge as efficiently indicating a highly rigid environment in the measured temperature domain.

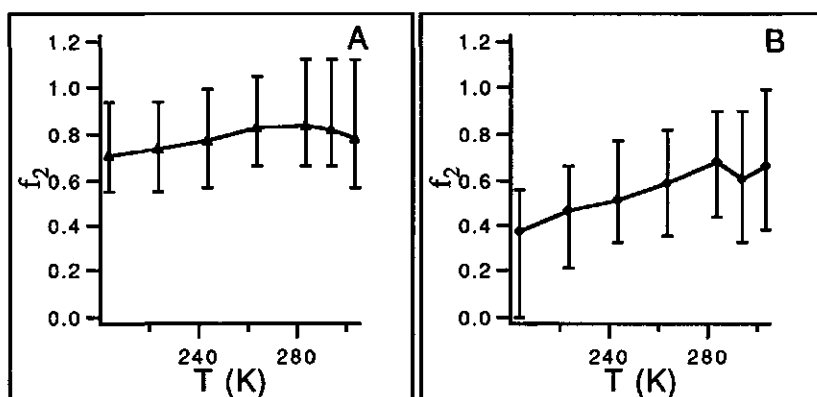


Fig.11: Fractional population (f_2) of transferring molecules upon edge excitation. Panel A: data for LipDH-AV, panel B: data for LipDH- $\Delta 14$.

The fractional population of transferring molecules (f_2) at a certain temperature can be calculated from the ratio of β_1 obtained at red-edge and main-band excitation (Fig.11A-B). Comparison of the f_2 -values of the two proteins at 203 K shows that the fractional population of photoselected unequilibrium solvates in LipDH-AV is much smaller than for LipDH- $\Delta 14$. The magnitude of the selection function depends on the relative width of the inhomogeneous broadening function as compared to the homogeneous broadening function. The deletion mutant has thus a more heterogeneous population of active sites as compared to the wild type enzyme. Furthermore, the fractional population of transferring protein molecules increases with temperature in LipDH- $\Delta 14$ whereas f_2 is practically temperature invariant in LipDH-AV.

The increase of f_2 with temperature in the deletion mutant is caused by a transition from a static to a dynamic inhomogeneously broadened system. Rapid relaxation of the surrounding (solvent) dipoles at higher temperatures causes energy transfer to take place from equilibrium excited states. It is remarkable that f_2 does not reach unity whereas rapid relaxation is observed for free FAD in 80% glycerol at temperatures above 263 K (chapter 3 of this thesis). This result is in agreement with a model where the modulation of the solvate energy levels is governed by two environments. One

environment with a small activation energy (solvent relaxation) and one with a higher activation energy (protein relaxation).

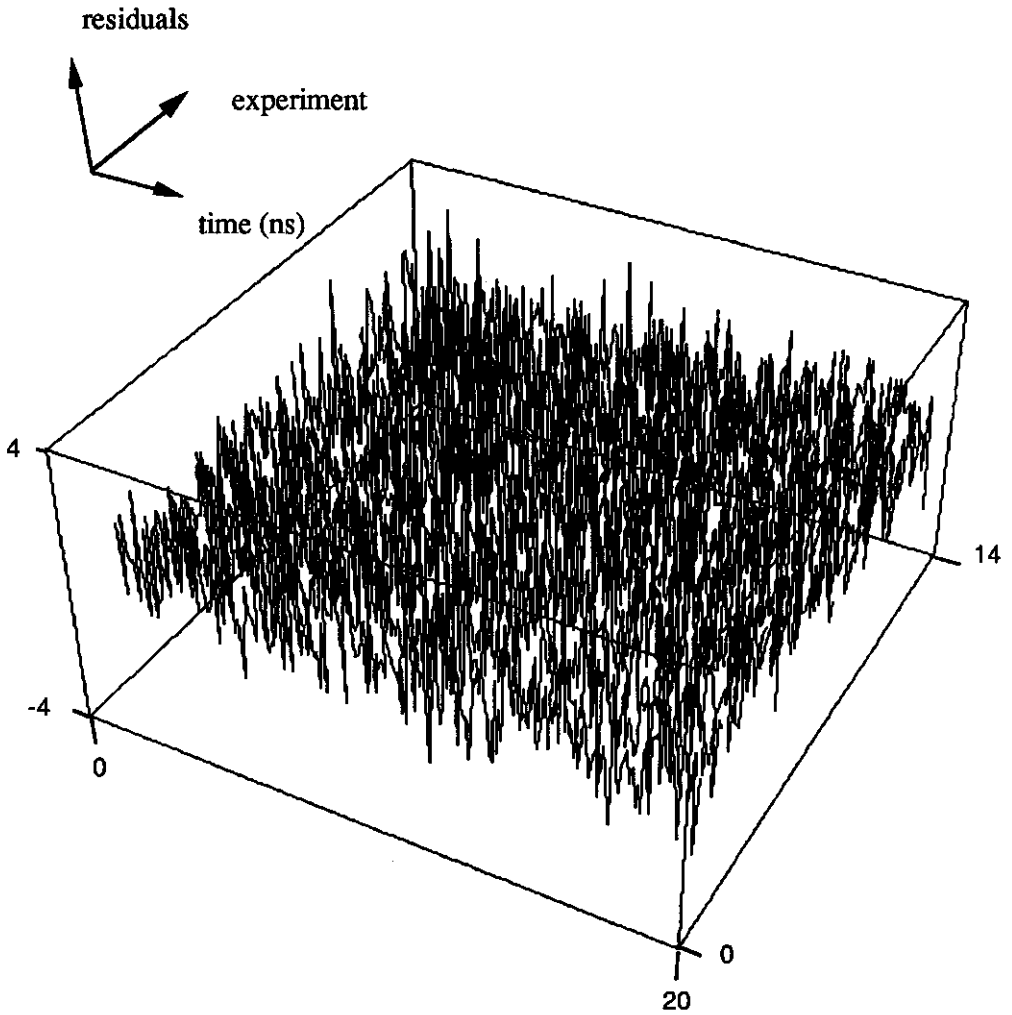


Fig.12: Weighted fluorescence anisotropy decay residual surface of the global fit of the fluorescence anisotropy decay of LipDH-AV to eqs. 10 and 12. The residual surface of the global fit of the fluorescence anisotropy decay of LipDH-D14 exhibited a similar pattern (not shown).

4.4 Discussion

In both LipDH-AV and LipDH- Δ 14 in 80% glycerol we observed a minimum of two lifetime classes as revealed by the inverse Laplace transforms of the fluorescence decays. Decrease of the fractional contribution of the shorter lifetime class upon lowering the temperature establishes that the two lifetime classes correspond to conformational substates of the proteins. A relatively large (>50 kJ/mol) undetermined activation barrier exists between the states, since the interconversion was slow on a fluorescence time scale. The high activation energy of transition between the two states possibly classifies them as conformational substates of the first tier (CS¹) [43, 44]. In contrast, the rate of exchange between conformational substates in LipDH-AV in aqueous solution is in the order of the fluorescence lifetime (chapter 2 of this thesis). The large effect of the solvent viscosity on the transition frequency indicates that considerable protein-domain rearrangements must be involved in the transition between the two conformers. An additional conformational state with higher transition enthalpy is also populated in aqueous solution (chapter 2 of this thesis). In 80% glycerol, protein dynamics is damped and the correlated atom movements do not contain enough kinetic energy to overcome the activation barrier to populate this conformational substate with higher enthalpy. The Gibbs free energy difference between conformational states is comparable in the wild type and mutant protein. However, the van 't Hoff plot of the conformational equilibrium constant is not linear below 263 K in case of the mutant protein. Equilibrium is then not established below 263 K due to a larger activation barrier between conformational states in LipDH- Δ 14 as compared to LipDH-AV. Removal of the 14 C-terminal amino acids by site-directed mutagenesis apparently affects the activation energy between the conformational states.

Both the maximum and the global analysis of the results revealed that the temperature dependence of the two observed lifetime classes is well described by one thermally activated and one temperature-independent radiative constant. By iodide quenching and molecular relaxation spectroscopy we have shown that the flavins are more solvent accessible in the mutant protein (chapter 3 of this thesis). The difference in the values of the rate constants and the effective activation energy of thermal quenching both reflect the difference in local environment of the flavins in the two proteins. The frequency factor and the effective

activation energy of thermal quenching are smaller for the solvent accessible flavins in the mutant than for the flavins in the wild type enzyme. In addition, the temperature-independent rate constants are larger for the flavins in LipDH- Δ 14. It is then tempting to assign the smaller lifetime class of LipDH-AV, with the lower activation energy, smaller frequency factor and larger temperature-independent rate constant, to a more "open" (substrate accessible) protein conformation.

The decrease in width of the lifetime distributions with increase in temperature possibly reflects rapid transitions between conformational substates of the third tier (CS³) [44]. From the slope of the FWHM on Arrhenius coordinates the empirical activation energy associated with this process was found to be between 4 and 20 kJ/mol. The magnitude of this activation energy is comparable to that of thermal quenching and possibly reflects the same dynamic mechanism (transitions between CS³). The local flavin environments in wild type and mutant lipomide dehydrogenase have distinct dynamic and structural properties as revealed by a smaller number of CS³ and lower activation barrier between states of tier 3 in LipDH- Δ 14, in agreement with the conclusions drawn from the parameters of thermal quenching of the fluorescence.

From the global analysis of fluorescence anisotropy data surface obtained at different temperatures and excitation wavelengths we could demonstrate that homo-energy transfer between the two flavins in both subunits of LipDH-AV is a mechanism which causes depolarization of the fluorescence. Red-edge spectroscopy in conjunction with temperature variation provides the necessary experimental axes to assess diagnostic methods to discriminate between reorientational dynamics and energy transfer. We can therefore exclude restricted motion of the flavins or hinge motion of the subunits as alternative mechanisms causing depolarization of the fluorescence [4].

LipDH-AV is an example of a biological macromolecule which can be used to test the validity of models describing the effect of excitation energy and dipolar relaxation on energy transfer between like chromophores. The capability of model testing arises from:

- i) the known crystal structure
- ii) the unique orientation of the non-mobile flavins

iii) the possibility to alter the electronic properties of the active site by site-directed mutagenesis.

The physical relations between the parameters of an anticipated model describing the anisotropy decay at different experimental conditions can be exploited by the use of global fit procedures in the analysis of data surfaces. The compartmental model used to describe the anisotropy decay surfaces of the proteins is a discrete state approximation of a qualitative physical model on failure of energy transfer [17, 33]. In a static inhomogeneously broadened system ($\tau_r \gg \tau_f$) the pure electronic transition energies are distributed as some continuous function (e.g. Gaussian). The experimental overlap integral J_{exp} of a dimeric system is then a static average of the overlap integrals J_i of the populations of dimers in energy configuration i :

$$J_{\text{exp}} = \sum_{i=1}^n A_i J_i \quad (17)$$

where A_i is the fractional population of dimers in energy configuration i . The rate of intersubunit energy transfer is then also a distributed function. In our model we assume that there is a predominant population (A_j) of dimers with energy configuration j within the population f_2 . This energy configuration j corresponds to equal transition energies of donor and acceptors. J_{exp} is then an overestimation of J_j and the rate of transfer k_T is a weighted average of the rates of each population i . In a dynamic inhomogeneously broadened system ($\tau_r \ll \tau_f$) all energy configurations are sampled during energy transfer and J_{exp} and thus k_T are dynamic averages [39]. The system behaves as if a single energy configuration j is present in all dimers. The rate of transfer k_T has then a discrete value independent of excitation energy proportional to J_{exp} . The model of Tanaka and Mataga (eq.10) is then adequate. Despite these assumptions in our model we obtained good agreement with experimental data. From the amplitudes of the anisotropy decay and transfer correlation time, geometrical information concerning the relative orientation and distance of the isoalloxazinic residues of the flavins in the subunits is obtained. The results as obtained for LipDH-AV are in excellent agreement with crystallographic data which validates the used energy transfer model. The interflavin distance and angle are slightly different in LipDH- $\Delta 14$ which is possibly caused by the perturbed interaction between the subunits.

The transfer correlation times and the fractional population of transferring molecules (f_2) are approximately temperature independent for LipDH-AV which we attribute to a rigid dipolar environment ($\tau_r \gg \tau_f$) of the flavins in the temperature range studied. The large population of transferring molecules (f_2) and the relatively small increase of the transfer correlation time upon edge excitation at 203 K shows that the photoselection of nonequilibrium solvates is small upon excitation at 514.5 nm. The inhomogeneous bandwidth is thus small and the isoalloxazines are located in a highly homogeneous, rigid (dipolar) protein environment. The temperature dependence of $\phi_T(T, 514.5)$ and f_2 in LipDH- $\Delta 14$ shows that effective dipolar relaxation takes place in this protein upon increase of the temperature. The interaction of the solvent dipoles with the isoalloxazines causes an increased inhomogeneity of the surrounding dipolar structure. At low temperatures (203 K) the immobilized solvent dipoles increase the inhomogeneous bandwidth as compared to the situation in the wild type enzyme. The increased inhomogeneous bandwidth results in an enhanced photoselection of unequilibrium solvates and larger shift of the emission spectra upon edge excitation. These factors contribute to red-edge failure of energy transfer by decreasing the overlap integral and the population of transferring molecules (f_2). Above 240 K, the fluctuating solvent dipoles cause partial up-relaxation and a decrease in the transfer correlation time at edge excitation. The more structured protein matrix surrounding the flavins hinders complete up-relaxation and failure of energy transfer is still observed at high temperature although to a lesser extent.

The Lip(SH₂)/NAD⁺ activity of LipDH- $\Delta 14$ in the dimeric form is extremely low (< 0.1% of wild type activity) whereas the diaphorase (NADH/DCPIP) activity is about 50% of the wild type enzyme. Although the dissociation constant of the subunits is three orders of magnitude larger [14], the mutated protein is present as a dimer under our experimental conditions. The removal of the 14 C-terminal amino acids has thus a most drastic effect on the Lip(SH₂) binding site which comprises amino acid residues from both subunits [12, 45]. Since the Lip(SH₂) binding site is composed of amino acid residues of both subunits and removal of the 14 C-terminal amino acids destabilizes the dimer, it is tempting to postulate that the C-terminal polypeptide of one subunit in LipDH-AV interacts via the Lip(SH₂) binding site of the other subunit and thereby stabilizes the dimer. The results as obtained in this study clearly demonstrate that the "disordered" C-terminal polypeptide in LipDH-AV has an

important effect on the local isoalloxazine micro-environment in LipDH-AV. We expect that the C-terminal tail folds back into the Lip(SH₂) binding site thereby shielding the active site from the solvent. One question remains open: what is the catalytic function of the two major conformations observed in the wild type enzyme in aqueous solution? If they do correspond to an "open" (Lip(SH₂) can bind) and "closed" (Lip(SH₂) cannot bind) enzyme conformation, the rate limiting step in catalysis could be the establishment of equilibrium between the two states in case the activation barrier between them is sufficiently large. In order to test this hypothesis substrate analogue binding studies must be undertaken. It is then expected that binding will result in the collapse of the enzyme into a single conformation.

4.5 References

1. Visser, A.J.W.G., Grande, H.J., Müller, F. and Veeger, C. (1974) *Eur. J. Biochem.*, 45, 99-107.
2. Visser, A.J.W.G., Grande, H.J. and Veeger, C. (1980) *Biophys. Chem.*, 12, 35-49.
3. Visser, A.J.W.G., Penners, N.H.G., van Berkel, W.J.H. and Müller, F. (1984) *Eur. J. Biochem.*, 143, 189-197.
4. de Kok, A. and Visser, A.J.W.G. (1987) *FEBS Lett.*, 218, 135-138.
5. Visser, A.J.W.G. (1989) *Time-Resolved Fluorescence Studies of Flavins in: Fluorescent Biomolecules* (Jameson, D.M. and Reinhart, D. eds.) pp. 319-341. Plenum Press, New York.
6. Bastiaens, P.I.H., Bonants, P.J.M., Müller, F. and Visser, A.J.W.G. (1989) *Biochemistry*, 28, 8416-8425.
7. Williams Jr, C.H. (1976) *The Enzymes*, 13, 89-173.
8. Reed, L.J. and Oliver, R.M. (1986) *Brookhaven Symp. Biol.*, 21, 397-412.
9. de Kok, A. and Visser, A.J.W.G. (1984) in: *Flavins and Flavoproteins* (Bray, R.C., Engel, P.C. and Mayhew S.G. eds.), pp. 149-152, Walter de Gruyter, Berlin.
10. de Kok, A., Bosma, H.J., Westphal, A.H. and Veeger, C. (1988) *Thiamine Pyrophosphate Biochemistry*, 2, 19-36.
11. Westphal, A.H. and de Kok, A. (1988) *Eur. J. Biochem.*, 172, 299-305.
12. Mattevi, A., Schierbeek, A.J. and Hol, W.G.J. (1991) *J. Mol. Biol.*, 220, 975-994.
13. Wahl, P., Auchet, J.C., Visser, A.J.W.G. and Veeger, C. (1975) *Eur. J. Biochem.*, 50, 413-418.

14. Schulze, E., Benen, J.A.E., Westphal, A.H. and de Kok, A. (1991) *Eur. J. Biochem.*, 200, 29-34.
15. Mattevi, A. (1991) Personal communication.
16. Rubinov, A.N. and Tomin, V.I. (1970) *Optics Spectrosc. (USSR)*, 29, 1082-1086.
17. Demchenko, A.P. (1987) *Ultraviolet Spectroscopy of Proteins* pp. 183-197. Springer-Verlag, Berlin.
18. O'Connor, D.V. and Phillips, D. (1984) *Time-Correlated Single Photon Counting*, Academic press, London.
19. van Hoek, A., Vos, K. and Visser, A.J.W.G. (1987) *IEEE J. Quantum Electron.*, QE-23, 1812-1820.
20. Gratton, E., Jameson, D.M. and Hall, R.D. (1984) *Ann. Rev. Biophys. Bioeng.*, 13, 105-124.
21. Lakowicz, J.R., Laczko, G. and Gryczynski, I. (1986) *Rev. Sci. Instrum.*, 57, 2499-2506.
22. Livesey, A.K. and Brochon, J.C. (1987) *Biophys. J.*, 52, 693-706.
23. Mérola, F., Rigler, R., Holmgren, A. and Brochon, J.C. (1989) *Biochemistry*, 28, 3383-3398.
24. Gentin, M., Vincent, M., Brochon, J.C., Livesey, A.K., Cittanova, N. and Gallay, J. (1990) *Biochemistry*, 29, 10405-10412.
25. Beechem, J.M., Gratton, E., Ameloot, M., Knutson, J.R. and Brand, L. (1991) *The global analysis of fluorescence intensity and anisotropy decay data in: Topics in Fluorescence Spectroscopy (Lakowicz, J.R. ed.) Vol 2, pp 241-305, Plenum Press, New York.*
26. Beechem, J.M. and Gratton, E. (1988) *Proc. SPIE*, 909, 70-81.
27. van Hoek, A. and Visser, A.J.W.G. (1981) *Rev. Sci. Instrum.*, 52, 1199-1205.
28. Vos, K., van Hoek, A. and Visser, A.J.W.G. (1987) *Eur. J. Biochem.*, 165, 55-63.
29. van Hoek, A. and Visser, A.J.W.G. (1985) *Anal. Instrum.*, 14, 359-378.
30. Spencer, R.D. and Weber, G. (1972) *In Structure and Function of Oxidation and Reduction Enzymes (Åkeson, Å. and Ehrenberg, A., eds.) pp 393-399, Pergamon Press, Oxford.*
31. Alcalá, R.J., Gratton, E. and Prendergast, F.G. (1987) *Biophys. J.*, 51, 597-604.
32. Galley, J.A. and Edelman, G.M. (1962) *Biochim. Biophys. Acta*, 60, 499-509.
33. Nemkovich, N.A., Rubinov, A.N. and Tomin, V.I. (1991) *Inhomogeneous Broadening of Electronic Spectra of Dye Molecules in: Topics in Fluorescence Spectroscopy (Lakowicz, J.R. ed.) Vol 2, pp 367-428, Plenum Press, New York.*

34. Tanaka, F. and Mataga, N. (1979) *Photochem. Photobiol.* 29, 1091-1097.
35. Nemkovich, N.A., Matseiko, V.I. and Tomin, V.I. (1980) *Optica Spectrosc. (USSR)*, 49, 274-282.
36. Tomin, V.I. and Rubinov, A.N. (1981) *J. Appl. Spectrosc (USSR)*, 35, 237-251.
37. Weber, G. (1952) *Biochem. J.* 51, 145-155
38. Johansson, L.B.-Å., Davidsson, Å., Lindblom, G. and Razi Naqvi, K. (1979) *Biochemistry*, 18, 4249-4253.
39. Dale, R.E., Eisinger, J. and Blumberg, W.E. (1979) *Biophys. J.*, 26, 161-194.
40. Förster, T. (1948) *Ann. Physik.*, 2, 55-75.
41. Steinberg, I.Z. (1971) *Ann. Rev. Biochem.*, 40, 83-114.
42. Visser, A.J.W.G. and Müller, F. (1979) *Helv. Chim. Acta*, 62, 593-608.
43. Austin, R.H., Beeson, K.W., Eisenstein, L., Frauenfelder, H. and Gunsalus, I.C. (1975) *Biochemistry*, 14, 5355-5373.
44. Frauenfelder, H. and Gratton, E. (1986) *Methods Enzymol.*, 127, 207-216.
45. Schierbeek, A.J., Swarte, M.B.A., Dijkstra, B.W., Vriend, G., Read, R.J., Hol, W.G.J., Drenth, J. and Betzel, C. (1989) *J. Mol. Biol.*, 206, 365-379.

Chapter 5

Energy Transfer between the two Flavin Chromophores of Electron-Transferring Flavoprotein from *Megasphaera elsdenii* as Inferred from Time-Resolved Red-Edge and Blue-Edge Fluorescence Spectroscopy

Bastiaens, P.I.H., Mayhew, S.G., O'Nualláin, E. M., van Hoek, A. and Visser, A.J.W.G.

Published in J. of Fluorescence (1991) 1, 95-103.

Abstract

Both a mode-locked argon-ion laser and synchrotron radiation were used as excitation source to obtain time-resolved polarized fluorescence of the two FAD prosthetic groups in electron transferring flavoprotein from *Megasphaera elsdenii*. Red-edge excited and blue-edge detected fluorescence anisotropy decay curves did not contain a fast relaxation process which was observed upon main-band excitation and detection. This relaxation was assigned to homo-energy transfer between the two FAD's. Failure of energy transfer as observed with edge spectroscopy on this protein excludes restricted reorientational motion of the flavins as a possible mechanism of depolarization. From the global analysis of the fluorescence anisotropy decay surface obtained at multiple excitation and detection wavelengths the distance between and the relative orientation of the flavins could be estimated. The methodology described has general applicability in other multichromophoric biopolymers and has the potential to acquire accurate geometrical parameters in these systems.

5.1 Introduction

The electron transferring flavoprotein (ETF) from *Megasphaera elsdenii* functions in the formation of short-chain fatty acids by coupling the oxidation of NADH or D-lactate dehydrogenase to the reduction of butyryl-CoA dehydrogenase [1]. ETF from *Megasphaera elsdenii* is unusual in comparison to ETF isolated from mammalian and other bacterial sources in that it contains two highly fluorescent noncovalently bound FAD prosthetic groups (quantum yield is 2.4 that of free FAD) instead of one per protein molecule [2]. The 74 kDa protein has a $\alpha\beta$ (α : 41

kDa, β : 33 kDa) dimeric quaternary structure with the two FAD prosthetic groups residing on the β subunit. No information is available on the spatial relationship of the flavins within the protein. One of the techniques to obtain insight in this spatial relationship is to monitor the fluorescence resonance energy transfer (FRET) between the isoalloxazinic residues of the flavins in a time-resolved fluorescence anisotropy experiment. Energy transfer between like chromophores, termed homo-transfer, cannot be observed in the decay of the fluorescence since this process does not affect the lifetime of the excited state. Instead, the relaxation of the excited state by dipole-dipole coupling in a homo-transfer system can be observed in the depolarization of the fluorescence when the direction of the transition moments do not coincide in the interacting moieties [3-5]. The rate of transfer can be obtained from the relaxation of the fluorescence anisotropy in a time-resolved experiment [3, 6]. The distance between the chromophores can be estimated with the Förster relation [7] given that the geometric parameter κ^2 and the overlap integral J are known. J can be determined from the overlap between absorption and fluorescence emission spectra of the chromophores in question. The exact value of the geometric factor κ^2 is hard to obtain, if not impossible under certain circumstances. Dale et al. [8] presented contour plots to estimate upper and lower boundaries of κ^2 provided that restricted reorientational motion of interacting chromophores takes place on a frequency scale which is much larger than the transfer rate (dynamic averaging regime). The axial depolarization due to restricted motion of the individual chromophores must be known for an estimate of κ^2 . In a completely rigid system with one unique configuration of the interacting chromophores, one cannot obtain information on κ^2 from a fluorescence experiment. Only an upper limit can be assigned to κ^2 leading to an upper limit of the distance between the chromophores [8].

One of the complications associated with the measurement of homo-transfer by fluorescence anisotropy, is that the depolarization of the fluorescence can arise not only from energy transfer, but also from restricted reorientational motion of the chromophores inside the protein. One solution to solve this ambiguity in the interpretation of the fluorescence anisotropy, is to alter the system in a biochemical fashion by selectively removing one of the noncovalently bound chromophores and comparing the anisotropy of this partial apo-protein with that of the holo-protein. In practice this is difficult to achieve, especially when the active sites are similar with comparable dissociation constants of the prosthetic groups. Another problem is that the

dynamical behavior of the chromophores inside the protein can be influenced by removal of one of them [5]. The other, physical solution is to excite the sample at the red-edge of the absorption band and monitoring the resulting decay of fluorescence anisotropy. In a system where the fluorescence depolarization is caused by homo-transfer, red-edge excitation in the absorption band will decrease the probability of transfer with a corresponding decrease of the transfer rate [5, 9-11]. Extreme edge excitation will result in complete failure of energy transfer as observed in aromatic fluorophores in viscous polar media at low temperature [12, 13]. This phenomenon will only take place in a system with inhomogeneously broadened fluorescence spectra and long dipolar relaxation time in comparison to the fluorescence lifetime [9-11, 14]. Such a situation may correspond to a chromophore in a polar protein environment where dynamical events take place on a time scale which is much longer than the fluorescence lifetime.

As energy transfer is directed from "blue" (large 0-0 energy separation) to "red" (small 0-0 energy separation) centers [11], a similar phenomenon to red-edge failure of energy transfer is expected upon detection at the blue edge of the emission band. Photons which are emitted at the blue edge of the emission have the largest energy and must therefore originate from chromophores which did not participate in energy transfer. Photons which originate from chromophores involved in energy transfer will have a lower polarization than photons from non-transferring chromophores. Both red-edge and blue-edge failure of energy transfer will be manifest in the anisotropy decay by an increase of the relaxation time constant associated with energy transfer and an increase of the fluorescence anisotropy.

To ascertain that energy transfer takes place between the flavins, we used both a synchrotron and a mode-locked argon-ion laser as excitation sources in order to perform a variable wavelength and time-resolved fluorescence experiment. The advantage of the former source is the continuous tunability of the excitation wavelength, with the disadvantage of the lower intensity and larger frequency band width in comparison to the latter excitation source. The argon-ion laser contains two excitation wavelengths which correspond to the main-band (457.9 nm) and red-edge (514.5 nm) of the normal flavin absorption spectrum. Therefore this pulsed excitation source is suitable to perform flavin red-edge spectroscopy. The narrow bandwidth in case of the 514.5 nm line (5 GHz bandwidth) enables highly selective excitation of nonequilibrium solvates at the red-edge of the absorption band [14].

Multiple fluorescence anisotropy decays of ETF have been collected as function of excitation and detection wavelengths. This set of curves can be combined to form a fluorescence anisotropy decay surface. Global analysis of this data surface to a single model by exploiting the relations between the parameters of the different experiments, allows for better model discrimination by statistical criteria and parameter recovery than single curve analysis of individual experiments [15-17].

5.2 Materials and methods

5.2.1 Biochemical manipulation

ETF was purified from *Megasphaera elsdenii* [2], and stored at 4° as a precipitate in ammonium sulphate (80% saturation). Prior to an experiment, the precipitate was dissolved in 50 mM KP_i pH 6.0 and 0.3 mM EDTA, and the solution chromatographed on a column of Biogel PDG-6 (Biorad) equilibrated with the same buffer to remove any protein-free FAD. The preparation was judged to be homogeneous by PAGE in the presence and absence of SDS. It was used as isolated without addition of FAD to saturate the flavin sites [2]. The visible absorption spectrum of the preparation showed that it contained a slight contamination of 8-OH-FAD [18], not exceeding 5% of the total FAD.

5.2.2 Steady-state spectra

Absorption spectra were recorded on a Cary 17 spectrophotometer and fluorescence emission spectra on an Aminco SPF-500 fluorimeter.

5.2.3 Time-resolved fluorometry

Time-correlated single photon counting (TCSPC) was used as the technique to measure fluorescence and fluorescence anisotropy decays [19]. For excitation with 457.9 and 514.5 nm light a mode-locked cw argon-ion laser was used (Coherent Radiation model CR-18). The pulses were about 100 ps FWHM with picojoule energies after the excitation rate was diminished from 76 MHz to 596 kHz by an electro-optic modulator [20]. The fluorescence was collected at 90° with respect to the direction of the exciting light beam. Between the sample and the microchannel plate detector (Hamamatsu 1645U) filters were placed to select blue-edge (Schott KV 500 + Balzers 501), main band (Schott OG 530 + Schott 539.4) and red-edge (Schott KV 500 + Schott 568.5)

portions of the flavin emission. Parallel- and perpendicular-polarized fluorescence intensities were collected with a computer controlled rotatable sheet polarizer (Polaroid HN38). The sequence of data acquisition consisted of 10 cycles of 10 seconds collection of parallel- and perpendicular-polarized sample fluorescence sandwiched between the collection of 2 cycles of 10 seconds of parallel and perpendicular pulse mimic (erythrosin B in water). The detection count rate was set at 30 kHz in the parallel-polarized detection to prevent pulse pile-up distortion of the data. Background fluorescence was sampled at one fifth of the sample acquisition time and was always below 1% of the sample count rate. Details of the experimental setup and detection electronics are presented in chapter 4 of this thesis. The data was transferred from the multichannel analyzer to a MicroVax station for data analysis.

For excitation at 435, 445, 451 and 515 nm, the synchrotron radiation facility at Daresbury U.K. was used [21]. The excitation wavelength was selected with a double monochromator with the slit width set at 1.5 nm. Detection wavelengths were selected by placing interference filters (Ealing, 10 nm bandpass) between the sample and the microchannel plate detector (Hamamatsu R-1564-U). Parallel- and perpendicular-polarized emission intensities were collected by sampling 1 cycle of 100 seconds of parallel and perpendicular fluorescence each. The pulse was acquired by placing a scatterer (Ludox in water) in the sample housing and tuning the excitation wavelength at the maximal transmission of the interference filter in use. The pulse was sampled in the parallel position of the polarizer until 20,000 counts in the peak were obtained. Background fluorescence of the buffer solution of ETF was in all cases negligible.

5.2.4 Data analysis

The fluorescence anisotropy data surface was analysed with a version especially designed for TCSPC data of the commercially available global analysis program (Globals Unlimited, Urbana IL) based on the iterative reconvolution method [17]. The total fluorescence decays were constructed from parallel- and perpendicular-polarized intensity decay files with the background subtracted and proper weighting applied [22]. For the deconvolution of the fluorescence decays obtained from laser excitation, the reference method was used with erythrosin B in water as a reference compound ($\tau_{\text{ref}} = 80$ ps) [22]. For the deconvolution of the fluorescence decays obtained with the synchrotron radiation source the pulse as acquired with a scatterer was used. The fluorescence decays of ETF were fitted to

a triple exponential function to obtain χ^2 values close to unity. This method does not give any insight into the physical process underlying the fluorescence decay, but allows for the analysis of the anisotropy decay surface. The optimized parameters of the fluorescence decays were fixed in the subsequent analysis of the fluorescence anisotropy decays eliminating six adjustable parameters. The fluorescence anisotropy decays obtained at different excitation and emission wavelengths were simultaneously fitted to a model described in the Results section. All parameters of the parallel- and perpendicular-polarized fluorescence intensity components of individual experiments were linked [17]. The fit of the data surface was subjected to rigorous error analysis to yield an estimate of the standard error of the anisotropy decay parameters [17].

5.3 Results

5.3.1 Fluorescence decay

Table1: Fluorescence decay parameters of ETF

excitation and detection wavelength:		parameters ³ :					
λ_{ex} (nm) ¹	λ_{em} (nm) ²	α_1	α_2	α_3	τ_1 (ns)	τ_2 (ns)	τ_3 (ns)
435 (S)	460	0.64	0.28	0.08	0.086	0.70	2.29
445 (S)	470	0.63	0.28	0.09	0.11	0.61	1.83
458 (L)	501	0.53	0.40	0.07	0.33	1.35	3.20
458 (L)	539	0.41	0.53	0.06	0.43	1.34	3.26
458 (L)	569	0.30	0.65	0.05	0.66	1.37	3.53
515 (L)	548	0.10	0.84	0.06	0.61	1.16	2.90

1) Excitation wavelength in nanometers where the alphabetical entry (S) denotes Synchrotron and (L) Laser as used excitation sources.

2) maximum transmission of used interference filter where the bandwidth at half maximum transmission was approximately 10 nm for all filters.

3) All fluorescence decays were fitted to a triple exponential function:

$$I(t) = \sum_{i=1}^3 \alpha_i \exp(-t/\tau_i)$$

In Table 1 the parameters of the triple exponential fit (χ^2 close to 1) of the fluorescence decays of ETF excited and detected at different wavelengths are gathered. The nonhomogeneous

fluorescence decay is often observed for intrinsic fluorophores in proteins and reflects the inhomogeneity of the chromophore environment. No effort was made to interpret the observed nonhomogeneous fluorescence decay in a quantitative fashion as our attention was directed to the spatial relationships of the FAD's as contained in the fluorescence anisotropy decay. The fluorescence decay parameters as listed in Table 1 were fixed in the analysis of the fluorescence anisotropy decay surface.

5.3.2 Fluorescence anisotropy decay

Let us assume as a working hypothesis that the depolarization of the flavin fluorescence in ETF is caused by: 1) homo-transfer between the FAD prosthetic groups and 2) protein tumbling. The model describing the anisotropy decay $r(t)$ is then given by [3, 5]:

$$r(t) = \{\beta_1 \exp(-t/\phi_T) + \beta_2\} \exp(-t/\phi_P) \quad (1)$$

where ϕ_P is the correlation time of protein tumbling related to the molecular volume (V) of the protein and viscosity of the solvent (η) by the Stokes-Einstein relation assuming that the protein is spherical and much larger than the solvent molecules. The transfer correlation time ϕ_T is reciprocally related to the rate of energy transfer k_T [4-6] as given in eq.13 of chapter 4 of this thesis. The amplitudes β_1 and β_2 contain geometrical information on intra- and intermolecular angles of absorption and emission transition moments of the interacting moieties [3, 23]. Since the amplitudes are only dependent on the relative positions of the transition moments of the chromophores in the protein, they should be physical invariants of excitation and detection wavelengths as long as the first electronic transition is excited. Consequently, the amplitudes can be linked in the fit of the anisotropy data surface as obtained by variation of excitation and emission wavelengths. The correlation time of protein tumbling is also independent of excitation or detection wavelengths and is thus also an overdetermined parameter in the fit of the data surface [24].

The probability of energy transfer is strongly dependent on the excitation and emission wavelengths. Upon excitation at the red-edge of the absorption, or detection at the blue-edge of the emission, the rate of transfer should approach zero if indeed failure of energy transfer occurs in the system under investigation. The corresponding transfer correlation time should then approach infinity. The observation of these phenomena

provides strong indications that the depolarization of the fluorescence upon main-band excitation and detection is caused by homo-energy transfer.

In our global analysis of the experiments, we have chosen not to include overlapping experiments obtained with the two excitation sources. We omitted the polarized decay curves arising from 450 and 515 nm synchrotron excitation. This was done because the quality of the data was not as good as that obtained with laser excitation, due to radiofrequency interference and detection of some white scattered light. In order to show the good reproducibility, however, we included the results of a separate analysis of experiments with synchrotron excitation at 450 and 515 nm (*vide infra*).

Table 2: Global link matrix

excitation and detection wavelength:		parameters ³ :			
λ_{ex}^1 : (nm)	λ_{em}^2 : (nm)	β_1	β_2	ϕ_p	ϕ_T
435 (S)	460	1	2	3	4
445 (S)	470	1	2	3	5
458 (L)	501	1	2	3	6
458 (L)	539	1	2	3	7
458 (L)	569	1	2	3	8
515 (L)	548	1	2	3	9

1) Excitation wavelength in nanometers where the alphabetical entry (S) denotes Synchrotron and (L) Laser as used excitation sources.

2) Maximum transmission of used interference filter where the bandwidth at half maximum transmission was approximately 10 nm for all filters.

3) Parameters of equation 1 (see text)

In Table 2 the global link matrix as used in the analysis of the data according to eq.1 is presented. One dimension represents the type of experiment (change of excitation and/or emission wavelength) and the other dimension the parameters of the model. Parameters which are linked have the same logic number in different experiments [17]. In Fig.1 the absorption and emission spectra of ETF are shown with arrows marking the used excitation and emission wavelengths. From Fig.1 it can be seen that a substantial overlap exists between the two spectra. Energy transfer may then be possible between both flavins.

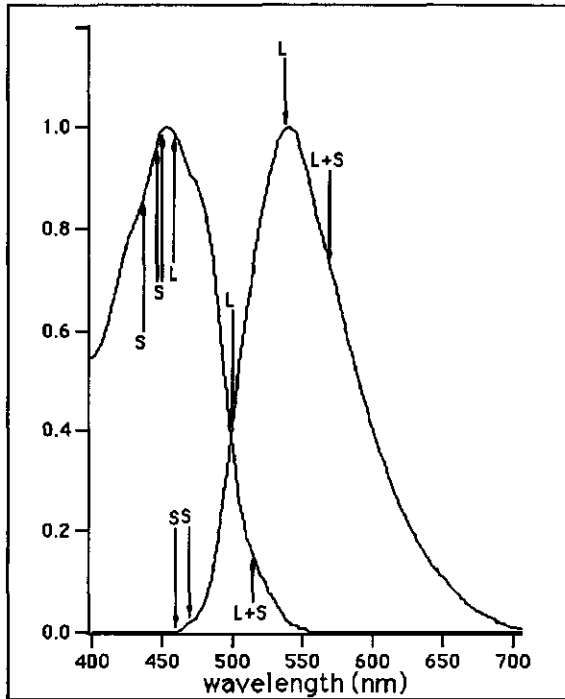


Fig.1: Absorption and emission spectra of electron transferring flavoprotein. Arrows on the absorption spectra (pointing upwards) indicate the used excitation wavelengths and source (S: Synchrotron, L: Laser). Arrows on the emission spectrum (pointing downwards) indicate the used detection wavelengths.

The anisotropy data surface of ETF was fitted to eq. 1 with the linkage between parameters of different decays presented in Table 2. The parameters are collected in Table 3 together with the standard errors as estimated from a rigorous error analysis (67% confidence interval). Fitting criteria, such as the residuals and local and global χ^2 values [25] are presented in Fig.2. This figure demonstrates that an optimized fit was achieved.

A global analysis with a linking scheme analogous to that in Table 2 was performed on the data originating from synchrotron excitation at 450 and 515 nm. The results are displayed and collected in Fig.3 and Table 4, respectively. It can be concluded that excellent agreement exists between the anisotropy decay parameters as obtained for both synchrotron and laser excitation at similar wavelength settings. It is also to be noted that different batches of protein were used.

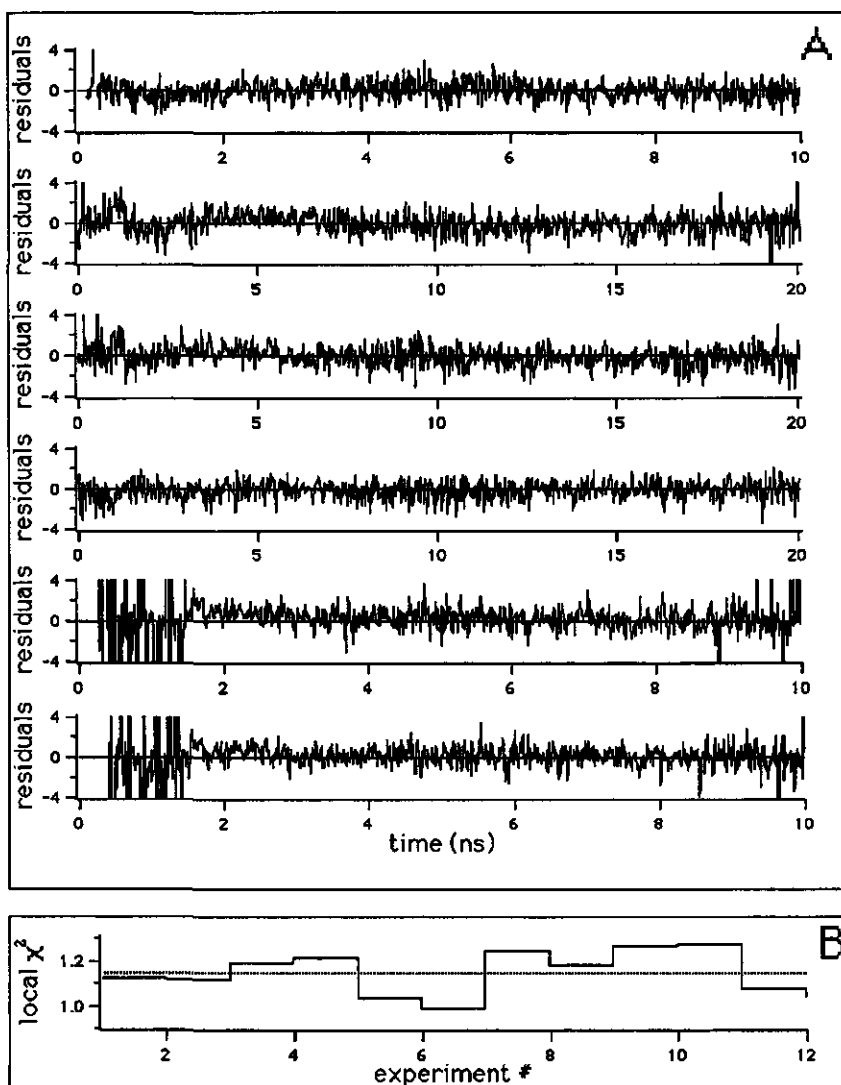


Fig. 2: Criteria of fit of fluorescence anisotropy data surface of electron transferring flavoprotein. A: Weighted residuals of anisotropy decays. From top to bottom of panel: λ_{ex} : 514.5 nm, λ_{em} : 539 nm (laser) ; λ_{ex} : 457.9 nm, λ_{em} : 501 nm (laser) ; λ_{ex} : 457.9 nm, λ_{em} : 548 nm (laser) ; λ_{ex} : 457.9 nm, λ_{em} : 569 nm (laser) ; λ_{ex} : 435 nm, λ_{em} : 460 nm (synchrotron) ; λ_{ex} : 445 nm, λ_{em} : 470 nm (synchrotron). B: Cityscape plot of local χ^2 of parallel and perpendicular components of the fluorescence decays. Local χ^2 is represented by a solid line and the global χ^2 by a broken line.

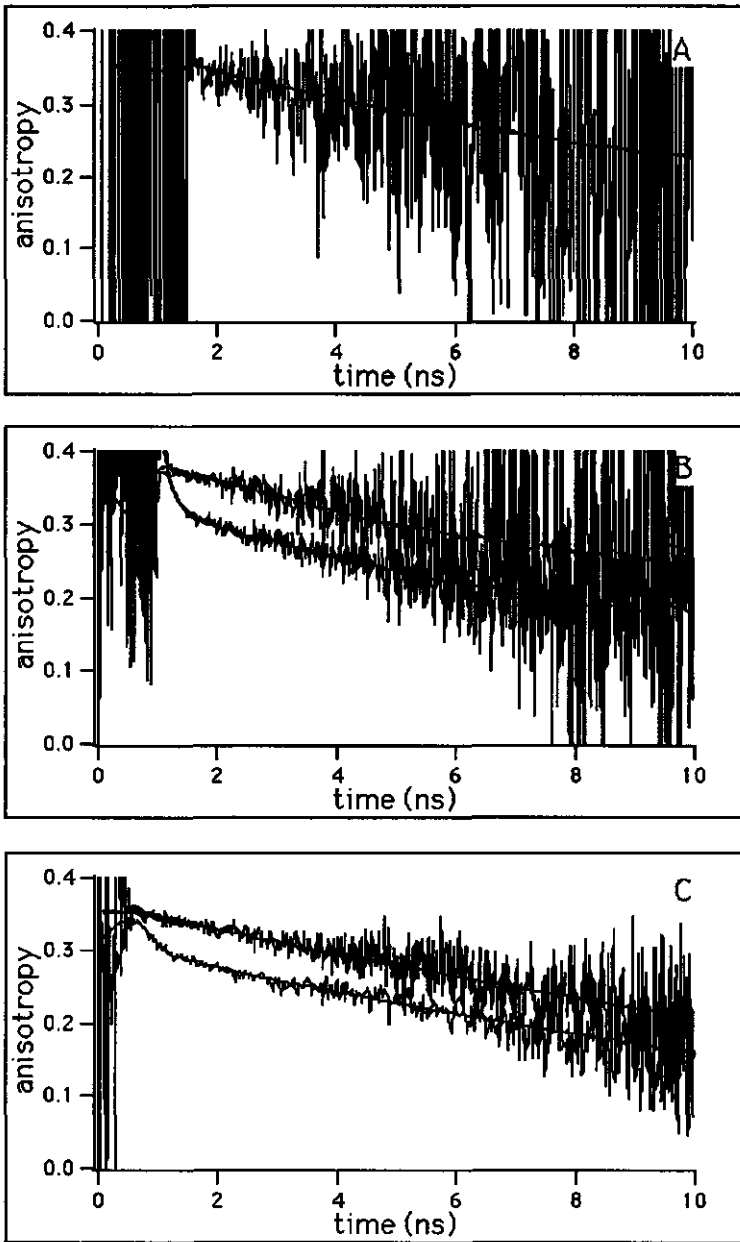


Fig. 3: Experimental and fitted anisotropy decays of electron transferring flavoprotein. Top panel: blue-edge excited and detected (Synchrotron). middle panel: main-band excited and detected (laser). bottom panel: red-edge excited and main-band detected (laser). Excitation and emission wavelengths are represented in the boxed legends in the figures.

Table 3: Fluorescence anisotropy decay parameters of ETF

excitation and detection wavelength:		value of parameters ³ :			
λ_{ex} (nm) ¹	λ_{em} (nm) ²	β_1	β_2	ϕ_p (ns)	ϕ_T (ns)
435 (S)	460	0.0556 (0.0491- 0.0645)	0.298 (0.288- 0.304)	14.5 (13.0-16.7)	45. 10 ³
445 (S)	470	"	"	"	18. 10 ⁴
458 (L)	501	"	"	"	1.71 (1.16-2.60)
458 (L)	539	"	"	"	0.437 (0.250- 0.706)
458 (L)	569	"	"	"	0.171 (0.0773- 0.317)
515 (L)	548	"	"	"	51.9

- 1) Excitation wavelength in nanometers where the alphabetical entry (S) denotes Synchrotron and (L) Laser as used excitation sources.
- 2) Maximum transmission of used interference filter where the bandwidth at half maximum transmission was approximately 10 nm for all filters.
- 3) Parameters of equation 1 (see text) with standard errors (at 67% confidence level) between brackets as obtained from a rigorous error analysis.

Table 4: Fluorescence anisotropy decay parameters of ETF as obtained by synchrotron excitation

excitation and detection wavelength:		value of parameters:			
λ_{ex} (nm)	λ_{em} (nm)	β_1	β_2	ϕ_p (ns)	ϕ_T (ns)
450 (S)	569	0.0646 (0.057- 0.075)	0.315 (0.305- 0.322)	12.5 (10.5-17.3)	0.141 (0.08-0.28)
515 (S)	569	"	"	"	98.9

See legend to Table 3 for explanation of symbols

From Tables 3 and 4 and Fig.3, it can be concluded that a fast process is present in the anisotropy decay upon main-band (435-460 nm) excitation and detection between 530 and 570 nm. This process becomes slower as apparent from an increase in correlation time upon blue-edge (501 nm) detection and vanishes

completely at the extreme blue-edge (460-470 nm). Upon red-edge (515 nm) excitation a completely analogous situation is encountered. Both extreme blue-edge detection and red-edge excitation thus abolish a process observed at main-band excitation and detection. This process must then be ascribed to homo-energy transfer between the FAD prosthetic groups.

From the pre-exponential amplitudes of eq. 1 the inter- and intramolecular angles between absorption and emission moments can be estimated (eqs. 15 and 16 of chapter 4 of this thesis). With the values of β_1 and β_2 as obtained from the global analysis (Table 2) we obtained an intramolecular angle δ of $16^\circ \pm 2^\circ$. An estimation of the intermolecular angle θ of absorption and emission transition moments can be made by assuming that the angles are equal in both directions of energy transfer (chapter 4 of this thesis). By subtraction of the pre-exponential amplitudes (eq.16 of chapter 4) we can then calculate an intermolecular angle θ of $31^\circ \pm 2^\circ$ or $149^\circ \pm 2^\circ$.

From red-edge excitation and blue-edge detected anisotropy experiments no depolarization process other than protein tumbling on a time scale comparable to the fluorescence emission was apparent. The value for the initial anisotropy is lower than the fundamental one of 0.4, which could originate from picosecond restricted motion. Alternatively, as outlined above, the intramolecular angle between absorption and emission transition moments is not zero. In the latter case the flavins are completely immobilized in the protein and the geometrical factor κ^2 of the Förster equation cannot be estimated. The only remedy is then to assign an upper limit of 4 to this parameter [8] to calculate a maximal possible distance between the isoalloxazine residues of the FAD's in ETF. From the transfer correlation time obtained at main-band excitation and detection we calculated a transfer rate k_T of 2.93 ns^{-1} . With the overlap integral as determined from the absorption and emission spectra in Fig.1 ($J = 5.53 \cdot 10^{-15} \text{ M}^{-1}\text{cm}^3$), the radiative rate of isoalloxazine ($\lambda_r = 0.0556 \text{ ns}^{-1}$) [26] and the refractive index ($n=1.4$) [27], we calculated from the Förster equation [7, 28] an upper limit for the intermolecular separation between the centers of the isoalloxazines of $21 \pm 2 \text{ \AA}$.

If the decrease of the fundamental anisotropy as observed for the isoalloxazines in ETF is due to picosecond reorientational motion, an upper and lower limit of the intermolecular distance can be estimated with the κ^2 -contour plots of Dale et al. [8]. From eqs. 15 and 16 of chapter 4 the transfer and axial depolarization factors can be readily calculated to be 0.60 and 0.88, respectively. The contour plot in Fig.6 in reference [8] was then used to estimate the upper (3.2) and lower (0.1) boundaries of κ^2 . By

taking into account the uncertainty in the transfer correlation time we obtained a distance of 12-23 Å for the FAD's in ETF.

5.4 Discussion

To our knowledge, this is the first report of failure of energy transfer as observed at the blue-edge of the fluorescence emission spectrum of a binary homo-transfer system. Possible interference of the presence of a trace amount of 8-OH-FAD can be discarded on the basis of two criteria. First, upon 515 nm excitation, 8-OH-FAD would be excited in the main absorption band, and back transfer to FAD (or 8-OH-FAD) leading to depolarization can still take place because there is substantial spectral overlap between emission of 8-OH-FAD and absorption of FAD [18]. Such an effect is not observed (Fig.3, Table 3). Second, upon excitation at 445 and detection at 470 nm, FAD is almost exclusively monitored and under these conditions energy transfer indeed is not detected.

Both the red-edge excited and blue-edge detected fluorescence anisotropy decay of ETF show that the depolarization of fluorescence upon main-band excitation and detection is caused by homo-energy transfer between the FAD's together with protein tumbling. Red-edge and blue-edge failure of energy transfer will only take place in a system with inhomogeneously broadened spectra and a dipolar relaxation time much longer than the average fluorescence lifetime [9-11]. Consequently, the chromophores must then be located in an effectively rigid environment (on the time scale of fluorescence emission) with multiple conformations as sustained by the nonhomogeneous fluorescence decay.

The anisotropy decays as obtained from edge spectroscopy did not exhibit a short relaxation process that could be ascribed to restricted reorientational motion of the flavins, in agreement with the abovepresented "solid-state" model of the active site of the protein. It is still possible that restricted reorientation of the flavins takes place on a time scale which is not resolvable by our experimental set-up. The value of the initial anisotropy as obtained from the global analysis of the data surface was indeed lower (0.35) than the expected fundamental anisotropy (0.4). This discrepancy can be explained by high frequency "rattling in a cage" of the isoalloxazines. It is, however, more probable that the absorption and emission transition moments in isoalloxazines do not coincide as the steady-state fluorescence anisotropy of flavins entrapped in rigid media do not exhibit the fundamental anisotropy of 0.4, but a value close to that found for the initial anisotropy of ETF [5]. Unfortunately, only an upper limit of the interflavin distance in ETF can be calculated in that instance. The

angular parameters determined from the analysis of the experiments are highly accurate as demonstrated by a similar study of a double FAD containing enzyme with known crystal structure (chapter 4 of this thesis). When the flavins undergo fast restricted motion, in addition to homo-transfer, the spread in the calculated distance is narrowed down considerably. This effect has been shown to occur in the biflavinyll-containing cytochrome P450 reductase, for which the three-dimensional structure is not yet known [5].

Concluding, it can be stated that a combination of edge spectroscopy and time-resolved fluorescence anisotropy adds an extra dimension to fluorescence depolarization methods. Both structural and dynamic information can be retrieved from the analysis of such a fluorescence anisotropy data surface.

5.5 References.

1. Brockman, H.L. and Wood, W.A. (1975) *J. Bacteriol.*, 124, 1447-1453.
2. Whitfield, C.D. and Mayhew, S.G. (1974) *J. Biol. Chem.*, 249, 2801-2810.
3. Tanaka, F. and Mataga, N. (1979) *Photochem. and Photobiol.*, 29, 1091-1097.
4. Bastiaens, P.I.H. , Bonants, P.J.M. , van Hoek, A. , Müller, F. and Visser, A.J.W.G. (1988) *Proc. SPIE*, 909, 257-262.
5. Bastiaens, P.I.H. , Bonants, P.J.M. , Müller, F. and Visser, A.J.W.G. (1989) *Biochemistry*, 28, 8416-8425.
6. Visser, A.J.W.G., Santema, J.S. and van Hoek, A. (1983) *Photobiophys.*, 6, 47-55.
7. Förster, T. (1948) *Ann. Physik.*, 2, 55-75.
8. Dale, R.E., Eisinger, J. and Blumberg, W.E. (1979) *Biophys. J.*, 26, 161-194.
9. Gullis, I.M. and Komjak, A.I. (1977) *J. Appl. Spectrosc. (U.S.S.R.)* 27, 841-845.
10. Gullis, I.M. and Komjak, A.I. (1980) *J. Appl. Spectrosc. (U.S.S.R.)* 32, 897-902.
11. Demchenko, A.P. (1987) *Ultraviolet Spectroscopy of Proteins* pp. 183-197, Springer-Verlag, Berlin.
12. Weber, G. (1960) *Biochem. J.*, 75, 335-345.
13. Weber, G. and Shinitzky, M. (1970) *Proc. Natl. Acad. Sci. U.S.A.*, 65, 823-830.
14. Nemkovich, N.A., Rubinov, A.N. and Tomin, V.I. (1991) *Inhomogeneous Broadening of Electronic Spectra of Dye Molecules in: Topics in Fluorescence Spectroscopy (Lakowicz, J.R. ed.) Vol 2, pp 367-428, Plenum Press, New York.*

15. Knutson, J.R., Beechem, J.M. and Brand, L. (1983) *Chem. Phys. Lett.*, 102, 501-507.
16. Beechem, J.M. and Gratton, E. (1988) *Proc. SPIE*, 909, 70-81.
17. Beechem, J.M., Gratton, E., Ameloot, M., Knutson, J.R. and Brand, L. (1991) *The Global Analysis of Fluorescence Intensity and Anisotropy Decay Data: Second Generation Theory and Programs in: Topics in Fluorescence Spectroscopy* (Lakowicz, J.R. ed.) vol 2., Principles, Plenum Press, New York
18. Ghisla, S. and Mayhew, S.G. (1973) *J. Biol. Chem.*, 248, 6568-6570.
19. O' Connor, D.V. and Philips, D. (1984) *Time Correlated Single Photon Counting*.
20. Van Hoek, A. and Visser, A.J.W.G. (1981) *Rev. Sci. Instrum.*, 52, 1199-1205.
21. Munro, I.H., Shaw, D. and Martin, M.M. (1985) *Anal. Instrum.*, 14, 465-482.
22. Vos, K., van Hoek, A. and Visser, A.J.W.G. (1987) *Eur. J. Biochem.*, 165, 55-63.
23. Szabo, A. (1984) *J. Chem. Phys.*, 81, 150-167.
24. Barkley, M.D., Kowalczyk, A. and Brand, L. (1981) *J. Chem. Phys.*, 75, 3581-3593.
25. Bevington, P.R. (1969) *Data Reduction and Error Analysis for the Physical Sciences*, McGraw-Hill, New York.
26. Visser, A.J.W.G. and Müller, F. (1979) *Helv. Chim. Acta.*, 62, 593-608.
27. Steinberg, I.Z. (1971) *Ann. Rev. Biochem.*, 40, 83-114.
28. Lakowicz, J.R. (1983) *Principles of Fluorescence Spectroscopy* pp. 303-305, Plenum Press, New York.

Chapter 6

Summarizing Discussion.

Refinements in technique and data analysis have opened new avenues for a detailed interpretation of protein fluorescence. What is more, by combining new insights in protein structure and dynamics with improved knowledge of photophysics of biological chromophores, the coupling between structure-function relationships and fluorescence properties is beginning to have a firm foundation. As a consequence of this interdisciplinary marriage, bidirectional information can be inferred from fluorescence spectroscopy of proteins.

In chapter 2 we could explain the time-resolved fluorescence parameters of FAD in glutathione reductase and lipoamide dehydrogenase by a different interplay between conformational substates in both enzymes. The existence of these states monitored by fluorescence relaxation spectroscopy, allowed us to postulate a new model of substrate binding prior to catalysis (Fig.1).

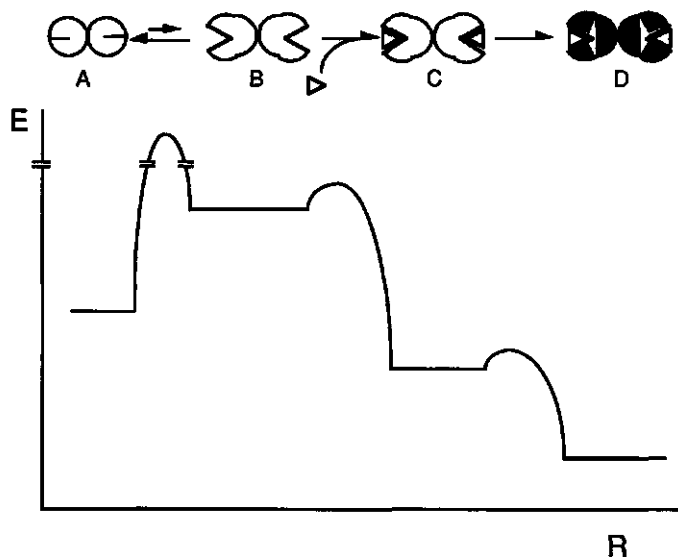


Fig.1: Schematic drawing of the role of conformational fluctuations in catalysis by oxidoreductases. A qualitative figure of the Gibbs free energy (E) versus reaction coordinate (R) is also presented. A break was introduced on the energy axis since the activation energy between "closed" (A) and "open" (B) enzyme conformation is much larger than the relative energy difference of these states. See text for details.

In this model, the majority of enzyme molecules in solution is present in an inaccessible conformation to substrate or cofactor ("closed" conformation, A in Fig.1). Structural (equilibrium) fluctuations give rise to a minor population of enzyme molecules with a proper conformation to bind substrate ("open" conformation, B in Fig.1). The equilibrium between "open" and "closed" enzyme conformations is shifted towards the "open" form in the presence of excess substrate or cofactor molecules (C in Fig.1) which reduce the flavin on the enzyme (D in Fig.1). The structural transition can be the rate limiting step in catalysis if the activation barrier between the "open" and "closed" enzyme structures is sufficiently large.

From time-resolved fluorescence anisotropy measurements as function of temperature one can distinguish between reorientational motion and energy transfer. In both dimeric proteins intersubunit energy transfer takes place between the FAD prosthetic groups. Furthermore, restricted reorientational motion of the flavin is only revealed in glutathione reductase. It is very likely that this flexible isoalloxazine is present in a minor population of enzyme molecules with a displaced Tyr197 making the flavin accessible to the cofactor (NADPH). This catalytically important enzyme species is not detected by X-ray crystallography and its observation requires a technique with high dynamic range of intensity such as time-resolved fluorescence. In order to derive the distance and relative orientation between the flavins, separate models describing fluorescence anisotropy must be applied to both proteins. The geometric arrangement of the flavins as derived from the analysis of the results is in excellent agreement with crystallographic data.

Chapter 3 of this thesis deals with the dynamic properties of the flavin environment in *Azotobacter vinelandii* lipoamide dehydrogenase as determined by steady-state fluorescence spectroscopy. As model systems the native enzyme and a deletion mutant lacking the 14 C-terminal amino acids were chosen. By fluorescence quenching and temperature dependent spectroscopy it was shown that the mutant has a flavin site accessible to solvent in contrast to wild type lipoamide dehydrogenase. We have to conclude from these observations and enzyme kinetic studies [1] that the C-terminal polypeptide of lipoamide-dehydrogenase is folded back onto the dehydrolipoamide binding site. This result is in agreement with the crystal structure of the *Pseudomonas putida* enzyme (A. Mattevi, personal communication) but in discrepancy with the disordered C-terminal tail of crystalline *A.vinelandii* lipoamide dehydrogenase [2]. In cryogenic solvents different dipolar relaxation behavior was found for mutant and native enzymes. The flavin

environment in the wild type enzyme was rigid on a nanosecond timescale while a conversion from slow to rapid relaxation was observed in the mutant protein from 203 to 303 K. The contributions to dipolar relaxation in the mutant enzyme were found to arise from solvent and protein dipoles. In aqueous solution, rapid relaxation was observed in both proteins indicating that rapid protein fluctuations are damped in viscogens. Because of the difference in dipolar relaxation in wild type and mutant proteins, the unique spatial arrangement of the two flavins makes this biological system an appropriate object to study the relationships between homo-energy transfer, dipolar relaxation and excitation energy. In this context a compartmental theoretical model is developed in chapter 4 on the basis of existing qualitative descriptions [3, 4]. The model was verified by global analysis of fluorescence anisotropy decay surfaces. The geometry and dynamics derived from the results were in excellent agreement with the protein-crystal geometry [2] and with the dipolar relaxation elaborated in chapter 3. In addition, thermodynamic parameters of equilibrium fluctuations in the protein structures could be determined from the maximum entropy analysis of the fluorescence decay. In agreement with Frauenfelder's concept of tiers of conformational substates [5, 6], the existence of two classes of states were established in lipoamide dehydrogenase (CS¹ and CS³). Thermal quenching of flavin fluorescence was related to transitions between conformational substates of category CS³ by comparing activation energy values.

In chapter 5 red- and blue-edge spectroscopy was applied to the electron-transferring flavoprotein from *Megasphaera elsdenii* which contains two FAD molecules within one subunit. Energy transfer between the two flavins was observed from time-resolved fluorescence depolarization experiments. We could demonstrate for the first time that energy transfer is not observable (as theoretically predicted) at the blue-edge of the emission band in an inhomogeneously broadened system. Interflavin distance and the relative orientation of the flavins could be determined for this protein with unknown three-dimensional structure.

In general, owing to a physical model based on conformational substates in proteins it is possible to use the complex fluorescence decay patterns in enzymes to explain certain aspects of catalysis. The analysis of the fluorescence decay in distributions of lifetimes by the maximum entropy method is then the logical choice since the information on conformational states is contained in the multiplicity of the distribution pattern. The advantage of the maximum entropy method is that no *a priori*

knowledge of the complex protein system needs to be encoded. According to the fluctuation-dissipation theorem [5] it is possible to monitor catalytically important protein conformations without substrate present. In order to test this hypothesis, fluorescence studies of binary enzyme-substrate complexes must be undertaken in the future. Catalytically important conformational substates will then be preferentially populated in contrast to the free enzyme.

We have also demonstrated that the validity of physical models on energy transfer in relation to dipolar relaxation can be tested in relatively complex biological systems. Precise goniometric information in bichromophoric proteins can be derived from fluorescence anisotropy relaxation. Temperature- and excitation energy-dependent studies of the fluorescence anisotropy provide a diagnostic method to distinguish reorientational motion from energy transfer. The described experimental and analytical methods have broad applicability to other biological systems containing identical fluorophores.

References

1. Schulze, E., Benen, J.A.E., Westphal, A.H. and de Kok, A. (1991) *Eur. J. Biochem.*, 200, 29-34.
2. Mattevi, A., Schierbeek, J.A. and Hol, W.G.J. (1991) *J. Mol. Biol.*, 220, 975-994.
3. Demchenko, A.P. (1987) *Ultraviolet Spectroscopy of Proteins* Springer-Verlag, Berlin.
4. Nemkovich, N.A., Rubinov, A.N. and Tomin, V.I. (1991) *Inhomogeneous Broadening of Electronic Spectra of Dye Molecules in: Topics in Fluorescence Spectroscopy* (Lakowicz, J.R. ed.) Vol 2, pp 367-428, Plenum Press, New York.
5. Frauenfelder, H. and Gratton, E. (1986) *Methods Enzymol.*, 127, 207-216.
6. Frauenfelder, H., Parak, F. and Young, R.D. (1988) *Ann. Rev. Biophys. Chem.*, 17, 451-479.

Samenvatting

Chemische reacties die zich in een levende cel afspelen, worden gekatalyseerd door enzymen. Deze belangrijke biomoleculen kunnen een chemische reactie tot een miljoen keer sneller laten verlopen, in vergelijking met dezelfde reactie in hun afwezigheid, waardoor het leven zoals wij het kennen mogelijk is. Elk organisme bevat eiwitten, welke alle opgebouwd zijn uit 20 verschillende aminozuren. De lineaire rangschikking van deze bouwstenen in een polypeptide wordt de primaire structuur genoemd. De primaire structuur, ofwel de chemische aminozuur samenstelling van dit polypeptide, bepaalt op zijn beurt de ruimtelijke structuur van een eiwit. Hierbij onderscheiden we de secundaire en tertiaire structuur. Met de secundaire structuur van het eiwit worden de specifieke vouwingspatronen van korte stukken polypeptiden bedoeld (b.v. α -helices, β -heets). De ruimtelijke coördinaten van alle atomen die in een eiwit voorkomen bepalen de tertiaire structuur. De assemblage van verschillende polypeptideketens tot een groter complex wordt aangeduid met de quaternaire structuur.

Tot in het begin van de jaren tachtig werd algemeen gedacht dat het werkingsmechanisme van een eiwit kon worden verklaard alleen al aan de hand van de primaire en statische tertiaire structuur zoals deze kan worden opgehelderd door middel van X-ray kristallografie. Er is echter een additioneel niveau van complexiteit die we in beschouwing moeten nemen. Als illustratie zullen we een simpel thermodynamisch rekenvoorbeeld aanhalen bedacht door Cooper en Dryden [1]. Stelt u zich een glaasje water voor met een volume van 1 ml. De warmtecapaciteit (C_v) van dit volume water is ongeveer 4.2 JK^{-1} . De statistische thermodynamica leert ons dat er een verband bestaat tussen de warmtecapaciteit en de grootte van energiefuctuaties ($\langle dE^2 \rangle$) van een systeem Dit verband is:

$$\langle dE^2 \rangle = kT^2 C_v \quad (1)$$

waarbij k de Boltzmann constante is en T de omgevings temperatuur in graad Kelvin. Bij een temperatuur van $27 \text{ }^\circ\text{C}$ (aangename zomerdag) treden dan energiefuctuaties op van $2.3 \cdot 10^{-9} \text{ J}$ wat overeenkomt met een temperatuurschommeling van $\pm 5.10 \cdot 10^{-10} \text{ }^\circ\text{C}$. In dit macroscopische systeem zijn we ons dus nauwelijks of niet bewust van fluctuaties. Neem nu een eiwit met een molecuulmassa van 25 kDa . De specifieke warmte capaciteit van verschillende eiwitten is zeer uniform en bedraagt ongeveer $1.3 \text{ JK}^{-1}\text{g}^{-1}$. Ons eiwit van 25 kDa heeft dan een warmte capaciteit

van $5.4 \cdot 10^{-20}$ JK⁻¹. Vullen we dit getal in vergelijking 1 in, dan levert dit energieflectuaties op met een amplitude van ongeveer $3 \cdot 10^{-19}$ J, wat overeenkomt met een temperatuur schommeling van ± 6 °C! De grootte van een systeem en het materiaal waarvan het gemaakt is (warmtecapaciteit) bepalen dus de amplitude van de energieflectuaties. Bovengenoemde additionele complexiteit betekent dus dat eiwitten structureel dynamische systemen zijn.

De vraag is hoe wij dit kunnen waarnemen en of structurele dynamica een rol in de katalyse speelt. Om de eerste vraag te beantwoorden moeten wij ons afvragen op welke tijdschaal dynamische processen zich binnen een eiwit afspeelen. Om een indruk te krijgen van deze tijdschaal zullen we uitrekenen hoe vaak een bolvormig eiwit, met een molekuul gewicht van 25 kDa in waterige oplossing, zich per seconde om zijn as wentelt. Met behulp van de Stokes-Einstein relatie wordt een verband gelegd tussen het volume (V) van een deeltje, de viscositeit van het oplosmiddel (η) en de temperatuur (T) enerzijds en de diffusieconstante (D) anderzijds:

$$D = \frac{6kT}{\eta V} \quad (2)$$

Om het volume van een eiwit van 25 kDa uit te rekenen moeten we het specifieke volume weten. Dit is weer een uniforme grootheid voor de meeste eiwitten met een waarde van 0.74 cm³/gr. Het volume van een eiwit van 25 kDa is dan $5.6 \cdot 10^{-20}$ cm³. Op een aangename zomerdag (27 °C) wentelt het eiwit zich dus per seconde drieëntachtig miljoen keer om zijn as, wat overeenkomt met één omwenteling per 12 ns (1 ns = $1 \cdot 10^{-9}$ seconde). Indien we dit willen waarnemen dan moeten we een interactie aangaan met het systeem (kleine verstoring) door middel van deeltjes of fotonen. Verder is het vereist dat de interactie plaatsvindt op dezelfde tijdschaal als het (omwentelings)proces. Indien de interactie te snel plaats vindt, dan heeft het systeem geen tijd om zich te equilibreren gedurende de interactie; indien te langzaam, dan is het proces al verlopen voordat we het kunnen meten.

Fluorescentie is een proces wat waarneembaar is, en tevens op dezelfde tijdschaal plaatsvindt als het omwentelen van het eiwit (1-10 ns). Kort gezegd komt fluorescentie op het volgende neer. Met behulp van een lichtbron wordt een electron van een molecuul aangeslagen naar een hoger energieniveau. Dit aangeslagen electron vervalt weer naar de grondtoestand door het uitzenden van een foton (licht). De energie (kleur van het licht) en de levensduur van de aangeslagen toestand (kans dat men een

foton op een bepaald tijdstip waarneemt) zijn gevoelige parameters voor de eigenschappen van de omgeving waarin het molecuul zich bevindt. Indien men ook nog verticaal gepolariseerd licht (electrisch veld van het licht trilt in één richting) op het molecuul afstuurt, dan bevatten de uitgezonden fotonen informatie over rotatie van het molecuul gedurende de aangeslagen toestand. Wil men fluorescentie waarnemen in eiwitten, dan moet men gebruik maken van fluorescente moleculen welke van nature binnen het eiwit aanwezig zijn of van zogenaamde "externe" fluorescente probes, welke aan een eiwit gebonden worden. Flavoproteïnen bevatten flavines als prothetische groep welke als natuurlijke, fluorescente "reporter" moleculen gebruikt kunnen worden. De flavines komen in verschillende gedaanten voor, maar zijn alle afgeleid van riboflavine, beter bekend onder de naam vitamine B2. Dit molecuul absorbeert blauw licht (waardoor het er geel uitziet) en fluoresceert groen licht.

Door verfijning van techniek en data-analyse zijn nieuwe mogelijkheden ontstaan om eiwitfluorescentie gedetailleerd te interpreteren. Door de combinatie van nieuwe inzichten omtrent eiwitstructuur en -dynamica aan de ene kant, en verbeterde kennis omtrent fotofysica van biologische moleculen aan de andere kant, is een "stevige fundering" ontstaan om structuur-functie relaties en fluorescentie-eigenschappen te koppelen. Een gevolg van dit interdisciplinaire "huwelijk" is dat bidirectionele informatie kan worden verkregen door de toepassing van fluorescentiespectroscopie aan eiwitten.

In dit proefschrift is het onderzoek beschreven aan de fluorescentie van Flavine Adenine Dinucleotide (FAD) gebonden aan Glutathione Reductase (GR), Lipoamide Dehydrogenase (LipDH) en Electron-Transferring Flavoprotein (ETF). Het doel van dit onderzoek was informatie te verkrijgen over de dynamische en structurele eigenschappen van deze eiwitten in oplossing. Tevens is getracht een verband te leggen tussen deze eigenschappen en de werking van eiwitten. Ook zijn de structureel gunstige eigenschappen van LipDH geëxploiteerd om fysische modellen omtrent energieoverdracht tussen gelijke chromoforen uit te breiden en te toetsen. In deze context hebben we dus biologisch materiaal gebruikt om fysische fenomenen te bestuderen.

In hoofdstuk 2 worden de tijdopgeloste fluorescentie-parameters van FAD gebonden aan GR en LipDH vergeleken. De dynamische interconversie tussen verschillende waargenomen conformatie toestanden van de twee eiwitten verschillen sterk ondanks hun vergelijkbare tertiaire structuur. Het bestaan van deze toestanden, zoals waargenomen door tijdopgeloste fluorescentie, heeft ons in staat gesteld om een nieuw model te

postuleren wat betrekking heeft op substraat-binding (substraat: in reactie om te zetten stof) voordat katalyse plaats vindt. In dit model wordt verondersteld dat de meeste enzymmoleculen aanwezig zijn in een toestand die ontoegankelijk is voor het substraat of de cofactor (gesloten conformatie). Structurele fluctuaties zorgen ervoor dat een eiwit molecuul in een geschikte conformatie komt om substraat te binden (open conformatie). Het evenwicht tussen gesloten en open conformatie verschuift naar de open conformatie doordat in aanwezigheid van een overmaat substraat- of cofactor moleculen de laatstgenoemde enzymvorm wordt weggevangen. Deze structurele fluctuaties kunnen de snelheidsbepalende stap in de katalyse zijn indien de activeringsenergie tussen de gesloten en open conformatie hoog is.

Met behulp van tijdopgeloste fluorescentie-anisotropiemetingen als functie van temperatuur, kan onderscheid gemaakt worden tussen reoriëntatie van FAD en energieoverdracht tussen de twee flavines in GR en LipDH. In beide eiwitten wordt energieoverdracht tussen de flavines waargenomen. Het flavine in LipDH is echter star gebonden (nauwelijks of geen reoriëntatie) maar in GR kan het bewegen met een maximale hoek van 26° . Het is erg waarschijnlijk dat dit flavine alleen beweeglijk is in de "open" (cofactor toegankelijke) GR-conformatie. Deze belangrijke enzymtoestand kan niet waargenomen worden d.m.v. röntgen diffractie aan kristallen, maar vereist een techniek met hoog-dynamisch bereik, zoals tijdopgeloste fluorescentie. De afstand en relatieve oriëntatie van de flavines kan goed berekend worden door verschillende modellen toe te passen op de fluorescentie-anisotropie van beide eiwitten. Deze resultaten zijn in overeenstemming met kristallografische gegevens.

In hoofdstuk 3 worden de dynamische eigenschappen van de flavine omgeving in LipDH behandeld gemeten met behulp van steady-state fluorescentie-spectroscopie. Het natieve enzym en een deletiemutant, welke 14 C-terminale aminozuren mist, zijn als modelsystemen gekozen. We laten d.m.v. fluorescentiedoving en temperatuurafhankelijke spectroscopie zien dat het flavine in de mutant toegankelijk is voor oplosmiddel in tegenstelling tot het natieve enzym. Door deze resultaten en enzymkinetische studies [2] kunnen we concluderen dat het C-terminale polypeptide in het natieve enzym een interactie aangaat met de dehydrolipoamide (substraat) bindingsplaats in tegenstelling tot wat m.b.v. röntgen diffractie aan kristallen van dit eiwit is gevonden [3].

Er werden duidelijke verschillen gevonden in dipolaire relaxatie tussen het natieve en het gemuteerde eiwit in een cryogeen oplosmiddel. De flavine omgeving is rigide te noemen op nanoseconde tijdschaal in het wild-type enzym, terwijl tussen 203

en 303 K een overgang van langzame naar snelle dipolaire relaxatie wordt waargenomen in de mutant. In hetzelfde hoofdstuk tonen we aan dat de dipolaire relaxatie in de omgeving van het flavine in de mutant veroorzaakt wordt door zowel oplosmiddel- als eiwitdipolen. Ultrasnelle relaxatie wordt voor beide eiwitten waargenomen in waterige oplossing. Dit toont aan dat eiwitfluctuaties worden gedempt in een oplosmiddel van hoge viscositeit.

Door het verschil in dipolaire relaxatie in het wild-type en de mutant alsmede de unieke ruimtelijke ordening van de twee flavines, is dit biologische systeem een geschikt object om de relatie tussen de energieoverdracht, de dipolaire relaxatie en de excitatieenergie te bestuderen. In deze context is in hoofdstuk 4 een compartimenteel model beschreven, uitgaande van bestaande kwalitatieve modellen [4,5]. Het model is geverifieerd door een simultane (globale) analyse van meerdere fluorescentie-anisotropievervalcurves, verkregen als functie van temperatuur en excitatieenergie. De geometrie en dynamische eigenschappen die uit de resultaten zijn afgeleid, blijken in overeenstemming te zijn met de eiwit-kristal geometrie [3] en met de dipolaire relaxatie zoals beschreven in hoofdstuk 3.

Door een maximale entropie analyse van fluorescentievervalcurven kunnen thermodynamische parameters van evenwichtsfluctuaties van de eiwitten bepaald worden. In overeenstemming met het concept dat een hiërarchie van conformatie toestanden bestaat [6,7], werden twee klassen van subtoestanden waargenomen in LipDH (CS^1 , CS^3). Door activeringsenergieën te vergelijken, is de temperatuursafhankelijke doving van de flavinefluorescentie gerelateerd aan overgangen tussen conformatie toestanden van de categorie CS^3 .

In hoofdstuk 5 wordt beschreven hoe spectroscopie met langgolvlige excitatie en kortgolvlige detectie is toegepast op ETF van *Megasphaera elsdenii* dat 2 FAD prosthetische groepen in een subunit bevat. Energieoverdracht tussen de flavines wordt waargenomen in de tijdopgeloste fluorescentieanisotropie. We hebben als eerste kunnen demonstreren dat energieoverdracht niet waarneembaar is aan de blauwe kant van het emissiespectrum van een inhomogeen verbreed systeem (zoals theoretisch was voorspeld). De afstand tussen de flavines en de relatieve oriëntatie konden worden geschat voor dit eiwit dat een onbekende driedimensionale structuur heeft

In het algemeen kunnen wij stellen dat het mogelijk is om m.b.v. een fysisch model, gebaseerd op conformatie toestanden in eiwitten, complexe fluorescentievervalpatronen van eiwitten te gebruiken om bepaalde aspecten van de katalyse te verklaren. De analyse van fluorescentieverval in distributies van levensduren

(d.m.v. de maximale entropie methode) is dan de logische keuze, omdat informatie over conformatie toestanden in de veelvoudigheid van het distributiepatroon is ondergebracht. Het voordeel van de maximale entropie methode is dat er geen voorafgaande kennis over het complexe eiwit systeem gecodeerd hoeft te worden.

Volgens het fluctuatie-dissipatie theorema [6] is het mogelijk om katalytisch belangrijke eiwitconformaties waar te nemen zonder dat het substraat aanwezig is. Om deze hypothese te testen moeten fluorescentie studies ondernomen worden aan het binaire enzym-substraat complex. De katalytisch belangrijke conformaties zullen dan bij voorkeur worden waargenomen in tegenstelling tot het vrije enzym.

We hebben ook laten zien dat fysische modellen die een verband leggen tussen dipolaire relaxatie en energieoverdracht, getoetst kunnen worden in relatief complexe biologische systemen. Precieze ruimtelijke informatie kan verkregen worden uit fluorescentieanisotropierelaxatie van eiwitten met twee identieke chromoforen. Temperatuur- en excitatieenergieafhankelijke metingen van de tijdopgeloste fluorescentieanisotropie is een diagnostische methode om onderscheid te maken tussen reoriëntatie beweeglijkheid of energieoverdracht. De beschreven experimentele en analytische methoden hebben een brede toepasbaarheid in andere biologische systemen met identieke en niet-gelijke chromoforen.

Referenties

1. Cooper, A. and Dryden, D.T.F. (1988) Thermodynamic Fluctuations and Functions in Proteins in: *The Enzyme Catalysis Process* (Cooper, A., Houben, J.L. and Chien, L.C., eds.) NATO ASI Series A: Life Sciences Vol.178, pp 159-171, Plenum Press, New York.
2. Schulze, E., Benen, J.A.E., Westphal, A.H. and de Kok, A. (1991) *Eur. J. Biochem.*, 200, 29-34.
3. Mattevi, A., Schierbeek, J.A. and Hol, W.G.J. (1991) *J. Mol. Biol.*, 220, 975-994.
4. Demchenko, A.P. (1987) *Ultraviolet Spectroscopy of Proteins* Springer-Verlag, Berlin .
5. Nemkovich, N.A., Rubinov, A.N. and Tomin, V.I. (1991) *Inhomogeneous Broadening of Electronic Spectra of Dye Molecules in: Topics in Fluorescence Spectroscopy* (Lakowicz, J.R. ed.) Vol 2, pp 367-428, Plenum Press, New York.
6. Frauenfelder, H. and Gratton, E. (1986) *Methods Enzymol.*, 127, 207-216.

7. Frauenfelder, H., Parak, F. and Young, R.D. (1988) *Ann. Rev. Biophys. Biophys Chem.*, 17, 451-479.

Curriculum vitae

Philippe Igor Henri Bastiaens werd geboren op 12 maart 1963 in Den Helder. In 1981 behaalde hij het diploma VWO aan het St. Joris College te Eindhoven. In datzelfde jaar werd de studie moleculaire wetenschappen aangevangen aan de landbouwuniversiteit te Wageningen. Het kandidaatsexamen werd afgelegd in 1985. Hierop volgde de doctoraalfase die bestond uit een verzwaard hoofdvak Biochemie en hoofdvak Moleculaire Fysica. Het eerste hoofdvak omvatte onderzoek naar structuur en werking van cytochroom P450-reductase onder leiding van Prof. Dr. F. Müller. Het laatste hoofdvak bestond uit hoge druk studies aan flavoproteïnen in het laboratorium van Prof. Dr. G. Weber aan het Department of Biochemistry van de University of Illinois te Urbana. De stageperiode is doorgebracht aan het Department of Biochemistry van de University of Georgia te Athens. Het onderzoek bestreek tijdopgeloste fluorescentie-studies aan bacterieel luciferase onder leiding van Prof. Dr. J. Lee. Het doctoraal examen werd met lof afgelegd in mei 1988.

In augustus 1988 is hij begonnen aan een promotieonderzoek aan het Department of Physiology and Biophysics van de Mount Sinai School of Medicine te New York onder leiding van Prof. Dr. J. Eisinger. Na een jaar heeft hij besloten om onderzoek te doen aan tijdopgeloste fluorescentie van flavoproteïnen bij de vakgroep Biochemie van de Landbouwuniversiteit onder leiding van Dr. A.J.W.G. Visser. Deze werkzaamheden hebben geresulteerd in dit proefschrift. Dit onderzoek is voorafgegaan aan een 3 maanden durende pilot studie aan proteïne kinase C gesubsidieerd door de Stichting voor Biofysica (NWO). Sinds juli 1991 werkt hij aan een project dat tot doel heeft de functie van proteïne kinase C in de differentiatie van embryonale carcinoma cellen vast te stellen. Dit onderzoek wordt gesubsidieerd door de Stichting Koningin Wilhelmina Fonds en wordt uitgevoerd bij de vakgroep Biochemie van de Landbouwuniversiteit te Wageningen.

Publications:

Bonants, P.J.M., Bastiaens, P.I.H., Visser, A.J.W.G. and Müller, F. (1987) Time-resolved fluorescence spectroscopy on NADPH-cytochrome P-450 reductase. In: *Flavins and Flavoproteins* (Edmondson, D.E. & McCormick, D.B., Eds.) pp. 357-360, de Gruyter, Berlin.

Brewer, J.M., Bastiaens, P.I.H. and Lee, J. (1987) Fluorescence lifetime and spectral study of the acid expansion of bovine serum albumin. *Biophys. Chem.*, 28, 22-27.

Brewer, J.M., Bastiaens, P.I.H. and Lee, J. (1987) Investigation of conformational changes in yeast enolase using dynamic fluorescence and steady-state quenching measurements. *BBRC*, 147, 329-334.

Brewer, J.M., Bastiaens, P.I.H. and Lee, J. (1988) Investigation of conformational changes in proteins using fluorescence and fluorescence anisotropy decay. *Proc. SPIE*, 909, pp. 150-154.

Bastiaens, P.I.H., Bonants, P.J.M., van Hoek, A., Müller, F. and Visser, A.J.W.G. (1988) Proof of Förster energy transfer between FAD and FMN in cytochrome P450 reductase by time-resolved red-edge spectroscopy. *Proc. SPIE*, 909, pp. 257-262.

Bastiaens, P.I.H., Bonants, P.J.M., van Hoek, A., Müller, F. and Visser, A.J.W.G. (1989) Time-resolved fluorescence spectroscopy of NADPH-cytochrome P-450 reductase: demonstration of energy transfer between the two prosthetic groups. *Biochemistry*, 28, 8416-8425.

Leenders, R., Bastiaens, P.I.H., Lunsche R., van Hoek, A. and Visser, A.J.W.G. (1990) Rotational resolution of methyl-group substitution and anisotropic rotation of flavins as revealed by picosecond-resolved fluorescence depolarization. *Chem. Phys. Lett.*, 165, 315-322.

Bastiaens, P.I.H., DeBeus, A., Lacker, M., Somerharju, P., Vauhkonen, M. and Eisinger (1990) Resonance energy transfer from a cylindrical distribution of donors to a plane of acceptors. - Location of apo-B100 protein on the human low-density lipoprotein particle. *Biophys. J.*, 58, 665-675.

Bastiaens, P.I.H. and Visser, A.J.W.G. (1991) Interflavin energy transfer as a tool to determine geometrical parameters in flavoproteins. In: *Flavins and Flavoproteins 1990* (Curti, B., Rondi, S. & Zanetti, G., Eds.) pp 73-78.

Tyrakowska, B., Koziolowa, A., Bastiaens, P.I.H. and Visser, A.J.W.G. (1991) Comparative fluorescence study of phototautomerism of lumichrome in dodecylammonium propionate reversed micelles. In: *Flavins and Flavoproteins 1990* (Curti, B., Rondi, S. & Zanetti, G., Eds.) pp. 46-48

Gadella Jr., T.W.J., Bastiaens, P.I.H., Visser, A.J.W.G. and Wirtz, K.W.A. (1991) Shape and lipid binding site of the non specific lipid-transfer protein (sterol carrier protein 2). A steady-state and time-resolved fluorescence study. *Biochemistry* **30**, 5555-5564.

Bastiaens, P.I.H., Mayhew, S.G., O'Nualláin, E.M., van Hoek, A. and Visser, A.J.W.G. (1991) Energy transfer between the flavin chromophores of electron-transferring flavoprotein from *Megasphaera elsdenii* as inferred from time-resolved red-edge and blue-edge fluorescence spectroscopy. *J. of Fluorescence*, **1**, 95-103.

Müller, F., Hopkins, T.R., Lee, J. and Bastiaens, P.I.H. (1991) Methanol oxidase. In: *Chemistry and Biochemistry of Flavoproteins* (Müller, F. ed.) Vol. 3, CRC Press, Boca Raton.

Bastiaens, P.I.H., van Hoek, A., Brochon, J.C. and Visser, A.J.W.G. (1992) Conformational dynamics in glutathione reductase. *Proc. SPIE*, in press

Shcherbatska, N.V., Bastiaens, P.I.H., Jonker, S.A., Warman, J.M. and Visser, A.J.W.G. (1992) Dipole moments in the ground- and excited state of flavin from molecular relaxation spectroscopy and microwave conductivity. *Proc. SPIE*, in press

Bastiaens, P.I.H. and Visser, A.J.W.G. (1992) Dynamics and geometry in dimeric flavoproteins from fluorescence relaxation spectroscopy. In: *Fluorescence Spectroscopy: New Methods and Applications* (Wolfbiss, ed.) Springer Verlag, in press

Bastiaens, P.I.H., van Hoek, A., Wolkers, W.F., Brochon, J.C. and Visser, A.J.W.G. (1992) Comparison of the dynamical structures of lipoamide dehydrogenase and glutathione reductase by time-resolved polarized flavin fluorescence. *Biochemistry*, submitted

Bastiaens, P.I.H., van Hoek, A., van Berkel, W.J.H., de Kok, A. and Visser, A.J.W.G. (1992) Molecular relaxation spectroscopy of flavin adenine dinucleotide in wild type and mutant lipoamide dehydrogenase from *azotobacter vinelandii*. *Biochemistry*, submitted

Bastiaens, P.I.H., van Hoek, A., Benen, J.A.E., Brochon, J.C. and Visser, A.J.W.G. (1992) Conformational dynamics and intersubunit energy transfer in wild type and mutant lipoamide dehydrogenase from *azotobacter vinelandii*. - A multidimensional time-resolved polarized fluorescence study. *Biophys. J.*, submitted